

Aus der Klinik für Neurologie

Geschäftsführender Direktor: Prof. Dr. Lars Timmermann

des Fachbereichs Medizin

der Philipps-Universität Marburg

**Multimodal view on resting-state brain activity in  
Parkinson's disease:  
examining the relation between functional resting-state  
networks and metabolic network activity**

Inaugural-Dissertation

zur Erlangung des Doktorgrades der Naturwissenschaften

dem Fachbereich Medizin der Philipps-Universität Marburg

vorgelegt von

**Marina Christine Ruppert-Junck  
(geb. Ruppert)**

aus Marburg

Marburg, 2023

Originaldokument gespeichert auf dem Publikationsserver der  
Philipps-Universität Marburg  
<http://archiv.ub.uni-marburg.de>



Dieses Werk steht unter einer  
Creative Commons  
Namensnennung  
Keine kommerzielle Nutzung  
Weitergabe unter gleichen Bedingungen  
4.0 International Lizenz.

Die vollständige Lizenz finden Sie unter:  
<https://creativecommons.org/licenses/by-nc-sa/4.0/deed.de>

Angenommen vom Fachbereich Medizin der Philipps-Universität Marburg am:  
31.05.2023

Gedruckt mit Genehmigung des Fachbereichs Medizin

Dekanin: Frau Prof. Dr. Denise Hilfiker-Kleiner

Referent: Herr PD Dr. David José Pedrosa Carrasco

1. Korreferent: Herr Prof. Dr. Igor Nenadić

*Widmung*

*Ich widme diese Arbeit meinem Großvater Walter.*

## Publications

Ruppert, M. C., Greuel, A., Tahmasian, M., Schwartz, F., Stürmer, S., Maier, F., Hammes, J., Tittgemeyer, M., Timmermann, L., van Eimeren, T., Drzezga, A., & Eggers, C. (2020). Network degeneration in Parkinson's disease: Multimodal imaging of nigro-striato-cortical dysfunction. *Brain : A Journal of Neurology*, 143(3), 944–959. <https://doi.org/10.1093/brain/awaa019>

Ruppert, M. C., Greuel, A., Freigang, J., Tahmasian, M., Maier, F., Hammes, J., van Eimeren, T., Timmermann, L., Tittgemeyer, M., Drzezga, A., & Eggers, C. (2021). The default mode network and cognition in Parkinson's disease: A multimodal resting-state network approach. *Human Brain Mapping*, 42(8), 2623–2641. <https://doi.org/10.1002/hbm.2539>

## Table of Content

<b>List of abbreviations .....</b>	<b>VII</b>
<b>1. Introduction.....</b>	<b>1</b>
1.1. Functional resting-state networks.....	1
1.2. Metabolic covariance patterns.....	2
1.3. Neurodegenerative disorders .....	2
1.4. Resting-state network dysfunction in neurodegenerative disorders .....	3
1.5. Coincidence of functional and metabolic deficits in neurodegeneration.....	4
1.6. Objective of the current work.....	5
<b>2. Results of the publications .....</b>	<b>6</b>
2.1. Network degeneration in Parkinson's disease: multimodal imaging of nigro-striato-cortical dysfunction .....	6
2.1.1. Statement of contribution.....	7
2.1.2. Cohort specification .....	7
2.1.3. Dopamine depletion in the posterior putamen in Parkinson's disease.....	7
2.1.4. Striatocortical hypoconnectivity in Parkinson's disease.....	8
2.1.5. Relation of striatocortical dysconnectivity and cortical glucose metabolism .....	8
2.1.6. Clinical impairment and multimodally assessed network dysfunction .....	9
2.2. The default mode network and cognition in Parkinson's disease: a multimodal resting-state network approach.....	10
2.2.1. Statement of contribution.....	10
2.2.2. Cohort specification .....	11
2.2.3. Spatial convergence of hemodynamic and metabolic networks.....	11
2.2.4. Metabolic activity in the default mode network in Parkinson's disease .....	11
2.2.5. Metabolic connectivity in the default mode network in Parkinson's disease .....	12
2.2.7. Default mode network hyperconnectivity and cognitive impairment.....	13
<b>3. Discussion .....</b>	<b>14</b>
3.1. Dopamine deficiency is accompanied by striatocortical dysconnectivity.....	15
3.2. Metabolic concomitant of striatocortical dysconnectivity .....	16
3.3. Metabolic and hemodynamic network convergence .....	17
3.4. Correspondence between metabolic and hemodynamic network changes .....	18
3.5. Relevance of default mode network dysfunction for cognitive impairment.....	19
3.6. Limitations .....	20
3.7. Outlook: Dynamic FDG-PET acquisition techniques .....	20
3.8. Conclusion .....	21

---

<b>4. Summary .....</b>	<b>22</b>
<b>5. Zusammenfassung .....</b>	<b>24</b>
<b>References .....</b>	<b>26</b>
<b>6. Appendix .....</b>	<b>34</b>
6.1. Network degeneration in Parkinson's disease: Multimodal imaging of nigro-striato-cortical dysfunction .....	34
6.2. Supplementary material .....	51
6.3. The default mode network and cognition in Parkinson's disease: a multimodal resting-state network approach.....	57
7.4. Supplementary material .....	77
7.5. Lebenslauf.....	85
7.6. Publikationsverzeichnis .....	87
1.7. Verzeichnis der akademischen Lehrer*innen.....	89
1.8. Danksagung .....	92
1.9. Ehrenwörtliche Erklärung.....	93

## List of abbreviations

AD .....	Alzheimer's disease
AGI .....	left angular gyrus
AGr .....	right angular gyrus
BDI-II .....	Beck's depression inventory II
BOLD .....	blood-oxygenation-level-dependent
DMN .....	default mode network
FDG .....	2-[18F]fluoro-2-deoxy-D-glucose
FDG-PET .....	2-[18F]fluoro-2-deoxy-D-glucose positron emission tomography
FDOPA .....	6-[18F]fluoro-L-Dopa
FDOPA-PET .....	6-[18F]fluoro-L-Dopa positron emission tomography
FDR .....	false discovery rate
fMRI .....	functional magnetic resonance imaging
FWE .....	family-wise error
GIFT .....	Group ICA of fMRI Toolbox
ICA .....	independent component analyses
IPC .....	inferior parietal cortex
LEDD .....	levodopa equivalent daily dose
MCI .....	mild cognitive impairment
MDS .....	Movement Disorder Society
MMSE .....	Mini-Mental State Examination
MNI .....	Montreal Neurological Institute
mPFC .....	medial prefrontal cortex
ParaHL .....	left parahippocampal cortex
ParaHR .....	right parahippocampal cortex
PC .....	precuneal cortex
PCC .....	posterior cingulate cortex
PD .....	Parkinson's disease
PD-MCI .....	Parkinson's disease with mild cognitive impairment
PD-NC .....	Parkinson's disease with normal cognition
pSMGI .....	left posterior supramarginal gyrus
pSMGls .....	left posterior superior supramarginal gyrus
pSMGrS .....	right posterior superior supramarginal gyrus
ROIs .....	regions of interest
rs-fMRI .....	resting-state functional magnetic resonance imaging
SFGI .....	left superior frontal gyrus



---

SFGr .....	right superior frontal gyrus
sLOCI .....	left superior lateral occipital cortex
sLOCr .....	right superior lateral occipital cortex
SPM12 .....	Statistical Parametric Mapping 12
uncorr .....	uncorrected
UPDRS-III .....	Unified Parkinson's Disease Rating Scale part III

# 1. Introduction

## 1.1. Functional resting-state networks

The architecture of human brain function is determined by ordered patterns of interregional correlations, even under resting conditions (Fox and Raichle 2007). Intrinsic connectivity between regions may be ascertained with functional magnetic resonance imaging (fMRI) by the degree of synchronization within the activity-dependent oxygenation of blood (Biswal et al. 2010). In a very specific context, resting-state functional connectivity between brain areas refers to a temporal correlation between fluctuations (typically  $< 0.1$  Hz) in the spontaneous blood-oxygenation-level-dependent (BOLD) signal (Fox and Raichle 2007). This intrinsic connectivity can be partially explained by direct structural connections between participating regions, yet may also result from more indirect interactions (Vincent et al. 2007; Biswal et al. 2010).

Numerous studies analyzing independent cohorts have consistently described the universal architecture of homotopic resting-state networks (Biswal et al. 2010). In their seminal study, Biswal and colleagues (1995) first provided evidence for functional coherence in the resting-state between cortical regions which are typically activated during motor tasks. The default mode network (DMN) represents the most often investigated resting-state network. It includes a set of brain regions, which are highly active at rest and deactivate during cognitive demanding tasks (Raichle et al. 2001). The posterior cingulate cortex (PCC) extending into the precuneal cortex (PC) and the medial prefrontal cortex (mPFC) are key hub regions of the DMN, meaning both have a high level of functional connections to other regions of the network, including the inferior parietal cortex (IPC), and parahippocampal gyri (Drzezga et al. 2011). Several resting-state networks have been described, e.g. the motor network (Biswal et al. 1995), the ventral attention network (Fox et al. 2006), the salience network (Seeley et al. 2007), and the primary visual network (Beckmann et al. 2005), all of which have been assigned to distinct cognitive features.

However, the underlying neurophysiological and metabolic principles of functional connectivity remain incompletely understood (Riedl et al. 2014) and less is known about the influence of different neurotransmitter systems on resting-state networks. Sparse evidence proposes a modulating effect of the dopaminergic system on resting brain activity, e.g. in the DMN (Cole et al. 2013; Conio et al. 2020) or even suggests dopaminergic nuclei as often neglected components of resting-state networks (Bär et al. 2016).

### 1.2. Metabolic covariance patterns

In contrast to fMRI which reflects a complex interaction between hemodynamic factors, among them blood flow, blood volume and the rate of oxygenation (Buxton 2010; Kim and Ogawa 2012), 2-[18F]fluoro-2-deoxy-D-glucose positron emission tomography (FDG-PET), uses a specific, radiolabeled glucose analog to directly measure the activity-dependent cellular glucose metabolism (Phelps et al. 1979). Although glucose serves as an essential cerebral source of energy, and oxidative phosphorylation is closely coupled to oxygen consumption according to basic physiological principles, fluctuations of glucose consumption at rest and their association to functional connectivity as metabolic component remain largely unknown (Tomasi et al. 2013; Riedl et al. 2014). Pioneering studies revealed evidence for a common substrate underlying intrinsic connectivity by combining both fMRI and FDG-PET (Di and Biswal 2012; Passow et al. 2015; Savio et al. 2017). In this context, the concept of metabolic connectivity emerged, which basically reflects the interaction among different brain regions, based on the interregional relation of glucose consumption measured with FDG-PET (Yakushev et al. 2017).

Previous studies focused on the analysis of metabolic resting-state covariance patterns by applying independent component analyses (ICA) on a group level, as single-subject analyses of interregional correlations were not possible due to a lack of temporal information in commonly acquired FDG-PET data (Savio et al. 2017; Amend et al. 2019). By applying this method, first evidence for equal variances of glucose metabolism in functional connected regions was observed for distinct resting-state networks, including the DMN and sensorimotor network (Di and Biswal 2012; Spetsieris et al. 2015; Savio et al. 2017). Therefore, FDG-PET represents a promising tool to investigate the metabolic basis of intrinsic network organization and fundamental relations between coherent hemodynamic networks and glucose consumption, which remain unresolved to date (Wehrl et al. 2013; Amend et al. 2019). In addition, studies suggest that metabolic connectivity may serve as a marker of cognitive functions, for example, working memory (Yakushev et al. 2013). A few studies pointed towards the potential of metabolic covariance as marker of cognitive dysfunction and neuronal pathologies (Amend et al. 2019; Spetsieris et al. 2015; Sala and Perani 2019).

### 1.3. Neurodegenerative disorders

Neurodegenerative disorders are accompanied by decline of distinct neuronal cell populations, resulting in heterogenous clinical presentations (Jellinger 2009). Among the most common neurodegenerative disorders are Alzheimer's disease (AD), frontotemporal dementia, Parkinson's disease (PD), dementia with Lewy bodies and

Huntington's disease (Erkkinen et al. 2018). Age is considered one of the main risk factors for neurodegenerative disorders like AD and PD and both mainly affect the elderly population (Hou et al. 2019). In result of the demographic change, case numbers will rise rapidly in the future and represent an enormous burden for the health care system and society (Shlisky et al. 2017). A pathological hallmark is the accumulation and/or dysregulated degradation of misfolded proteins in neural tissue, characterizing the diseases as "proteinopathies" with partly overlapping features (Jellinger 2009). In addition to these molecular pathological hallmarks, functional changes within neuronal circuits can be found (Palop et al. 2006). For example, in AD accumulation of distinct  $\beta$ -amyloid species coincides with hypometabolism and connectivity changes in the DMN (Buckner et al. 2005; Drzezga et al. 2011).

PD is the second common neurodegenerative disease with a prevalence of 1% in the population above 60 years (Lau and Breteler 2006). The cardinal symptoms of PD include rigidity, bradykinesia and tremor (Postuma et al. 2015). In addition, non-motor symptoms have gained in importance and may manifest in autonomic dysfunction, sleep problems, cognitive deficits and dementia among others (Zach et al. 2017). Neuropathological hallmarks include Lewy-bodies, containing, among other proteins, aggregated forms of a  $\alpha$ -synuclein (Spillantini et al. 1998), that are typically found in midbrain nuclei like the Substantia Nigra from stage three on and enter neocortical areas in later disease stages (Braak et al. 2004). In classical models of PD pathophysiology, degeneration of dopaminergic neurons in the Substantia Nigra, is accompanied by dysregulations in striato-thalamo-cortical circuits responsible for bradykinesia (DeLong 1990). Modern theories assume that this focal loss of dopaminergic cells induces more widespread functional changes in a stereotypic manner by disturbing the efficient interplay of oscillatory brain activity. In this context, the term "circuitopathy" emerged, which describes dysregulated activity within disease-vulnerable networks (McIntyre and Anderson 2016), which can be examined *in vivo* with functional imaging.

### 1.4. Resting-state network dysfunction in neurodegenerative disorders

A large body of studies focused on dysfunction of resting-state networks in neurodegenerative disorders as a potential prospective imaging biomarker of dysregulated oscillatory activity. The resting-state approach offers a unique advantage for the study of neurodegenerative disorders, unbiased by difficulties with understanding specific tasks or instructions and the easy applicability to clinical settings. Particularly, under different neurodegenerative conditions, connectivity deficits were observed in defined networks and increased as symptoms worsened (Drzezga et al. 2011).

In PD, reduced functional connectivity has been reported along striatocortical connections of the sensorimotor network as revealed by resting-state fMRI (rs-fMRI) studies (Helmich et al. 2010; Helmich et al. 2015). A few studies reported altered functional connectivity of the DMN in PD patients with or without cognitive impairment and drew a relation to cognitive symptoms (Tessitore et al. 2012; Baggio et al. 2015; Lucas-Jiménez et al. 2016; Karunanayaka et al. 2016; Lopes et al. 2017), but findings delineating altered DMN connectivity based on rs-fMRI were heterogenous, suggesting predominant decreases or increases in DMN functional connectivity alike (Tessitore et al. 2012; Krajcovicova et al. 2012; Baggio et al. 2015; Amboni et al. 2015; Karunanayaka et al. 2016; Lopes et al. 2017; Zhan et al. 2018).

Pioneering studies examined interregional metabolic interactions based on static FDG-PET scans on a group level in PD patients. Spetsieris et al. (2015) thereby concluded that DMN function is spared from pathological alterations in the early disease stage but followed by dopamine-responsive decreased network expression at advanced stages. Using sparse-inverse covariance estimation and an interregional correlation approach, Sala and colleagues (2017) assessed altered metabolic connectivity in cognitively unimpaired PD patients and reported changes on multiple scales. They observed decreased frontal metabolic coupling in several important resting-state networks on one hand and enhanced coupling in the posterior cortex in comparison to age-matched controls on the other hand (Sala et al. 2017). Given the heterogeneity prevalent in unimodal studies, multimodal examinations may provide an opportunity to understand disease-related hemodynamic and metabolic network alterations at more a holistic level.

### 1.5. Coincidence of functional and metabolic deficits in neurodegeneration

A better understanding of metabolic brain activity in coherently active regions could enable insights into the abovementioned dysfunction of resting-state networks in neurodegenerative diseases (Savio et al. 2017). According to the hypothesis of circuitopathy, i.e., local degeneration possibly leading to remote aberrant synchronization, extensive degenerative processes occur in a network-dependent manner. Multimodal neuroimaging studies showed a topographic convergence between univariate metabolic deficits and impairments of functional connectivity within distinct disease-vulnerable networks (Drzezga et al. 2011; Scherr et al. 2019). Moreover, in AD, for example, a specific topographic distribution of molecular pathology, cerebral atrophy, hypometabolism and functional network degeneration has been described (Buckner et al. 2005; Drzezga et al. 2011; Hoenig et al. 2018).

In PD specifically, as the leading neurodegenerative disorder of the motor system, similar spatial associations between hemodynamic and metabolic changes remain to be studied to date. But, a network perspective on 2-[18F]fluoro-2-deoxy-D-glucose (FDG) metabolism has emerged in the field of PD and has been demonstrated as a robust technique to identify a characteristic topographical pattern of PD-related metabolic changes in independent patient cohorts (Niethammer and Eidelberg 2012). Multimodal resting-state studies are necessary to clarify if and how metabolic and functional connectivity are associated with each other and how altered functional connectivity in PD relates to metabolic changes or if they mutually depend on each other during the diseases course. This would not only result in a more complete view on PD pathophysiology from a network perspective, but also enhance the establishment of multimodal progression markers for PD.

### 1.6. Objective of the current work

According to the current state of research, there are hardly any studies which combine resting-state FDG-PET acquisitions and fMRI in the same cohort of PD patients to analyze the topography of intrinsic neuronal networks and alterations therein in PD. But it is urgently emphasized in current literature that such multimodal resting-state studies could provide fundamental insights into the energetic principles of neural connectivity (Yakushev et al. 2017). Further, it represents a promising approach for clarifying the organization of resting-state activity in healthy subjects and its pathological changes under neurodegenerative conditions (Spetsieris et al. 2015). The combination of multimodal resting-state acquisitions of the same subjects further involves the advantage that FDG-PET offers more robust data in terms of signal-to-noise ratio and reproducibility (Yakushev et al. 2017). Multimodal resting-state network analyses could enable a better understanding of the metabolic component of intrinsic functional network activity and the clarification of the missing link between metabolic changes and functional dysconnectivity in neurodegenerative disorders like PD.

Given the current state of knowledge, the following research questions arise:

1. Is there a spatial association between striatocortical functional connectivity changes and glucose hypometabolism in a multimodally examined PD cohort?
2. Does a direct comparison between resting-state fMRI and static FDG-PET scans reveal a spatial convergence of identified hemodynamic and metabolic networks?
3. Do PD patients show characteristic changes within defined functional resting-state networks and are changes in metabolic activity and connectivity detectable within the same network?

## 2. Results of the publications

### 2.1. Network degeneration in Parkinson's disease: multimodal imaging of nigro-striato-cortical dysfunction

The present work was published as an original article in *Brain – A Journal of Neurology*: doi:10.1093/brain/awaa019. The references to figures and tables always refer to items in the original publication (see section 7.1. and 7.2.).

In a first study, coregistered 6-[18F]fluoro-L-Dopa positron emission tomography (FDOPA-PET) scans, static FDG-PET scans and resting-state fMRI data from 42 patients with PD and 14 healthy controls of the KFO219 TP10 cohort (Deutsche Forschungsgemeinschaft 2022) were used to investigate multimodal correlates of neurodegeneration in PD in relation to motor and non-motor symptoms. With the precise localization of dopamine deficiency in PD using voxel-wise group comparisons of 6-[18F]fluoro-L-Dopa (FDOPA) uptake, the analysis enabled an investigation of the impact of impaired nigrostriatal dopaminergic transmission on striatocortical resting-state networks. Seed-to-voxel functional connectivity networks of the study-specific striatal dopaminergic deficit were obtained and compared between patients and controls. FDG uptake was compared voxel-wise on a whole brain level and mean values of FDG metabolism were extracted from clusters with significantly reduced striatocortical functional connectivity in PD patients to examine the spatial association between changes in functional connectivity and metabolic activity. Finally, the clinical relevance of multimodally observed functional changes was exploratively examined via correlation analyses.

Preprocessing and neuroimaging analyses were performed in *MATLAB* (The MathWorks, Inc. 2016) using the Statistical Parametric Mapping 12 (SPM12) (The Wellcome Centre for Human Neuroimaging 2022) or the CONN Toolbox v.17 (Whitfield-Gabrieli and Nieto-Castanon 2017). Second-level rs-fMRI analysis were performed based on a General Linear Model with Likelihood Ratio Tests allowing making decisions regarding hypotheses defined by individual contrast matrices. For group-level and between-group comparisons, statistics based on *t*-distribution were derived by the transformations of the Lambda distribution implemented in CONN (Nieto-Castanon 2020). Descriptive statistics on demographic, clinical and behavioral data and correlation analyses with neuroimaging data were performed in R (R Core Team 2018). Results were considered significant if  $p < 0.05$ . For neuroimaging analyses, correction for multiple comparisons was performed by using the family-wise error (FWE) rate.

### 2.1.1. Statement of contribution

Statistical analysis of clinical, behavioral, fMRI and FDG-PET imaging data and of associations between the findings, manuscript writing, submission and revision were performed by Marina C. Ruppert-Junck. Preprocessing of fMRI scans was performed in collaboration with Andrea Greuel.

### 2.1.2. Cohort specification

In total, 14 healthy controls ( $64.50 \pm 8.29$  years old, seven males) out of 25 and 42 PD patients ( $67.24 \pm 7.94$  years old, 26 males) out of 60 completed the trimodal neuroimaging protocol. Only those were included in the presented analyses and for clarifying associations between the processes assessed with all three modalities. There were no group differences regarding demographic and behavioral variables (see Table 1 for clinical and demographic data). PD patients were categorized into tremor-dominant and non-tremor-dominant subtypes according to previously published criteria (Eggers et al. 2011). All included PD patients were classified as having mid-stage PD with on average  $28.33 \pm 3.79$  points on the Unified Parkinson's Disease Rating Scale part III (UPDRS-III) for tremor-dominant patients and  $24.49 \pm 8.96$  points for non-tremor-dominant patients in the OFF-state of medication (12 h for levodopa, 72 h for longer acting agonists). There were no significant differences between the patient groups in terms of disease severity or level of dopaminergic medication. Twenty patients each reported left or right side of onset and two reported that there was no initial symptom lateralization (Table 1). Demographic, behavioral, and clinical data of the entire cohort can be found in Supplementary Table 1 (section 7.2.).

### 2.1.3. Dopamine depletion in the posterior putamen in Parkinson's disease

The whole brain group comparison of FDOPA scans indicated a significant dopaminergic deficit in the bilateral putamen in PD patients compared to healthy controls (Montreal Neurological Institute (MNI)-coordinates: -30, -10, 0 and 28, -6, 2,  $p_{FWE} < 0.001$  peak-level corrected, see Fig. 1C and Table 3). The exact localization confined to the posterior putamen was confirmed by an MNI structural template assuming the anterior commissure as anterior-posterior border as suggested by Helmich et al. (2010). An asymmetric dopaminergic deficit was observed in the present cohort with a slightly larger cluster in the left striatum (see Table 3).



### 2.1.4. Striatocortical hypoconnectivity in Parkinson's disease

The obtained study-specific posterior putamen cluster (see section 2.1.3.) comprising the dopamine-deficient tissue in the present PD cohort, served as seed for seed-to-voxel resting-state fMRI analysis. First, functional connectivity maps, reflecting Fisher-transformed bivariate correlation coefficients between the seed's BOLD signal time course and every other voxel in the brain, were calculated separately in healthy controls and PD patients via voxel-wise one sample *t*-tests. Group-based analysis revealed significant correlations of BOLD signal fluctuations between the bilateral putaminal seed and the precentral gyrus, supplementary motor area, cerebellum, postcentral gyrus and parts of the parietal association cortex (see Fig. 2 and Supplementary Tables 3 and 4). The subsequently performed between-group analysis in form of voxel-wise two-sample *t*-tests of putaminal functional connectivity maps with bilateral or unilateral FDOPA-defined seeds revealed a specific pattern of reduced functional connectivity for patients (patients < controls,  $p_{FWE} < 0.05$ , Fig. 2C and Table 4). In PD patients, the bilateral posterior putaminal cluster exhibited significantly reduced functional connectivity with the precentral gyrus, supplementary motor area, brainstem, superior frontal gyrus and clusters in the bilateral IPC, comprising the anterior and posterior part of the supramarginal gyrus as well as the neighboring left and right opercular cortices. In sum, most of the regions with reduced functional connectivity in PD, were part of the sensorimotor network. Additionally, the putamina showed reduced functional connectivity with the precuneus and the IPC, which both are central nodes of the DMN. Interestingly, when focusing on the left putamen, a more widespread dysconnectivity was observed in PD patients and regions with reduced functional connectivity were mainly located on the left cortical hemisphere for both putaminal seeds (not shown).

### 2.1.5. Relation of striatocortical dysconnectivity and cortical glucose metabolism

At first, whole brain comparisons of FDG uptake were performed between PD patients and healthy controls to investigate the spatial association between striatocortical functional connectivity and cortical FDG metabolism. Between-group comparisons of FDG uptake by voxel-wise two-sample *t*-tests between PD patients and healthy controls resulted in three clusters of regional hypometabolism in patients ( $p_{FWE} < 0.05$  cluster-level corrected). Hypometabolism was identified in a cortical cluster covering parts of the bilateral occipital fusiform gyri, inferior lateral occipital cortex and superior lateral occipital cortex (MNI coordinates: 26, -90, -10,  $p_{FWE} < 0.001$ , Fig. 1A and Table 2). A second cluster was found on the left hemisphere, where hypometabolism expanded into the

posterior middle temporal gyrus (MNI coordinates:  $-66, -44, -4$ ,  $p_{FWE} = 0.019$ , Fig. 1A and Table 2). The third cluster, with the most significant hypometabolism in PD patients, was located in the midbrain (MNI coordinates:  $-10, -20, -20$ ,  $p_{FWE} < 0.001$  cluster-level corrected; Fig. 1A, B and Table 2). The hypometabolic midbrain cluster partly covered the left lateral caudal substantia nigra pars compacta as identified with a probabilistic human atlas (Pauli et al. 2018).

When hypometabolic regions and areas with hypoconnectivity to the posterior putamen in PD patients were spatially overlaid, low spatial similarity was apparent. An additional analysis of mean metabolic activity of clusters with striatocortical hypoconnectivity was performed to investigate the relation between striatocortical functional connectivity changes and cortical FDG tracer uptake. In the PD group, but not in controls, a significant positive correlation was found between mean functional connectivity values and normalized FDG uptake in the right and the left IPC cluster (IPC left:  $r = 0.35$ ,  $p = 0.021$ , IPC right:  $r = 0.36$ ,  $p = 0.018$ , Fig. 3A and B, corrected for age and levodopa equivalent daily dose (LEDD)). Hence, significant reduction of striatocortical functional connectivity in PD patients with predominant akinetic-rigid symptoms was associated with concomitant changes in cortical metabolism in the IPC.

### 2.1.6. Clinical impairment and multimodally assessed network dysfunction

In an exploratory correlation analysis, the clinical relevance of the observed functional network changes was scrutinized. Firstly, functional measures of nigrostriatal integrity significantly correlated with contralateral bradykinetic symptoms quantified by the UPDRS-III right hemibody score in PD patients (FDG: Fig. 4A,  $r = -0.40$ ,  $p = 0.010$ ; FDOPA: Fig. 4B,  $r = -0.38$ ,  $p = 0.014$ ). For cortical clusters, including motor regions, which showed dysconnectivity to the posterior putamen, no significant correlation between functional connectivity values and motor impairment could be observed except for a negative linear trend between UPDRS-III right body scores and left IPC functional connectivity values (coordinates  $-68 -26 22$ , Fig. 4D,  $r = -0.31$ ,  $p = 0.053$ , corrected for age, LEDD and Mini-Mental State Examination (MMSE)). Interestingly, there was a trend towards a relationship between normalized FDG uptake values and contralateral motor impairment in this hypoconnected IPC cluster (Fig. 4E,  $r = -0.31$ ,  $p = 0.057$ , corrected for age, LEDD, MMSE and disease duration). In addition, striatocortical connectivity values of the left IPC cluster showed a positive correlation with total cognition MMSE scores in patients (Fig. 4E,  $r = 0.42$ ,  $p = 0.005$ , corrected for age, LEDD, and akinesia-rigidity-score).

### 2.2. The default mode network and cognition in Parkinson's disease: a multimodal resting-state network approach

The presented work was published as an original article in Human Brain Mapping:10.1002/hbm.25393. The references to figures and tables always refer to items in the original publication (see section 7.3. and 7.4.).

In a second study, fMRI and static FDG-PET scans from 51 PD patients ( $66.45 \pm 8.53$  years; 18 female) and 16 elderly healthy controls ( $64.63 \pm 8.33$  years; nine female) from the KFO219 TP10 cohort (Deutsche Forschungsgemeinschaft 2022) were analyzed in terms of multimodal DMN representation and concordant metabolic and hemodynamic deficits in relation to cognitive performance. The scans from 16 controls and 16 randomized PD patients who underwent both modalities (Supplementary Table S3) were fed into separate ICA for both modalities to obtain metabolic and fMRI-based resting-state networks. One DMN component per modality was identified. FDG uptake, group-level metabolic connectivity, as well as functional connectivity of multimodally defined DMN regions were compared between healthy controls, all PD patients with mild cognitive impairment (MCI) or without cognitive impairment (PD-NC), categorized after level II criteria published by the Movement Disorder Society (MDS) (Litvan et al. 2012).

Preprocessing and neuroimaging analyses were performed in *MATLAB* (The MathWorks, Inc. 2016) using the SPM12 (The Wellcome Centre for Human Neuroimaging 2022) or the CONN Toolbox v.17 (Whitfield-Gabrieli and Nieto-Castanon 2017). ICA conducted on FDG-PET data was performed in the Group ICA of fMRI toolbox (GIFT) (Translational Research in Neuroimaging & Data Science 2016). Descriptive statistics on demographic, clinical and behavioral data and correlation analyses were performed in R (R Core Team 2018). Results were considered significant if  $p < 0.05$ . For neuroimaging analyses, false-discovery rate- (FDR-) correction was applied. In parts, exploratory results with uncorrected (uncorr) p-values are presented.

#### 2.2.1. Statement of contribution

Intensity normalization of FDG-PET data, statistical analyses of clinical, behavioral and imaging data and of associations between the findings, manuscript writing, submission and revision were performed by Marina C. Ruppert-Junck. Preprocessing of rs-fMRI scans was performed in collaboration with Andrea Greuel. Calculation of standardized z-scores per cognitive domain had previously been carried out by Dr. Franziska Maier.

### 2.2.2. Cohort specification

Twelve PD patients presented with MCI and 36 exhibited normal cognitive performance. Demographic, clinical, and behavioral characteristics of all subgroups are depicted in Table 1. Healthy controls did not differ from the PD groups in terms of age and gender, but in education years, Beck's depression inventory II (BDI-II) scores and global cognition (Table 1 and 2). No significant differences in demographics and motor severity were observed between the patient groups. Significantly lower z-scores were observed for PD-MCI patients in the cognitive composite score and all domains compared to controls and PD-NC patients, except for the domains language and executive functioning, in which they only differed from control subjects (Table 2).

### 2.2.3. Spatial convergence of hemodynamic and metabolic networks

The ICA-based network identification conducted on concatenated static FDG-PET and rs-fMRI data of the same 32 subjects resulted in 5 distinct components in both modalities. The clearest visually recognizable resting-state network represented a DMN component in each modality, although some differences in spatial expansion were apparent. Individual regions were identified as parts of the functional DMN component, but not present in the metabolic component or vice versa. This was especially true for prefrontal areas, which were absent in the FDG-PET component (Figure 2). The superior frontal gyrus and juxtapositional lobule were covered by both DMN components, but only the metabolic component included the anterior cingulate gyrus and paracingulate gyrus. The bilateral parahippocampal gyri were part of the fMRI component, but not the metabolic pattern. In addition, parts of the cerebellar cortex were identified in the metabolic component, but not in the fMRI component, and the parietal cluster extended into the cuneal cortex and occipital pole in the metabolic component (Figure 2). In general, the spatial correspondence between the metabolic and the fMRI DMN component was fair (dice coefficient = 0.25). However, especially for posterior DMN regions (PC, PCC, bilateral superior lateral occipital cortex) higher correspondence was observed (dice coefficient = 0.27) (Figure 2). For the other networks identified, e.g. the motor network, less correspondence was observed between the modalities.

### 2.2.4. Metabolic activity in the default mode network in Parkinson's disease

For all 15 multimodally obtained regions of interest (ROIs) in the DMN, significant differences in the extracted mean normalized FDG uptake values were observed between the groups (Figure 3, Kruskal-Wallis test,  $p < 0.05$ , Supplementary Table S4).

Particularly, a significant trend towards an increasing metabolic deficit from healthy controls via cognitively unimpaired patients to patients with MCI was identified for all DMN regions (Figure 3, Jonckheere-Terpstra-test;  $p < 0.01$ , Supplementary Table S4). Patients differed most from healthy controls in the metabolic activity of the following regions: PC, the right posterior superior supramarginal gyrus (pSMGr), right superior lateral occipital cortex (sLOCr), right angular gyrus (AGr). Despite the significant trend, no major differences between impaired and unimpaired patients were seen for some regions which were exclusively part of the hemodynamic network (e.g. the mPFC).

### 2.2.5. Metabolic connectivity in the default mode network in Parkinson's disease

In an exploratory analysis of interregional metabolic connectivity between DMN ROIs, gradual changes were observed at a group level between healthy controls and both patient groups. Patients with normal cognition exhibited an increased metabolic connectivity between DMN regions, especially along fronto-parietal connections, which proceeded in PD-MCI. This type of changes concerned, e.g. the connection between the right superior frontal gyrus (SFG<sub>r</sub>) and the AGr. In the PD-NC group an increased metabolic connectivity between these regions was demonstrated ( $z = 2.61$ ,  $p\text{-value} = 0.009$ , Figure 4a), which was also found in PD-MCI patients compared to controls ( $z = -3.56$ ,  $p\text{-value} < 0.001$ ). In addition, PD-MCI patients showed a corresponding increase in metabolic connectivity to additional posterior DMN regions including the posterior division of the left superior supramarginal gyrus (pSMG<sub>l</sub>) ( $z = -2.13$ ,  $p\text{-value} = 0.033$ ), and the left superior lateral occipital cortex (sLOC<sub>l</sub>) ( $z = -2.03$ ,  $p\text{-value} = 0.043$ , Figure 4b). A trend towards an increased metabolic connectivity between posterior DMN regions, e.g. the AGr and LOC<sub>r</sub>, was identified in both patient groups compared to healthy controls (Figure 4a, b). Only the PD-NC group showed a significantly increased metabolic connectivity between the left parahippocampal cortex (ParaHL) and posterior regions, e.g. the left posterior supramarginal gyrus (pSMG<sub>l</sub>) ( $z = 2.57$ ,  $p\text{-value} = 0.010$ , Figure 4a, b). However, in PD-MCI, a reduced connectivity could be detected for individual connections in comparison to cognitively unimpaired patients. This concerned the following regions: right parahippocampal cortex (ParaHR) and the pSMG<sub>l</sub> ( $z = 2.48$ ,  $p\text{-value} = 0.013$ ) and left angular gyrus (AG<sub>l</sub>) ( $z = 2.01$ ,  $p\text{-value} = 0.045$ ) (Figure 4c).

### 2.2.6. Default Mode Network functional connectivity in Parkinson's disease

A separate exploratory analysis of between-group differences in interregional hemodynamic connectivity between the 15 DMN ROIs revealed primarily an increase

along fronto-parietal connections in cognitively impaired patients compared to unimpaired patients and healthy controls. PD patients without MCI showed an increased fronto-parietal functional connectivity, e.g. between the PC and the LOCI in comparison to controls (Figure 5A 1,  $p_{\text{uncorr}} = 0.041$ ). Additionally, PD-NC patients showed decreased functional connectivity between DMN regions, namely the AGr and the PCC ( $p_{\text{FDR}} = 0.013$ ), ParaHL and the left superior frontal gyrus (SFGI) ( $p_{\text{uncorr}} = 0.024$ ), and between both the AGI ( $p_{\text{uncorr}} = 0.046$ ) and the pSMGrs ( $p_{\text{uncorr}} = 0.043$ ) and the ParaHR compared to controls (Fig. 5A 1, Table 3). Additional connections with hypoconnectivity in PDNC were: SFGI and PCC ( $p_{\text{uncorr}} = 0.011$ ) or AGr ( $p_{\text{FDR}} = 0.047$ ). In PD-MCI, reduced functional connectivity patients in comparison to controls was exclusively found for the pSMGrs and SFGI ( $p_{\text{uncorr}} = 0.033$ ). In PD-MCI patients, increased functional connectivity was demonstrated between the SFGI and the PC ( $p_{\text{uncorr}} = 0.043$ ) and between the pSMGIs and SFGI ( $p_{\text{uncorr}} = 0.005$ ) as well as between the mPFC and both the AGr and SFGI in comparison to controls (Figure 5A 2,  $p_{\text{uncorr}} < 0.05$ ).

Further a comparison of ROI-based connectivity among both patient groups indicated a higher functional connectivity in PD-MCI for the following ROIs: PC, AGr, and PCC (Figure 5A 3, Table 3). Additional connections, for which a higher connectivity was observed in MCI, included the PC and ParaHL ( $p_{\text{uncorr}} = 0.013$ ), the PCC and mPFC ( $p_{\text{uncorr}} = 0.021$ ) and the AGr and the SFGI ( $p_{\text{FDR}} = 0.030$ , Figure 5A 3, Table 3). The obtained changes of increased connectivity in the PD-MCI group remained significant after controlling for UPDRS-III, disease duration and LEDD. The comparison between both patient groups revealed no significant decreases of functional connectivity among DMN regions in PD-MCI.

### 2.2.7. Default mode network hyperconnectivity and cognitive impairment

An exploratory partial correlation analysis revealed a relation between cognitive composite z-scores and functional connectivity along frontoparietal connections and among posterior DMN regions in PD patients, e.g. between the 1) PCC and AGr ( $r = -0.43$ ,  $p = 0.005$ , Figure 5b 1), when including age, sex, LEDD, UPDRS-III, disease duration and BDI-II as covariates. Visuospatial z-scores and attention domain z-scores were related to posterior DMN connectivity, e.g. between the AGr and PCC ( $r = -0.39$ ,  $p = 0.010$ ) and PC-PCC ( $r = -0.32$ ,  $p = 0.037$ ). No significant correlation was observed between motor scores or disease duration and DMN functional connectivity. Metabolic activity, especially in superior frontal and parietal DMN regions, was exclusively related to executive domain z-scores and disease severity, quantified by UPDRS-III, LEDD and disease duration.

## 3. Discussion

The current work sought to investigate the association between resting-state functional connectivity and metabolic network activity. The main aim was to scrutinize the relation between changes in both functional measures and their relevance for cognitive symptoms in PD patients. A multimodal imaging protocol including FDOPA-PET, FDG-PET and rs-fMRI was applied to a well-defined cohort to more holistically investigate network destruction in PD.

The first study opened new perspectives by combining three imaging modalities to investigate functional correlates of neurodegeneration in PD. Impaired nigrostriatal dopaminergic transmission in PD was accompanied by specific disturbances in striatocortical functional connectivity. Dysconnectivity was mainly confined to the sensorimotor network but pointing towards an additional DMN involvement. Despite low spatial convergence between whole-brain metabolic deficits and impaired striatocortical functional connectivity in PD, concomitant changes in both functional correlates were identified in the IPC. This suggests that reduced input from the striatum is accompanied by metabolic changes in the disconnected cortical areas. Lower striatocortical functional connectivity in the IPC related to global cognitive performance in PD patients. For the current work, the findings revealed first hints at 1) an association between metabolic changes and striatocortical functional connectivity in DMN regions and 2) the importance of DMN alterations for cognitive symptoms in PD.

In a second work, fMRI and static FDG-PET scans were analyzed in a data-driven, multivariate ICA approach to investigate consistency of both measures of neuronal activity in relation to cognitive symptoms in PD. A fair spatial convergence was observed between modality-specific DMN components with higher spatial convergence in parieto-occipital regions. Metabolic activity declined gradually in all DMN ROIs in PD patients with strongest metabolic deficits in the posterior DMN in PD-MCI. By integrating both modalities, first evidence for a predominant increase in frontoparietal hemodynamic and metabolic network coherency was detected in PD-NC patients compared to healthy controls and proceeded (i.e. further increased) in PD-MCI patients. Worse performance in cognitive testing was associated with increased functional connectivity along frontoparietal connections and within the posterior DMN in PD patients. For the current work, the results revealed evidence for 1) a commonly organized network structure and metabolic underpinnings of resting-state networks, particularly in the posterior DMN and 2) multimodally assessable network reorganization in PD patients with increasing cognitive decline.

#### 3.1. Dopamine deficiency is accompanied by striatocortical dysconnectivity

The observed pattern of striatocortical dysconnectivity, starting from the posterior putamina with dopamine deficiency, suggests specific involvement in the connectivity changes in PD patients. In line with the current findings, Helmich et al. (2010) reported similar putaminal hypoconnectivity in PD patients between the anatomically defined posterior putamen and mainly the sensorimotor network, including the bilateral precentral gyrus and postcentral gyrus, the supplementary motor area but also the IPC. However, the here presented integrative analyses revealed robust information on cohort-specific spatial extent of dopamine depletion and its involvement in vulnerable networks, whose progressive changes can be analyzed longitudinally in the disease course. In a recently published follow-up project by Steidel and Ruppert (2022), the association between striatal dopamine depletion and striatocortical resting-state connectivity was analyzed longitudinally using the same approach in a small subset of the current cohort who underwent a follow-up visit. The obtained results revealed longitudinal evidence for the proposed relation. In compliance with the well-described posterior-anterior gradient of dopamine deficiency (Nandhagopal et al. 2009), dopamine depletion proceeded into more anterior striatal regions at follow-up, especially the caudate nucleus (Steidel et al. 2022). The dopamine deficient caudate cluster exhibited reduced striatocortical functional connectivity at follow-up in comparison to baseline, while putaminal dopamine deficiency and functional connectivity did not differ significantly, indicating that putaminal impairment might already have reached a maximum or less changes were apparent in this striatal sub compartment (Steidel et al. 2022). The results suggest that proceeding pathophysiological changes are traceable on all three proposed level: midbrain hypometabolism proceeded and extended laterally, striatal dopamine deficiency involved additional anterior striatal clusters and striatocortical functional dysconnectivity concerned additional cortical areas at follow-up (Steidel et al. 2022). Especially anterior striatal seeds exhibited more changes at follow-up in comparison to healthy controls than at baseline in comparison to controls (Steidel et al. 2022). The results confirm the idea, raised by Helmich et al. (2010), that in the course of reorganization towards desegregated striatocortical loops in PD, there is a potentially compensatory increased coupling of the regions not yet so severely affected by dopamine deficiency. In the cohort investigated, striatal clusters that were initially spared by dopamine deficiency, showed an increased functional connectivity to a cluster in the occipito-parietal cortex at baseline compared with controls, but profoundly reduced connectivity at follow-up visit ( $13.8 \pm 4.1$  months) when they were more severely affected by dopamine depletion, as shown by FDOPA-PET comparisons between the visits (Steidel et al. 2022).



#### 3.2. Metabolic concomitant of striatocortical dysconnectivity

The first aim of the current work was to unravel whether there is a spatial convergence between impairments of striatocortical functional connectivity and metabolic changes in a multimodal PD cohort (section 1.6). The voxel-wise examination of hypometabolism in PD patients' FDG-PET revealed no direct spatial convergence with striatocortical dysconnectivity patterns (section 2.1.5.). However, the indirect correlates of midbrain degeneration detected in this way gave important impulses for the proposed model underlying PD pathophysiology with midbrain hypometabolism as the most caudally detectable correlate of nigrostriatal degeneration. The additional correlation analysis between normalized FDG uptake and striatocortical functional connectivity in clusters with putaminal hypoconnectivity showed a significant association between both measures in PD in the bilateral IPC, suggesting concomitant metabolic changes.

A previous meta-analysis has attributed hypometabolism in the IPC in PD mainly to cognitive symptoms (Albrecht et al. 2019). Further evidence for functional connectivity changes of the bilateral IPC in PD is given in a quantitative neuroimaging meta-analysis (Tahmasian et al. 2017). Interestingly, the IPC is also involved in sensory feedback processing during movement tasks (Mattingley et al. 1998) with adequate sensorimotor integration hinging considerably upon this brain area (Wang et al. 2017). This stands in agreement with the here observed association between contralateral motor impairments and global cognition quantified by MMSE scores and striatocortical connectivity of the left IPC. According to functional subdivisions defined by Wang et al. (2017), the identified IPC clusters with striatal hypoconnectivity encompass areas responsible for sensorimotor processing and default mode activity. The concurrent functional changes in the IPC and their relevance for PD symptoms imply that dysfunction of additional resting-state networks, e.g. the DMN, might result secondarily from dopamine depletion (van Eimeren et al. 2009; Wu et al. 2012). One may posit that striatocortical dysconnectivity may entrail aberrant communication within the DMN which may ultimately promote cognitive decline. From a broader point of view, the IPC could represent a link between motor and cognitive deficits in PD or at least to those subtypes with significant non-motor involvement (Selikhova et al. 2009; Eggers et al. 2012).

Together, the findings are suggestive of pathological processes targeting predefined neural networks and a putative role for dopamine depletion as conjoining element, which provokes functional and metabolic imbalance in cortical regions that form the network in healthy controls. Variability of the clinical course in different subtypes might partially depend on which non-motor networks are impaired and thereby determine susceptibility to non-motor symptoms.

#### 3.3. Metabolic and hemodynamic network convergence

The second aim of the present work was to scrutinize the spatial correspondence between the data-driven obtained spatial extend of metabolic and hemodynamic networks in the same cohort (see 1.6.). A few studies have conducted ICA-based decomposition of static FDG-PET data in healthy and diseased subjects to date. The fair spatial correspondence between hemodynamic and metabolic DMN components observed in the second study stands in accordance with a previous MR-PET hybrid scanner study which analyzed simultaneously acquired data from 22 healthy, mid-aged subjects (Savio et al. 2017). The latter study also indicated a moderate spatial convergence between metabolic and fMRI derived DMN components and similar differences between the modalities in frontal and cerebellar areas (Savio et al. 2017). In line with the identified stronger correspondence in posterior DMN regions, Biswal (2012) described the identification of a metabolic component with only posterior DMN regions. In contrast, Yakushev et al. (2013) observed the classical DMN topology in FDG-PET data with expected involvement of the prefrontal cortex by conducting a comparable ICA (GIFT, five components) in 35 mid-aged healthy subjects. Despite these differences, the comparable spatial overlap identified across different populations suggests that metabolic covariance networks can robustly be detected in the resting brain. Together the results underscore that hemodynamic networks are paralleled by covariant metabolic activity. Residual differences between both imaging modalities might result from different methodology of network identification by using static FDG-PET (one image per subject) or fMRI data (timeseries per subject). Frame selection and parameters of the PET acquisition protocol might also provoke discrepancies among studies. In addition, only a few studies included multimodal data sets of the same cohort (Savio et al. 2017).

The other identified networks showed less correspondence between the modalities. A direct comparison of obtained motor network components revealed a symmetrical subcortical PET motor network (midbrain, bilateral putamen, thalamus) and an fMRI pattern largely sparing the subcortical part. These differences in network characteristics might result from their difference in resolution for deep brain structures vs. cortical areas. Frame-wise connectivity analysis of the motor network in a subset of patients for which multiframe FDG-PET acquisitions were available (6 frames,  $n = 5$ ) provided insights concerning the dependency of tracer flooding and metabolic connectivity. The approach in these studies (bolus injection) resulted in differing metabolic connectivity between individual frames and gradual increases with tracer enrichment. This strong influence of the application method in mind, future studies should consider multiple frames or / and apply acquisition techniques with constant tracer concentration (cf. 3.7.).

#### 3.4. Correspondence between metabolic and hemodynamic network changes

The third aim of the present work was to unravel if there are metabolic equivalents of functional dysconnectivity detectable in resting-state networks with altered functional connectivity and if both measures reflect cognitive functioning in PD (section 1.6.). The obtained trend towards a progressive metabolic decline in the DMN with increasing cognitive impairment fits well with the described DMN hypometabolism in other neurodegenerative disorders, e.g. AD (Drzezga et al. 2011), which is clinically mainly characterized by progressive cognitive impairment. The identification of glucose hypometabolism in occipito-parietal and frontal regions in PD-MCI compared to patients with normal cognition is also consistent with comparable PD studies (Huang et al. 2008; Hosokai et al. 2009; Lyoo et al. 2010; Pappatà et al. 2011). In addition, the observed metabolic deficits in the lateral occipital regions of the identified network in cognitively unimpaired patients stand in accordance with the hypometabolism in the voxel-wise group-comparison of the first study (cf. section 2.1.5.). In the second study, further insights into the relationship between the reduction of glucose metabolism and network coherence were obtained: posterior DMN regions with the strongest metabolic deficits and gradual decline (PC, sLOCr, AGr, and pSMGrS), showed the strongest increases in both metabolic and functional connectivity. Therefore, the results point at a spatial convergence between degeneration on one hand and network reorganization on the other hand. It could be speculated that the metabolic decline in the DMN, observed by FDG-PET, which specifically affected all associated regions, per se is also reflected in the higher synchrony within the network, because these changes affect all regions in a comparable way and reinforce the commonalities of the regions in relation to the independent influences from outside the network. This could also be related to the hypothesis of the secondary effect of reduced striatocortical inputs revealed by the first study (cf. 3.2.), as these reflect a reduced external influence in the same sense.

A direct comparison of functional and metabolic connectivity changes of DMN regions indicated similarities between both measures of network connectivity. In particular, both modalities revealed evidence for an increased connectivity between frontal and posterior DMN regions in PD patients with or without MCI compared to control subjects. For some frontoparietal connections with hyperconnectivity in patients, e.g. the connectivity between the SFGGr and pSMGI, similar changes in metabolic connectivity were observed in PD patients with MCI compared to controls. However, no consistent changes were found for some connections. One technical reason for this could be the rough nature of metabolic connectivity due to the difference in calculating connectivity measures that distinguishes fMRI from static FDG-PET (single subject vs. group measure).

In the following, dysconnectivity results of the respective modalities are placed in the context of the respective current literature. Consistent with an enhanced metabolic coupling in the posterior cortex in PD patients compared to age-matched controls reported by Sala and colleagues (2017), an increased metabolic connectivity was found in posterior DMN regions in PD patients in the current cohort. Toussaint et al. (2012) also reported an increase in correlated metabolic activity between parietal and temporal hypometabolic regions in MCI patients with conversion to AD compared to controls. They also noticed a pronounced increase in correlation between frontal and parietal regions in MCI converters (Toussaint et al. 2012). In fMRI data, Zhan et al. (2018) also described increased functional connectivity between the PCC and the bilateral mid frontal gyri in cognitively impaired PD patients compared to unaffected ones. An increased functional correlation between the DMN and posterior cortical regions in PD patients with and without cognitive impairment compared to controls was also identified by Baggio et al. (2015). Similar to the observed association between the functional connectivity of the PC, PCC, and mPFC and objective cognition in PD patients, the authors also drew a relation to cognitive symptoms, especially visuospatial performance (Baggio et al. 2015). Notably, some fMRI studies emphasize decreased functional connectivity among DMN regions, but most of these studies examined PD patients in their ON-state (Amboni et al. 2015; Lucas-Jiménez et al. 2016) and are therefore biased by the suspected modulatory role of dopamine with decreasing effects on DMN connectivity (Conio et al. 2020).

#### 3.5. Relevance of default mode network dysfunction for cognitive impairment

Differing connectivity between groups with different degrees of cognitive impairment ultimately raises the question of the clinical implication for PD patients. An increased metabolic coupling in frontal and occipital areas, like in the present study, has been postulated as a compensatory mechanism to maintain cognitive function in PD patients (Sala et al. 2017). By contrast, the increasing functional connectivity within the posterior DMN and along fronto-parietal connections with worse cognitive functioning in PD-MCI in the present cohort supports this hypothesis, but could also represent a maladaptive response to neurodegeneration as posited by Gardini (2015). The increased coherent DMN activity in PD patients in the OFF-state reported in the current study may also reflect the inability to deactivate during cognitive tasks described by previous studies (van Eimeren et al. 2009; Ibarretxe-Bilbao et al. 2011), which has also been linked to poor cognitive performance (Gardini et al. 2015). Further studies using the test battery applied here for categorization and including patients with PD dementia as a more advanced stage are required to resolve whether hyperconnectivity represents a mechanism

contributing to cognitive decline or maintaining cognitive function. When examining DMN involvement in cognitive dysfunction in the AD spectrum, Toussaint et al. (2012) found a similar increased synchronization to break down during transition from MCI to AD.

In summary, decreased metabolic activity and increased coherent activity within posterior DMN regions might precede clinically manifest cognitive impairment. It yet remains debatable if cortical hypometabolism relates to network reorganization and striatocortical PD pathology, alike. Together with the first study's results one may speculate about dysregulations within cortical regions which partly constitute the DMN in consequence of striatocortical dysconnectivity. Additionally, posterior cortical dysfunction might be linked to degeneration of cholinergic pathways (Hilker et al. 2005; Klein et al. 2010). Future studies, combining comprehensive analyses of multiple neurotransmitter systems and directional connectivity, are needed to complete our knowledge about directionality in network dysfunction in the PD spectrum.

#### 3.6. Limitations

A limitation concerning both studies is the low number of control subjects which limits the power for identifying group differences. Additionally, imaging procedures were performed consecutively, limiting the informative value regarding simultaneity of the processes. However, the adherence of standard conventions in terms of subject instruction, scanner environment and cross-modal registration enabled a sufficient intra- and inter-subject comparability. Another critical point represents the fact that metabolic connectivity studies with static FDG-PET in the second study were restricted to group-level analysis, resulting in one correlation measure per group, in contrast to fMRI analyses, where interregional correlations were assessed on a subject level.

#### 3.7. Outlook: Dynamic FDG-PET acquisition techniques

The analysis of interregional metabolic interactions is essentially limited by the static character of commonly acquired FDG-PET data. The latter might be causative for the only moderate spatial coincidence of resting-state networks (Savio et al. 2017) (section 2.2.3). Further, reliability in covariance analysis of group data is essentially influenced by the cohorts' homogeneity, normalization of between-group effects and variability of image acquisition (Veronese et al. 2019). But there are dynamic acquisition techniques, which start to acquire repetitively in parallel with injections or use continuous tracer application (Carson et al. 1993; Villien et al. 2014). List-mode acquisition and offline reconstruction allow obtaining timeseries of glucose dynamics with this technique, which enables measures of fluctuations of glucose consumption on a single subject level

(Amend et al. 2019; Ionescu et al. 2021). Rat studies revealed region-depending dynamics of glucose consumption encoded in dynamic FDG-PET data, not covered by static FDG-PET (Wehrl et al. 2013). Particularly, constant infusion techniques allow the measurement of metabolic connectivity, independently of hemodynamic confounding effects due to constant plasma availability (Amend et al. 2019). The simultaneous application in a MR-PET hybrid system revealed a greater correspondence between dynamically assessed metabolic connectivity and functional connectivity (Jamadar et al. 2020) and first applications as a measure of cognitive functions were carried out (Voigt et al. 2022).

The approach further enables direct comparisons of the temporal and spatial course of hemodynamics and glucose consumption (Villien 2015) and thereby would enable the investigation of interregional metabolic connectivity on subject level. This could revolutionize the field of metabolic connectivity in neurodegenerative disorders, because it allows the aptitude of individual connectivity values as signature of metabolic brain activity for diagnostics, regression analyses with clinical and neuropsychological deficits or as progression marker (Sala and Perani 2019). In consequence, a subsequent study was initiated to broaden the existing competences of static FDG-PET by means of dynamic acquisition protocols in a way, which allows analyzing metabolic connectivity of a single subject level and clinicopathological correlations (Study 146/19). In the course of the study, 10 healthy controls and 10 PD patients underwent a multimodal imaging protocol consisting of sequentially performed resting-state fMRI and dynamic FDG-PET acquisitions after Villien and colleagues (2014). At the time, the present work was submitted, all 20 participants were enrolled into the self-initiated study.

#### 3.8. Conclusion

The two studies render evidence for metabolic and hemodynamic network reorganization within the sensorimotor network and the DMN in PD and highlight how multimodal resting-state studies may foster our understanding of (patho-)physiological organization of brain activity. Particularly, the second study deepened the knowledge of DMN dysfunction and its relevance for cognitive symptoms in PD, for which the first study provided initial multimodal evidence. The self-initiated study further laid the ground for multimodal characterization of metabolic and hemodynamic network changes on single-subject level and the evaluation of dynamic PET-based connectivity as metabolic network marker for neurodegenerative disorders like PD.

### 4. Summary

Research focusing on the pathophysiology of neurodegenerative disorders has undergone a fundamental shift towards a network perspective in the last decades. Besides regional aggregation of misfolded proteins and changes in cellular metabolism, accompanying changes of synaptic activity evolve and evoke dysregulation within neural circuits including remote brain regions. Modern theories of neurodegeneration propose a stereotypic pattern of these cerebral pathologies, which partly are *in vivo* accessible by multimodal neuroimaging techniques. The most often used indirect measurement of functional network integrity is resting-state functional magnetic resonance imaging, which depends on a complex interplay of hemodynamics, blood volume, and blood flow. Less is known about a potential metabolic component underlying resting-state networks in healthy brains and changes thereof in neurodegeneration and the influence of different transmitter systems. The current work therefore sought to investigate the association between functional resting-state networks and metabolic network activity and focused on metabolic consequences of nigrostriatal and striatocortical dysfunction in Parkinson's disease.

In the current work, a multimodal data set of the TP10 KFO219 cohort was analyzed regarding 1) the impact of nigrostriatal dopamine depletion on resting-state networks and 2) the relation between changes in functional connectivity and metabolic network activity. The first study addressed the subset of the KFO219 TP10 cohort who completed the trimodal imaging protocol (42 patients vs. 14 controls). Dopamine deficiency in Parkinson's patients was examined by voxel-wise comparison of 6-[<sup>18</sup>F]fluoro-L-Dopa positron emission tomography scans. Resulting clusters served as seeds for resting-state functional connectivity maps that were compared between both groups by voxel-wise *t*-tests. Metabolic activity was extracted from 2-[<sup>18</sup>F]fluoro-2-deoxy-D-glucose positron emission tomography scans for respective cortical clusters with striatocortical dysconnectivity and the relation to functional connectivity values was analyzed. In a separate study, functional and metabolic resting-state networks were obtained by performing spatial independent component analyses in a subset of the same cohort who underwent 2-[<sup>18</sup>F]fluoro-2-deoxy-D-glucose positron emission tomography and functional magnetic resonance imaging (56 vs 16) and completed neuropsychological testing. Multimodally obtained regions of interest in the default mode network were defined and metabolic activity as well as metabolic connectivity compared to functional connectivity differences between patients without or with mild cognitive impairment and healthy controls. Moreover, a third study was initiated in the context of the present work with the aim of establishing a dynamic 2-[<sup>18</sup>F]fluoro-2-deoxy-D-glucose positron

emission tomography acquisition with a constant infusion protocol for examining interregional metabolic connectivity on single subject level and enable comparable analysis of hemodynamic and metabolic fluctuations in Parkinson's disease.

In the first study, a significant association between striatocortical functional connectivity changes of the data-driven defined dopamine depleted posterior putamen and metabolic activity of the cortical target area in the inferior parietal cortex was found in Parkinson's disease. Interestingly, striatocortical connectivity of the inferior parietal cortex was associated with motor and cognitive impairment. In a second study, the multivariate approach revealed a moderate spatial convergence for the posterior default mode network in functional and metabolic data. For all multimodally obtained default mode network regions, a significant trend towards an increment of metabolic deficits from healthy controls via unimpaired patients to patients with mild cognitive impairment was identified. In addition, posterior default mode network regions with the strongest metabolic deficits and gradual decline in comparison to controls, also showed the strongest increases in both metabolic and functional connectivity compared to controls. The verification of the applicability of a constant infusion dynamic 2-[<sup>18</sup>F]fluoro-2-deoxy-D-glucose positron emission tomography protocol in Parkinson's disease patients was started in a self-initiated study, which finished the acquisition phase with 10 participants per group by the time the current work was submitted.

Together the first two studies highlight the added value of multimodal imaging in investigating human brain function and the pathophysiology of neurodegenerative disorders, in particular their great potential for identifying links between individual pathologies. The second study partly continued, and answered questions raised in response to the first study, which hinted at an involvement of default mode network regions in cognitive symptoms of Parkinson's disease and a relation between functional network degeneration and metabolic activity. The current work shows exemplary the complementarity of both measures of brain network activity and their individual significance for cognitive symptoms in Parkinson's disease. The presented work highlights how multimodal resting-state studies can provide new insights into the (patho-)physiological network organization of brain activity by confirming insights obtained by one modality and deepen our understanding of disease processes. The self-initiated study further laid the ground for multimodal characterization of metabolic and hemodynamic network changes on single-subject level and the evaluation of dynamic positron emission tomography-based connectivity as metabolic network marker for Parkinson's disease.



### 5. Zusammenfassung

Die Erforschung der Pathophysiologie neurodegenerativer Erkrankungen hat in den letzten Jahrzehnten einen grundlegenden Wandel hin zu einer Netzwerkperspektive vollzogen. Neben der regionalen Akkumulation fehlgefalteter Proteine und Veränderungen des zellulären Metabolismus kommt es zu Veränderungen der synaptischen Aktivität, die Dysregulationen in neuronalen Schaltkreisen, einschließlich entfernter Hirnregionen, hervorrufen. Moderne Theorien der Neurodegeneration postulieren eine stereotypische Ausbreitung dieser Pathologien, die teilweise mittels neurobildgebender Verfahren *in vivo* darstellbar sind. Die am häufigsten angewendete Methode zur Messung der Integrität von Ruhenetzwerken ist die funktionelle Magnetresonanztomografie, die von einem komplexen Zusammenspiel von Hämodynamik, Blutvolumen und Blutfluss abhängt. Die mögliche metabolische Komponente der Ruhenetze im gesunden Gehirn, Veränderungen dieser bei neurodegenerativen Erkrankungen sowie der Einfluss spezifischer Transmittersysteme, sind hingegen weniger erforscht. Die vorliegende Arbeit untersuchte daher die Assoziation zwischen funktionellen Ruhenetzwerken und metabolischer Aktivität und fokussierte insbesondere metabolische Konsequenzen der dopaminergen nigrostriatalen und striatokortikalen Dysfunktion bei Morbus Parkinson.

Ein multimodaler Datensatz der TP10 KFO219 Kohorte wurde daher hinsichtlich 1) des Einflusses des nigrostriatalen Dopaminmangels auf striatokortikale Ruhenetze und 2) der Beziehung zwischen Veränderungen der funktionellen Konnektivität und metabolischer Netzwerkaktivität bei der Parkinson Erkrankung analysiert. Die erste Studie untersuchte eine Subgruppe von Patient\*innen und Kontrollen mittels trimodaler Bildgebung (42 vs. 14). Anhand eines Vergleichs der 6-[<sup>18</sup>F]fluoro-L-Dopa Positronen-Emissions-Tomografie Daten wurde der Dopaminmangel der Patient\*innen lokalisiert. Die resultierenden Cluster dienten als Ausgangsvolumen für einen Vergleich der striatokortikalen Konnektivität anhand einer funktionellen Magnetresonanztomografie. Die metabolische Aktivität der kortikalen Cluster mit striatokortikaler Dyskonnektivität wurde mittels der 2-[<sup>18</sup>F]fluoro-2-deoxy-D-Glukose-Positronen-Emissions-Tomografie Daten extrahiert und deren Beziehung zu funktionellen Konnektivitätswerten untersucht. In einer separaten Studie wurden mittels Unabhängigkeitsanalysen der Subgruppe, welche eine 2-[<sup>18</sup>F]fluoro-2-deoxy-D-Glukose-Positronen-Emissions-Tomografie, eine funktionelle Magnetresonanztomografie und eine neuropsychologische Untersuchung erhalten hatte (56 vs. 16), funktionelle und metabolische Ruhenetze herausgearbeitet. Multimodal erhobene Regionen des Default-Mode Netzwerks wurden definiert und Veränderung der metabolischen Aktivität sowie der metabolischen und

funktionellen Konnektivität zwischen Gruppen mit verschiedenem kognitiven Leistungsprofil verglichen. Zudem wurde eine dritte Studie mit dem Ziel der Etablierung eines dynamischen Akquisitionsprotokolls für die Untersuchung von interregionaler metabolischer Konnektivität auf Einzelsubjektebene und vergleichbare Analysen von hämodynamischen und metabolischen Fluktuationen bei Parkinson initiiert.

In der ersten Studie wurde eine signifikante Assoziation zwischen striatokortikalen Konnektivitätsänderungen des Dopamin defizienten posterioren Putamens und der metabolischen Aktivität der kortikalen Projektionsareale im inferior parietalen Kortex bei Parkinson gefunden. Interessanterweise zeigte sich hierbei auch ein Zusammenhang der striatokortikalen Konnektivität mit der motorischen und kognitiven Beeinträchtigung der Patient\*innen in dieser Region des Default-Mode Netzwerks. In einer zweiten Studie zeigte ein multivariater Ansatz eine moderate räumliche Konvergenz für das posteriore Default-Mode Netzwerk in beiden Bildgebungsmodalitäten. Für alle multimodal herausgearbeiteten Regionen des Netzwerks wurde ein Trend hinsichtlich eines zunehmenden metabolischen Defizits mit zunehmender kognitiver Beeinträchtigung festgestellt. Außerdem zeigten posteriore Default-Mode Netzwerk Regionen mit den stärksten metabolischen Defiziten und graduellen Veränderungen im Vergleich zu Kontrollen, auch die stärksten Veränderungen in der metabolischen und funktionellen Konnektivität. Die Überprüfung der Durchführbarkeit eines dynamischen Positronen-Emissions-Tomografie Akquisitionsprotokolls mit konstanter Infusion wurde im Rahmen einer selbstinitiierten Studie begonnen, welche die Akquisitionsphase mit 10 Teilnehmer\*innen pro Gruppe zum Zeitpunkt der Einreichung erfolgreich beendete.

Gemeinsam heben beide Studien den Vorteil der multimodalen Bildgebung für die Untersuchung der Hirnfunktion und der Pathophysiologie neurodegenerativer Erkrankungen, insbesondere für Verbindungen zwischen einzelnen Pathologien, hervor. Die zweite Studie beantwortete teilweise Fragen, die aus der ersten resultierten und auf eine Relevanz des Default-Mode Netzwerks für kognitive Symptome der Parkinson Erkrankung und einen Zusammenhang zwischen funktioneller Netzwerkdegeneration und metabolischer Aktivität hinwiesen. Die vorliegende Arbeit zeigt exemplarisch die Komplementarität beider Hirnnetzwerkaktivitätsmaße und deren individuelle Bedeutung für kognitive Symptome bei Parkinson. Mit der eigens initiierten Studie konnte abschließend eine methodische Grundlage für die multimodale Charakterisierung von metabolischen und hämodynamischen Netzwerkveränderungen auf Einzelsubjektebene und die Evaluation der Konnektivität basierend auf dynamischen Positronen-Emissions-Tomografie-Daten als metabolischer Netzwerkmarker für die Parkinson Erkrankung geschaffen werden.

## References

- Albrecht, Franziska; Ballarini, Tommaso; Neumann, Jane; Schroeter, Matthias L. (2019): FDG-PET hypometabolism is more sensitive than MRI atrophy in Parkinson's disease: A whole-brain multimodal imaging meta-analysis. In *NeuroImage. Clinical* 21, p. 101594. DOI: 10.1016/j.nicl.2018.11.004.
- Amboni, Marianna; Tessitore, Alessandro; Esposito, Fabrizio; Santangelo, Gabriella; Picillo, Marina; Vitale, Carmine et al. (2015): Resting-state functional connectivity associated with mild cognitive impairment in Parkinson's disease. In *Journal of neurology* 262 (2), pp. 425–434. DOI: 10.1007/s00415-014-7591-5.
- Amend, Mario; Ionescu, Tudor M.; Di, Xin; Pichler, Bernd J.; Biswal, Bharat B.; Wehrl, Hans F. (2019): Functional resting-state brain connectivity is accompanied by dynamic correlations of application-dependent 18FFDG PET-tracer fluctuations. In *NeuroImage* 196, pp. 161–172. DOI: 10.1016/j.neuroimage.2019.04.034.
- Baggio, Hugo-Cesar; Segura, Bàrbara; Sala-Llonch, Roser; Marti, Maria-José; Valldeoriola, Francesc; Compta, Yaroslau et al. (2015): Cognitive impairment and resting-state network connectivity in Parkinson's disease. In *Human brain mapping* 36 (1), pp. 199–212. DOI: 10.1002/hbm.22622.
- Bär, Karl-Jürgen; La Cruz, Feliberto de; Schumann, Andy; Koehler, Stefanie; Sauer, Heinrich; Critchley, Hugo; Wagner, Gerd (2016): Functional connectivity and network analysis of midbrain and brainstem nuclei. In *NeuroImage* 134, pp. 53–63. DOI: 10.1016/j.neuroimage.2016.03.071.
- Beckmann, Christian F.; DeLuca, Marilena; Devlin, Joseph T.; Smith, Stephen M. (2005): Investigations into resting-state connectivity using independent component analysis. In *Philosophical transactions of the Royal Society of London. Series B, Biological sciences* 360 (1457), pp. 1001–1013. DOI: 10.1098/rstb.2005.1634.
- Biswal, Bharat; Zerrin Yetkin, F.; Haughton, Victor M.; Hyde, James S. (1995): Functional connectivity in the motor cortex of resting human brain using echo-planar mri. In *Magn. Reson. Med.* 34 (4), pp. 537–541. DOI: 10.1002/mrm.1910340409.
- Biswal, Bharat B.; Mennes, Maarten; Zuo, Xi-Nian; Gohel, Suril; Kelly, Clare; Smith, Steve M. et al. (2010): Toward discovery science of human brain function. In *Proceedings of the National Academy of Sciences of the United States of America* 107 (10), pp. 4734–4739. DOI: 10.1073/pnas.0911855107.
- Braak, Heiko; Ghebremedhin, Estifanos; Rüb, Udo; Bratzke, Hansjürgen; Del Tredici, Kelly (2004): Stages in the development of Parkinson's disease-related pathology. In *Cell and tissue research* 318 (1), pp. 121–134. DOI: 10.1007/s00441-004-0956-9.
- Buckner, Randy L.; Snyder, Abraham Z.; Shannon, Benjamin J.; LaRossa, Gina; Sachs, Rimmon; Fotenos, Anthony F. et al. (2005): Molecular, structural, and functional characterization of Alzheimer's disease: evidence for a relationship between default activity, amyloid, and memory. In *The Journal of neuroscience : the official journal of the Society for Neuroscience* 25 (34), pp. 7709–7717. DOI: 10.1523/JNEUROSCI.2177-05.2005.
- Buxton, Richard B. (2010): Interpreting oxygenation-based neuroimaging signals: the importance and the challenge of understanding brain oxygen metabolism. In *Frontiers in neuroenergetics* 2, p. 8. DOI: 10.3389/fnene.2010.00008.

- Carson, Richard E.; Channing, Michael A.; Blasberg, Ronald G.; Dunn, Bonnie B. Cohen, Robert M.; Rice, Kenner C.; and Herscovitch, Peter (1993): Comparison of Bolus and Infusion Methods for Receptor Quantitation: Application to [18F]Cyclofoxy and Positron Emission Tomography.
- Cole, David M.; Beckmann, Christian F.; Oei, Nicole Y. L.; Both, Stephanie; van Gerven, Joop M. A.; Rombouts, Serge A. R. B. (2013): Differential and distributed effects of dopamine neuromodulations on resting-state network connectivity. In *NeuroImage* 78, pp. 59–67. DOI: 10.1016/j.neuroimage.2013.04.034.
- Conio, Benedetta; Martino, Matteo; Magioncalda, Paola; Escelsior, Andrea; Inglese, Matilde; Amore, Mario; Northoff, Georg (2020): Opposite effects of dopamine and serotonin on resting-state networks: review and implications for psychiatric disorders. In *Molecular psychiatry* 25 (1), pp. 82–93. DOI: 10.1038/s41380-019-0406-4.
- DeLong, Mahlon R. (1990): Primate models of movement disorders of basal ganglia origin. In *Trends in Neurosciences* 13 (7), pp. 281–285. DOI: 10.1016/0166-2236(90)90110-V.
- Deutsche Forschungsgemeinschaft (2022): Konnektivitätsstörungen als pathologischer Link zwischen striatalen und kortikalen Auffälligkeiten bei Subtypen der Parkinson-Erkrankung. Eine longitudinale multimodale Bildgebungsstudie. Projektnummer 101434521. Available online at <https://gepris.dfg.de/gepris/projekt/233511284?context=projekt&task=showDetail&id=233511284&>, checked on 11/2/2022.
- Di, Xin; Biswal, Bharat B. (2012): Metabolic brain covariant networks as revealed by FDG-PET with reference to resting-state fMRI networks. In *Brain connectivity* 2 (5), pp. 275–283. DOI: 10.1089/brain.2012.0086.
- Drzezga, Alexander; Becker, J. Alex; van Dijk, Koene R. A.; Sreenivasan, Aishwarya; Talukdar, Tanveer; Sullivan, Caroline et al. (2011): Neuronal dysfunction and disconnection of cortical hubs in non-demented subjects with elevated amyloid burden. In *Brain : a journal of neurology* 134 (Pt 6), pp. 1635–1646. DOI: 10.1093/brain/awr066.
- Eggers, Carsten; Kahraman, Deniz; Fink, Gereon R.; Schmidt, Matthias; Timmermann, Lars (2011): Akinetic-rigid and tremor-dominant Parkinson's disease patients show different patterns of FP-CIT single photon emission computed tomography. In *Movement disorders : official journal of the Movement Disorder Society* 26 (3), pp. 416–423. DOI: 10.1002/mds.23468.
- Eggers, Carsten; Pedrosa, David J.; Kahraman, Deniz; Maier, Franziska; Lewis, Catharine J.; Fink, Gereon R. et al. (2012): Parkinson subtypes progress differently in clinical course and imaging pattern. In *PloS one* 7 (10), e46813. DOI: 10.1371/journal.pone.0046813.
- Erkkinen, Michael G.; Kim, Mee-Ohk; Geschwind, Michael D. (2018): Clinical Neurology and Epidemiology of the Major Neurodegenerative Diseases. In *Cold Spring Harbor perspectives in biology* 10 (4). DOI: 10.1101/cshperspect.a033118.
- Fox, Michael D.; Corbetta, Maurizio; Snyder, Abraham Z.; Vincent, Justin L.; Raichle, Marcus E. (2006): Spontaneous neuronal activity distinguishes human dorsal and ventral attention systems. In *Proceedings of the National Academy of Sciences* 103 (26), pp. 10046–10051. DOI: 10.1073/pnas.0604187103.

- Fox, Michael D.; Raichle, Marcus E. (2007): Spontaneous fluctuations in brain activity observed with functional magnetic resonance imaging. In *Nature reviews. Neuroscience* 8 (9), pp. 700–711. DOI: 10.1038/nrn2201.
- Gardini, Simona; Venneri, Annalena; Sambataro, Fabio; Cuetos, Fernando; Fasano, Fabrizio; Marchi, Massimo et al. (2015): Increased functional connectivity in the default mode network in mild cognitive impairment: a maladaptive compensatory mechanism associated with poor semantic memory performance. In *Journal of Alzheimer's disease : JAD* 45 (2), pp. 457–470. DOI: 10.3233/JAD-142547.
- Helmich, Rick C.; Derikx, Loes C.; Bakker, Maaïke; Scheeringa, René; Bloem, Bastiaan R.; Toni, Ivan (2010): Spatial remapping of cortico-striatal connectivity in Parkinson's disease. In *Cerebral cortex (New York, N.Y. : 1991)* 20 (5), pp. 1175–1186. DOI: 10.1093/cercor/bhp178.
- Helmich, Rick C.; Thaler, Avner; van Nuenen, Bart F. L.; Gurevich, Tanya; Mirelman, Anat; Marder, Karen S. et al. (2015): Reorganization of corticostriatal circuits in healthy G2019S LRRK2 carriers. In *Neurology* 84 (4), pp. 399–406. DOI: 10.1212/WNL.0000000000001189.
- Hilker, R.; Thomas, A. V.; Klein, J. C.; Weisenbach, S.; Kalbe, E.; Burghaus, L. et al. (2005): Dementia in Parkinson disease: functional imaging of cholinergic and dopaminergic pathways. In *Neurology* 65 (11), pp. 1716–1722. DOI: 10.1212/01.wnl.0000191154.78131.f6.
- Hoenig, Merle C.; Bischof, Gérard N.; Seemiller, Joseph; Hammes, Jochen; Kukolja, Juraj; Onur, Özgür A. et al. (2018): Networks of tau distribution in Alzheimer's disease. In *Brain : a journal of neurology* 141 (2), pp. 568–581. DOI: 10.1093/brain/awx353.
- Hosokai, Yoshiyuki; Nishio, Yoshiyuki; Hirayama, Kazumi; Takeda, Atsushi; Ishioka, Toshiyuki; Sawada, Yoichi et al. (2009): Distinct patterns of regional cerebral glucose metabolism in Parkinson's disease with and without mild cognitive impairment. In *Movement disorders : official journal of the Movement Disorder Society* 24 (6), pp. 854–862. DOI: 10.1002/mds.22444.
- Hou, Yujun; Dan, Xiuli; Babbar, Mansi; Wei, Yong; Hasselbalch, Steen G.; Croteau, Deborah L.; Bohr, Vilhelm A. (2019): Ageing as a risk factor for neurodegenerative disease. In *Nature reviews. Neurology* 15 (10), pp. 565–581. DOI: 10.1038/s41582-019-0244-7.
- Huang, C.; Mattis, P.; Perrine, K.; Brown, N.; Dhawan, V.; Eidelberg, D. (2008): Metabolic abnormalities associated with mild cognitive impairment in Parkinson disease. In *Neurology* 70 (16 Pt 2), pp. 1470–1477. DOI: 10.1212/01.wnl.0000304050.05332.9c.
- Ibarretxe-Bilbao, Naroa; Zarei, Mojtaba; Junque, Carme; Martí, Maria Jose; Segura, Barbara; Vendrell, Pere et al. (2011): Dysfunctions of cerebral networks precede recognition memory deficits in early Parkinson's disease. In *NeuroImage* 57 (2), pp. 589–597. DOI: 10.1016/j.neuroimage.2011.04.049.
- Ionescu, Tudor M.; Amend, Mario; Hafiz, Rakibul; Biswal, Bharat B.; Wehrl, Hans F.; Herfert, Kristina; Pichler, Bernd J. (2021): Elucidating the complementarity of resting-state networks derived from dynamic 18FFDG and hemodynamic fluctuations using simultaneous small-animal PET/MRI. In *NeuroImage*, p. 118045. DOI: 10.1016/j.neuroimage.2021.118045.

- Jamadar, Sharna D.; Ward, Phillip G. D.; Liang, Emma Xingwen; Orchard, Edwina R.; Chen, Zhaolin; Egan, Gary F. (2020): Metabolic and haemodynamic resting-state connectivity of the human brain: a high-temporal resolution simultaneous BOLD-fMRI and FDG-fPET multimodality study.
- Jellinger, Kurt A. (2009): Recent advances in our understanding of neurodegeneration. In *Journal of neural transmission (Vienna, Austria : 1996)* 116 (9), pp. 1111–1162. DOI: 10.1007/s00702-009-0240-y.
- Karunanayaka, Prasanna R.; Lee, Eun-Young; Lewis, Mechelle M.; Sen, Suman; Eslinger, Paul J.; Yang, Qing X.; Huang, Xuemei (2016): Default mode network differences between rigidity- and tremor-predominant Parkinson's disease. In *Cortex; a journal devoted to the study of the nervous system and behavior* 81, pp. 239–250. DOI: 10.1016/j.cortex.2016.04.021.
- Kim, Seong-Gi; Ogawa, Seiji (2012): Biophysical and physiological origins of blood oxygenation level-dependent fMRI signals. In *Journal of cerebral blood flow and metabolism : official journal of the International Society of Cerebral Blood Flow and Metabolism* 32 (7), pp. 1188–1206. DOI: 10.1038/jcbfm.2012.23.
- Klein, J. C.; Eggers, C.; Kalbe, E.; Weisenbach, S.; Hohmann, C.; Vollmar, S. et al. (2010): Neurotransmitter changes in dementia with Lewy bodies and Parkinson disease dementia in vivo. In *Neurology* 74 (11), pp. 885–892. DOI: 10.1212/WNL.0b013e3181d55f61.
- Krajcovicova, L.; Mikl, M.; Marecek, R.; Rektorova, Irena (2012): The default mode network integrity in patients with Parkinson's disease is levodopa equivalent dose-dependent. In *Journal of neural transmission (Vienna, Austria : 1996)* 119 (4), pp. 443–454. DOI: 10.1007/s00702-011-0723-5.
- Lau, Lonneke M. L. de; Breteler, Monique M. B. (2006): Epidemiology of Parkinson's disease. In *The Lancet Neurology* 5 (6), pp. 525–535. DOI: 10.1016/S1474-4422(06)70471-9.
- Litvan, Irene; Goldman, Jennifer G.; Tröster, Alexander I.; Schmand, Ben A.; Weintraub, Daniel; Petersen, Ronald C. et al. (2012): Diagnostic criteria for mild cognitive impairment in Parkinson's disease: Movement Disorder Society Task Force guidelines. In *Movement disorders : official journal of the Movement Disorder Society* 27 (3), pp. 349–356. DOI: 10.1002/mds.24893.
- Lopes, Renaud; Delmaire, Christine; Defebvre, Luc; Moonen, Anja J.; Duits, Annelien A.; Hofman, Paul et al. (2017): Cognitive phenotypes in parkinson's disease differ in terms of brain-network organization and connectivity. In *Human brain mapping* 38 (3), pp. 1604–1621. DOI: 10.1002/hbm.23474.
- Lucas-Jiménez, Olaia; Ojeda, Natalia; Peña, Javier; Díez-Cirarda, María; Cabrera-Zubizarreta, Alberto; Gómez-Esteban, Juan Carlos et al. (2016): Altered functional connectivity in the default mode network is associated with cognitive impairment and brain anatomical changes in Parkinson's disease. In *Parkinsonism & related disorders* 33, pp. 58–64. DOI: 10.1016/j.parkreldis.2016.09.012.
- Lyoo, Chul Hyung; Jeong, Yong; Ryu, Young Hoon; Rinne, Juha O.; Lee, Myung Sik (2010): Cerebral glucose metabolism of Parkinson's disease patients with mild cognitive impairment. In *European neurology* 64 (2), pp. 65–73. DOI: 10.1159/000315036.

- Mattingley, J. B.; Husain, M.; Rorden, C.; Kennard, C.; Driver, J. (1998): Motor role of human inferior parietal lobe revealed in unilateral neglect patients. In *Nature* 392 (6672), pp. 179–182. DOI: 10.1038/32413.
- McIntyre, Cameron C.; Anderson, Ross W. (2016): Deep brain stimulation mechanisms: the control of network activity via neurochemistry modulation. In *Journal of neurochemistry* 139 Suppl 1, pp. 338–345. DOI: 10.1111/jnc.13649.
- Nandhagopal, R.; Kuramoto, L.; Schulzer, M.; Mak, E.; Cragg, J.; Lee, Chong S. et al. (2009): Longitudinal progression of sporadic Parkinson's disease: a multi-tracer positron emission tomography study. In *Brain : a journal of neurology* 132 (Pt 11), pp. 2970–2979. DOI: 10.1093/brain/awp209.
- Niethammer, Martin; Eidelberg, David (2012): Metabolic brain networks in translational neurology: concepts and applications. In *Annals of neurology* 72 (5), pp. 635–647. DOI: 10.1002/ana.23631.
- Nieto-Castanon, Alfonso (2020): Handbook of functional connectivity magnetic resonance imaging methods in CONN. Boston, MA: Hilbert Press.
- Palop, Jorge J.; Chin, Jeannie; Mucke, Lennart (2006): A network dysfunction perspective on neurodegenerative diseases. In *Nature* 443 (7113), pp. 768–773.
- Pappatà, Sabina; Santangelo, G.; Aarsland, D.; Viciomini, C.; Longo, K.; Bronnick, K. et al. (2011): Mild cognitive impairment in drug-naïve patients with PD is associated with cerebral hypometabolism. In *Neurology* 77 (14), pp. 1357–1362. DOI: 10.1212/WNL.0b013e3182315259.
- Passow, Susanne; Specht, Karsten; Adamsen, Tom Christian; Biermann, Martin; Brekke, Njål; Craven, Alexander Richard et al. (2015): Default-mode network functional connectivity is closely related to metabolic activity. In *Human brain mapping* 36 (6), pp. 2027–2038. DOI: 10.1002/hbm.22753.
- Pauli, Wolfgang M.; Nili, Amanda N.; Tyszka, J. Michael (2018): A high-resolution probabilistic in vivo atlas of human subcortical brain nuclei. In *Scientific data* 5, p. 180063. DOI: 10.1038/sdata.2018.63.
- Phelps, M. E.; Huang, S. C.; Hoffman, E. J.; Selin, C.; Sokoloff, L.; Kuhl, D. E. (1979): Tomographic measurement of local cerebral glucose metabolic rate in humans with (F-18)2-fluoro-2-deoxy-D-glucose: validation of method. In *Annals of neurology* 6 (5), pp. 371–388. DOI: 10.1002/ana.410060502.
- Postuma, Ronald B.; Berg, Daniela; Stern, Matthew; Poewe, Werner; Olanow, C. Warren; Oertel, Wolfgang et al. (2015): MDS clinical diagnostic criteria for Parkinson's disease. In *Movement disorders : official journal of the Movement Disorder Society* 30 (12), pp. 1591–1601. DOI: 10.1002/mds.26424.
- R Core Team (2018): R: A Language and Environment for Statistical Computing. Edited by R Foundation for Statistical Computing. Vienna, Austria.
- Raichle, M. E.; MacLeod, A. M.; Snyder, A. Z.; Powers, W. J.; Gusnard, D. A.; Shulman, G. L. (2001): A default mode of brain function. In *Proceedings of the National Academy of Sciences* 98 (2), pp. 676–682. DOI: 10.1073/pnas.98.2.676.
- Riedl, Valentin; Bienkowska, Katarzyna; Strobel, Carola; Tahmasian, Masoud; Grimmer, Timo; Förster, Stefan et al. (2014): Local activity determines functional connectivity in the resting human brain: a simultaneous FDG-PET/fMRI study. In *The*

- Journal of neuroscience : the official journal of the Society for Neuroscience* 34 (18), pp. 6260–6266. DOI: 10.1523/JNEUROSCI.0492-14.2014.
- Sala, Arianna; Caminiti, Silvia Paola; Presotto, Luca; Premi, Enrico; Pilotto, Andrea; Turrone, Rosanna et al. (2017): Altered brain metabolic connectivity at multiscale level in early Parkinson's disease. In *Scientific reports* 7 (1), p. 4256. DOI: 10.1038/s41598-017-04102-z.
- Sala, Arianna; Perani, Daniela (2019): Brain Molecular Connectivity in Neurodegenerative Diseases: Recent Advances and New Perspectives Using Positron Emission Tomography. In *Frontiers in neuroscience* 13, p. 617. DOI: 10.3389/fnins.2019.00617.
- Savio, Alexandre; Fänger, Sarah; Tahmasian, Masoud; Rachakonda, Srinivas; Manoliu, Andrei; Sorg, Christian et al. (2017): Resting-State Networks as Simultaneously Measured with Functional MRI and PET. In *Journal of nuclear medicine : official publication, Society of Nuclear Medicine* 58 (8), pp. 1314–1317. DOI: 10.2967/jnumed.116.185835.
- Scherr, Martin; Utz, Lukas; Tahmasian, Masoud; Pasquini, Lorenzo; Grothe, Michel J.; Rauschecker, Josef P. et al. (2019): Effective connectivity in the default mode network is distinctively disrupted in Alzheimer's disease-A simultaneous resting-state FDG-PET/fMRI study. In *Human brain mapping*. DOI: 10.1002/hbm.24517.
- Seeley, William W.; Menon, Vinod; Schatzberg, Alan F.; Keller, Jennifer; Glover, Gary H.; Kenna, Heather et al. (2007): Dissociable intrinsic connectivity networks for salience processing and executive control. In *The Journal of neuroscience : the official journal of the Society for Neuroscience* 27 (9), pp. 2349–2356. DOI: 10.1523/JNEUROSCI.5587-06.2007.
- Selikhova, M.; Williams, D. R.; Kempster, P. A.; Holton, J. L.; Revesz, T.; Lees, A. J. (2009): A clinico-pathological study of subtypes in Parkinson's disease. In *Brain : a journal of neurology* 132 (Pt 11), pp. 2947–2957. DOI: 10.1093/brain/awp234.
- Shlisky, Julie; Bloom, David E.; Beaudreault, Amy R.; Tucker, Katherine L.; Keller, Heather H.; Freund-Levi, Yvonne et al. (2017): Nutritional Considerations for Healthy Aging and Reduction in Age-Related Chronic Disease. In *Advances in nutrition (Bethesda, Md.)* 8 (1), pp. 17–26. DOI: 10.3945/an.116.013474.
- Spetsieris, Phoebe G.; Ko, Ji Hyun; Tang, Chris C.; Nazem, Amir; Sako, Wataru; Peng, Shichun et al. (2015): Metabolic resting-state brain networks in health and disease. In *Proceedings of the National Academy of Sciences of the United States of America* 112 (8), pp. 2563–2568. DOI: 10.1073/pnas.1411011112.
- Spillantini, Maria Grazia; Crowther, R. Anthony; Jakes, Ross; Hasegawa, Masato; Goedert, Michel (1998):  $\alpha$ -Synuclein in filamentous inclusions of Lewy bodies from Parkinson's disease and dementia with Lewy bodies. In *Proceedings of the National Academy of Sciences* 95 (11), pp. 6469–6473.
- Steidel, Kenan; Ruppert, Marina C.; Greuel, Andrea; Tahmasian, Masoud; Maier, Franziska; Hammes, Jochen et al. (2022): Longitudinal trimodal imaging of midbrain-associated network degeneration in Parkinson's disease. In *NPJ Parkinson's disease* 8 (1), p. 79. DOI: 10.1038/s41531-022-00341-8.
- Tahmasian, Masoud; Eickhoff, Simon B.; Giehl, Kathrin; Schwartz, Frank; Herz, Damian M.; Drzezga, Alexander et al. (2017): Resting-state functional reorganization in Parkinson's disease: An activation likelihood estimation meta-analysis. In *Cortex; a*



*journal devoted to the study of the nervous system and behavior* 92, pp. 119–138. DOI: 10.1016/j.cortex.2017.03.016.

Tessitore, Alessandro; Esposito, Fabrizio; Vitale, Carmine; Santangelo, Gabriella; Amboni, Marianna; Russo, Antonio et al. (2012): Default-mode network connectivity in cognitively unimpaired patients with Parkinson disease. In *Neurology* 79 (23), pp. 2226–2232. DOI: 10.1212/WNL.0b013e31827689d6.

The MathWorks, Inc. (2016): MATLAB Version 2016b. Available online at <https://de.mathworks.com/products/matlab.html>, checked on 11/2/2022.

The Wellcome Centre for Human Neuroimaging (2022): Statistical Parametric Mapping 12. UCL Queen Square Institute of Neurology. London, UK. Available online at <https://www.fil.ion.ucl.ac.uk/spm/software/spm12/>, checked on 11/2/2022.

Tomasi, Dardo; Wang, Gene-Jack; Volkow, Nora D. (2013): Energetic cost of brain functional connectivity. In *Proceedings of the National Academy of Sciences of the United States of America* 110 (33), pp. 13642–13647. DOI: 10.1073/pnas.1303346110.

Toussaint, Paule-Joanne; Perlberg, Vincent; Bellec, Pierre; Desarnaud, Serge; Lacomblez, Lucette; Doyon, Julien et al. (2012): Resting state FDG-PET functional connectivity as an early biomarker of Alzheimer's disease using conjoint univariate and independent component analyses. In *NeuroImage* 63 (2), pp. 936–946. DOI: 10.1016/j.neuroimage.2012.03.091.

Translational Research in Neuroimaging & Data Science (2016): Group ICA of FMRI Toolbox. Available online at <https://trendscenter.org/software/gift/>, checked on 11/2/2022.

van Eimeren, Thilo; Monchi, Oury; Ballanger, Benedicte; Strafella, Antonio P. (2009): Dysfunction of the default mode network in Parkinson disease: a functional magnetic resonance imaging study. In *Archives of neurology* 66 (7), pp. 877–883. DOI: 10.1001/archneurol.2009.97.

Veronese, Mattia; Moro, Lucia; Arcolin, Marco; Dipasquale, Ottavia; Rizzo, Gaia; Expert, Paul et al. (2019): Covariance statistics and network analysis of brain PET imaging studies. In *Scientific reports* 9 (1), p. 2496. DOI: 10.1038/s41598-019-39005-8.

Villien, Marjorie (2015): Simultaneous functional imaging using fPET and fMRI. In *EJNMMI physics* 2 (Suppl 1), A66. DOI: 10.1186/2197-7364-2-S1-A66.

Villien, Marjorie; Wey, Hsiao-Ying; Mandeville, Joseph B.; Catana, Ciprian; Polimeni, Jonathan R.; Sander, Christin Y. et al. (2014): Dynamic functional imaging of brain glucose utilization using fPET-FDG. In *NeuroImage* 100, pp. 192–199. DOI: 10.1016/j.neuroimage.2014.06.025.

Vincent, J. L.; Patel, G. H.; Fox, M. D.; Snyder, A. Z.; Baker, J. T.; van Essen, D. C. et al. (2007): Intrinsic functional architecture in the anaesthetized monkey brain. In *Nature* 447 (7140), pp. 83–86. DOI: 10.1038/nature05758.

Voigt, Katharina; Liang, Emma X.; Misic, Bratislav; Ward, Phillip G. D.; Egan, Gary F.; Jamadar, Sharna D. (2022): Metabolic and functional connectivity provide unique and complementary insights into cognition-connectome relationships. In *Cerebral cortex (New York, N.Y. : 1991)*. DOI: 10.1093/cercor/bhac150.

Wang, Jiaojian; Xie, Sangma; Guo, Xin; Becker, Benjamin; Fox, Peter T.; Eickhoff, Simon B.; Jiang, Tianzi (2017): Correspondent Functional Topography of the Human Left Inferior Parietal Lobule at Rest and Under Task Revealed Using Resting-State

fMRI and Coactivation Based Parcellation. In *Human brain mapping* 38 (3), pp. 1659–1675. DOI: 10.1002/hbm.23488.

Wehrl, Hans F.; Hossain, Mosaddek; Lankes, Konrad; Liu, Chih-Chieh; Bezrukov, Ilja; Martirosian, Petros et al. (2013): Simultaneous PET-MRI reveals brain function in activated and resting state on metabolic, hemodynamic and multiple temporal scales. In *Nature medicine* 19 (9), pp. 1184–1189. DOI: 10.1038/nm.3290.

Whitfield-Gabrieli, S.; Nieto-Castanon, Alfonso (2017): CONN - functional connectivity toolbox v17. Edited by Massachusetts Institute of Technology. Gabrieli Lab. McGovern Institute for Brain Research. Available online at <http://www.nitrc.org/projects/conn>, updated on 4/25/2019.

Wu, Tao; Wang, Jue; Wang, Chaodong; Hallett, Mark; Zang, Yufeng; Wu, Xiaoli; Chan, Piu (2012): Basal ganglia circuits changes in Parkinson's disease patients. In *Neuroscience letters* 524 (1), pp. 55–59. DOI: 10.1016/j.neulet.2012.07.012.

Yakushev, Igor; Chételat, Gael; Fischer, Florian U.; Landeau, Brigitte; Bastin, Christine; Scheurich, Armin et al. (2013): Metabolic and structural connectivity within the default mode network relates to working memory performance in young healthy adults. In *NeuroImage* 79, pp. 184–190. DOI: 10.1016/j.neuroimage.2013.04.069.

Yakushev, Igor; Drzezga, Alexander; Habeck, Christian (2017): Metabolic connectivity: methods and applications. In *Current opinion in neurology* 30 (6), pp. 677–685. DOI: 10.1097/WCO.0000000000000494.

Zach, H.; Walter, U.; Liepelt-Scarfone, I.; Maetzler, W. (2017): Diagnostik des klinischen und prodromalen idiopathischen Parkinson-Syndroms : Neue Kriterien. In *Der Nervenarzt* 88 (4), pp. 356–364. DOI: 10.1007/s00115-017-0290-6.

Zhan, Zhou-Wei; Lin, Li-Zhen; Yu, Er-Han; Xin, Jia-Wei; Lin, Lin; Lin, Hai-Long et al. (2018): Abnormal resting-state functional connectivity in posterior cingulate cortex of Parkinson's disease with mild cognitive impairment and dementia. In *CNS neuroscience & therapeutics* 24 (10), pp. 897–905. DOI: 10.1111/cns.12838.

## 6. Appendix

### 6.1. Network degeneration in Parkinson's disease: Multimodal imaging of nigro-striato-cortical dysfunction

# Network degeneration in Parkinson's disease: multimodal imaging of nigro-striato-cortical dysfunction

**Marina C. Ruppert,<sup>1,2,\*</sup> Andrea Greuel,<sup>1,\*</sup> Masoud Tahmasian,<sup>3</sup> Frank Schwartz,<sup>4</sup> Sophie Stürmer,<sup>5,6</sup> Franziska Maier,<sup>7</sup> Jochen Hammes,<sup>8</sup> Marc Tittgemeyer,<sup>5,9</sup> Lars Timmermann,<sup>1,2</sup> Thilo van Eimeren,<sup>6,8,10,11</sup> Alexander Drzezga<sup>8,11,12</sup> and Carsten Eggers<sup>1,2</sup>**

\*These authors contributed equally to this work.

The spreading hypothesis of neurodegeneration assumes an expansion of neural pathologies along existing neural pathways. Multimodal neuroimaging studies have demonstrated distinct topographic patterns of cerebral pathologies in neurodegeneration. For Parkinson's disease the hypothesis so far rests largely on histopathological evidence of  $\alpha$ -synuclein spreading in a characteristic pattern and progressive nigrostriatal dopamine depletion. Functional consequences of nigrostriatal dysfunction on cortical activity remain to be elucidated. Our goal was to investigate multimodal imaging correlates of degenerative processes in Parkinson's disease by assessing dopamine depletion and its potential effect on striatocortical connectivity networks and cortical metabolism in relation to parkinsonian symptoms. We combined <sup>18</sup>F-DOPA-PET, <sup>18</sup>F-fluorodeoxyglucose (FDG)-PET and resting state functional MRI to multimodally characterize network alterations in Parkinson's disease. Forty-two patients with mild-to-moderate stage Parkinson's disease and 14 age-matched healthy control subjects underwent a multimodal imaging protocol and comprehensive clinical examination. A voxel-wise group comparison of <sup>18</sup>F-DOPA uptake identified the exact location and extent of putaminal dopamine depletion in patients. Resulting clusters were defined as seeds for a seed-to-voxel functional connectivity analysis. <sup>18</sup>F-FDG metabolism was compared between groups at a whole-brain level and uptake values were extracted from regions with reduced putaminal connectivity. To unravel associations between dopaminergic activity, striatocortical connectivity, glucose metabolism and symptom severity, correlations between normalized uptake values, seed-to-cluster  $\beta$ -values and clinical parameters were tested while controlling for age and dopaminergic medication. Aside from cortical hypometabolism, <sup>18</sup>F-FDG-PET data for the first time revealed a hypometabolic midbrain cluster in patients with Parkinson's disease that comprised caudal parts of the bilateral substantia nigra pars compacta. Putaminal dopamine synthesis capacity was significantly reduced in the bilateral posterior putamen and correlated with ipsilateral nigral <sup>18</sup>F-FDG uptake. Resting state functional MRI data indicated significantly reduced functional connectivity between the dopamine depleted putaminal seed and cortical areas primarily belonging to the sensorimotor network in patients with Parkinson's disease. In the inferior parietal cortex, hypoconnectivity in patients was significantly correlated with lower metabolism (left  $P = 0.021$ , right  $P = 0.018$ ). Of note, unilateral network alterations quantified with different modalities corresponded with contralateral motor impairments. In conclusion, our results support the hypothesis that degeneration of nigrostriatal fibres functionally impairs distinct striatocortical connections, disturbing the efficient interplay between motor processing areas and impairing motor control in patients with Parkinson's disease. The present study is the first to reveal trimodal evidence for network-dependent degeneration in Parkinson's disease by outlining the impact of functional nigrostriatal pathway impairment on striatocortical functional connectivity networks and cortical metabolism.

Received August 28, 2019. Revised November 21, 2019. Accepted December 11, 2019. Advance Access publication February 14, 2020

© The Author(s) (2020). Published by Oxford University Press on behalf of the Guarantors of Brain. All rights reserved.

For permissions, please email: journals.permissions@oup.com

- 1 Department of Neurology, University Hospital of Marburg, Germany
- 2 Center for Mind, Brain and Behavior - CMBB, Universities Marburg and Gießen, Germany
- 3 Institute of Medical Science and Technology, Shahid Beheshti University, Tehran, Iran
- 4 Department of Neurology, Hospital of the Brothers of Mercy, Trier, Germany
- 5 Max Planck Institute for Metabolism Research, Cologne, Germany
- 6 Department of Neurology, Medical Faculty and University Hospital Cologne, University Hospital Cologne, Germany
- 7 Department of Psychiatry, University Hospital Cologne, Medical Faculty, Cologne, Germany
- 8 Multimodal Neuroimaging Group, Department of Nuclear Medicine, Medical Faculty and University Hospital Cologne, University Hospital Cologne, Germany
- 9 Cluster of Excellence in Cellular Stress and Aging Associated Disease (CECAD), Cologne, Germany
- 10 Cognitive Neuroscience, Institute of Neuroscience and Medicine (INM-3), Research Center Jülich, Germany
- 11 German Center for Neurodegenerative Diseases (DZNE), Germany
- 12 Cognitive Neuroscience, Institute of Neuroscience and Medicine (INM-2), Research Center Jülich, Germany

Correspondence to: Univ-Prof. Dr Carsten Eggers

Department of Neurology

University Hospital of Marburg

Baldingerstraße

35033 Marburg

Germany

E-mail: marina.ruppert@uni-marburg.de or Andrea.greuel@med.uni-marburg.de

**Keywords:** neurodegeneration; network degeneration; Parkinson's disease; multimodal imaging

**Abbreviations:** BOLD = blood oxygen level-dependent; DMN = default mode network; FDG = fluorodeoxyglucose; IPC = inferior parietal cortex; LEDD = levodopa equivalent daily dose; MMSE = Mini-Mental State Examination; ROI = region of interest; SN(pc) = substantia nigra (pars compacta); UPDRS = Unified Parkinson's Disease Rating Scale

## Introduction

Although consequences of selective neural cell death in the substantia nigra pars compacta (SNpc) gave rise to landmark insights into Parkinson's disease pathophysiology by identifying an imbalance between motor-inhibiting and motor-promoting pathways (Kish *et al.*, 1988; Albin *et al.*, 1989; DeLong, 1990), they are not capable of clarifying the entire spectrum of parkinsonian symptoms. Therefore, a more systemic approach is needed as Parkinson's disease is a multifarious disorder, characterized by a complex pattern of progressively worsening symptoms (Obeso *et al.*, 2017). Choosing a unique methodological approach, Braak and colleagues were the first to systematically map stages of Parkinson's disease pathology based on post-mortem examination of cerebral  $\alpha$ -synuclein distribution. As the SNpc is not affected until Braak stage 3 and neocortical areas become involved much later, their observations are suggestive of an ascending progressive pathology (Braak *et al.*, 2003).

Based on the assumption that neural pathologies spread out along existing networks, the network degeneration hypothesis of neurodegeneration has moved into the focus of research in the past decade (Palop *et al.*, 2006; Seeley *et al.*, 2009; Tahmasian *et al.*, 2016; Drzezga, 2018; Bischof *et al.*, 2019). Multimodal neuroimaging studies have reported a spatial coincidence between patterns of brain atrophy in several forms of dementia and functional network organization in healthy subjects (Seeley *et al.*, 2009). Accumulating evidence suggests a distinct topographic

aggregation of molecular, structural and functional abnormalities in Alzheimer's disease (Bischof *et al.*, 2016; Dronse *et al.*, 2017), preferentially detectable within specific brain networks (Buckner *et al.*, 2005; Zhou *et al.*, 2012; Hoenig *et al.*, 2018). More precisely, disturbances in functional connectivity were found to arise at important densely connected network 'hubs' (Drzezga *et al.*, 2011), which also have been reported to exhibit a higher tau and amyloid burden (Buckner *et al.*, 2009; Cope *et al.*, 2018).

Unfortunately, because of the lack of reliable  $\alpha$ -synuclein tracers, functional neuroimaging techniques are not capable of specifically tracing  $\alpha$ -synuclein distribution in the living human Parkinson's brain. However, in contrast to histopathological studies, functional neuroimaging allows longitudinal monitoring of cerebral pathologies, which may reflect indirect functional correlates of selective neural cell death and unravel disease mechanisms implicated in aetiology and disease progression (Politis, 2014; Pagano *et al.*, 2016). Using  $^{18}\text{F}$ -fluorodeoxyglucose (FDG)-PET, a metabolic spatial covariance pattern, the Parkinson's disease-related pattern, has been repeatedly validated in populations of patients with Parkinson's disease (Schindlbeck and Eidelberg, 2018). It is characterized by increased activity in pallidothalamic, pontocerebellar and primary motor regions, and reduced activity in pre-motor cortex, supplementary motor and parietal association areas (Niethammer and Eidelberg, 2012).

Dopaminergic deficits in Parkinson's disease can reliably be assessed *in vivo* by  $^{18}\text{F}$ -DOPA-PET and typically are most severe in the posterior putamen (Sawle *et al.*, 1994).

Despite their high sensitivity for diagnosis, no first-line diagnostic neuroimaging tool has been established for clinical practice; metabolic and dopaminergic imaging are still considered as adjuvant tools (Politis, 2014).

In Parkinson's disease, denervation of striatal structures—mainly the putamen—and consequential neurochemical alterations in the basal ganglia are hypothesized to impair functional integrity of remote brain regions, which may be involved in motor symptoms (Wu *et al.*, 2009). In accordance with known patterns of neural degeneration within the basal ganglia, dysfunctional resting activity of the posterior putamen is hypothesized to underlie motor abnormalities seen in Parkinson's disease (Hacker *et al.*, 2012). There is also growing interest in dysfunctional connectivity that extends beyond the sensorimotor network, affecting e.g. the default mode network (DMN), as possible correlates of non-motor symptoms, including cognitive impairment (Prodoehl *et al.*, 2014). Functional network alterations in resting state functional MRI in Parkinson's disease have been analysed with different methodological approaches, including seed-based analysis (Helmich *et al.*, 2010; Prodoehl *et al.*, 2014; Tahmasian *et al.*, 2015a, 2017; Mohan *et al.*, 2016) or multivariate network approaches (Ghasemi and Mahloojifar, 2013; Cerasa *et al.*, 2016; Vo *et al.*, 2017; Ehgoetz Martens *et al.*, 2018). For instance, a functional connectivity equivalent of the Parkinson's disease-related pattern was recently detected using independent component analysis (Vo *et al.*, 2017), highlighting the capability of resting state functional MRI to unravel pathological correlates of motor dysfunction and non-motor symptoms (Schindlbeck and Eidelberg, 2018).

Cross-modal inspection of cerebral pathologies identified by different imaging methods in the same subjects holds the potential to uncover pathophysiological mechanisms and topographic overlaps of different degenerative processes (Drzezga *et al.*, 2011; Bischof *et al.*, 2016; Hoenig *et al.*, 2018). Associations between different cerebral pathological features identified by functional imaging in Parkinson's disease have not been thoroughly examined so far and therefore are poorly understood. In particular, the extent to which topographically preceding pathologies such as nigral degeneration and putaminal dopamine depletion affect cortical abnormalities and their putative effect on parkinsonian symptoms remains to be elucidated to clarify if network degeneration is at play and pave the way for developing multimodal imaging markers as diagnostic and progression tracking tools.

## Materials and methods

### Subject inclusion and clinical assessment

After declaring informed consent in conformation with the Declaration of Helsinki and according to the institutional guidelines of the local ethics committee (ethical clearance number EK12-265), 25 healthy controls and 60 patients with

idiopathic Parkinson's disease, diagnosed according to the UK Brain Bank criteria, were included. Subjects were recruited via the neurological outpatient clinic at the University Hospital of Cologne and associated neurological practices. Healthy control subjects were reached by advertising. For PET imaging, the Federal Bureau for Radiation gave permission to apply radiation in patients and healthy controls. Exclusion criteria were age <40 years, suspected atypical parkinsonian syndromes, advanced parkinsonism [i.e. Hoehn and Yahr stage >3 (Hoehn and Yahr, 1967)], dementia, CNS diseases other than Parkinson's disease, and any safety concerns for MRI scanning. Dementia was excluded according to criteria published by the Movement Disorder Society by using a neuropsychological test battery and an assessment of the patient's ability to manage daily life (Emre *et al.*, 2007). Global cognitive screening was performed using the Mini-Mental State Examination (MMSE) (Folstein *et al.*, 1975). Functional, anatomical and clinical data were collected at the Max Planck institute for Metabolism Research Cologne and the University Hospital Cologne, Department of Neurology. MRI images were acquired from all subjects, while limited numbers of subjects were available for PET imaging (Table 1). Levodopa-equivalent daily dose (LEDD) was calculated for total antiparkinsonian medication and separately for dopamine agonists based on standard conventions (Tomlinson *et al.*, 2010). Clinical examination and functional imaging were carried out in the OFF state, defined as a 12-h period without dopaminergic medication (Langston *et al.*, 1992) (72 h in cases of dopamine agonists). Disease severity was quantified by the Unified Parkinson's Disease Rating Scale (UPDRS) part III (Fahn *et al.*, 1987). Subscores for akinesia-rigidity were calculated for the whole body and left/right hemibody from subsets of UPDRS-III items (Supplementary material). Subdivision of patients into tremor-dominant and non-tremor-dominant subtypes was performed according to strict criteria as previously described (Eggers *et al.*, 2011) (Supplementary material).

### Image acquisition and analysis

#### <sup>18</sup>F-FDG- and <sup>18</sup>F-DOPA-PET

All PET scans were acquired on an ECAT HRRT-PET-Scanner (CTI) at the Max-Planck-Institute for Metabolism Research in Cologne. Both <sup>18</sup>F-FDG- and <sup>18</sup>F-DOPA-PET were performed within a 2-day interval, each in the morning after overnight fasting and OFF dopaminergic medication. In case of <sup>18</sup>F-DOPA, 100 mg of carbidopa was administered 1 h before tracer injection. Otherwise, except for scan duration, protocols were identical for both PET scans, as follows. Under standardized conditions (dimmed light, closed eyes, quiet room) subjects were positioned along the kantho-meatal line. Following a transmission scan, 185 MBq of the radioligand was injected intravenously and tomographic images were acquired in a dynamic PET scan (60 min for <sup>18</sup>F-FDG and 90 min for <sup>18</sup>F-DOPA). Using camera-specific filters, PET data were corrected for attenuation and scattered radiation, and reconstructed to 207 slices with a 256 × 256 matrix and 1.22 mm voxel size, creating one frame per 10 min. Frames were realigned for motion correction by rigid-body transformation and frames numbered three to six (<sup>18</sup>F-FDG) or four to nine (<sup>18</sup>F-DOPA) were averaged into one for further analysis.



**Table 1 Subject characteristics and clinical data**

Demographic and behavioural data: subjects with all imaging modalities				
	Healthy controls	Parkinson's disease	P-value	Test statistic
<i>n</i>	14	42 <sup>a</sup>	-	-
Gender male / female	7 / 7	26 / 16	0.43	$\chi^2 = 0.61$
Age, years	64.50 ± 8.29	67.24 ± 7.94	0.27	<i>t</i> = 1.11
MMSE	28.86 ± 1.03	28.36 ± 1.85	0.54	<i>W</i> = 262
Clinical characteristics: Parkinson's disease patients by subtype				
	Non-TD subtype	TD subtype	P-value	Test statistic
<i>n</i>	39	3	-	-
Disease duration, years	4.49 ± 3.42	3.17 ± 2.36	0.71	<i>W</i> = 66.5
UPDRS III off	24.49 ± 8.96	28.33 ± 3.79	0.21	<i>W</i> = 32.5
Total score				
UPDRS III off	10.51 ± 5.08	4.67 ± 0.58	0.03	<i>W</i> = 103
AR score				
UPDRS III off	9.26 ± 4.22	11.67 ± 3.51	0.26	<i>W</i> = 35
Right body score				
UPDRS III off	9.23 ± 4.54	13.00 ± 5.00	0.18	<i>W</i> = 30.5
Left body score				
UPDRS III off	8.41 ± 3.45	6.67 ± 2.08	0.31	<i>W</i> = 79.5
Right body non-tremor score				
UPDRS III off	8.36 ± 3.86	10.00 ± 4.36	0.46	<i>W</i> = 43
Left body non-tremor score				
Hoehn and Yahr	2.31 ± 0.37	2.17 ± 0.29	0.59	<i>W</i> = 69
LEDD, mg	433.82 ± 236.45	401.67 ± 152.51	0.81	<i>W</i> = 64
LEDD <sub>A</sub> , mg	127.37 ± 96.96	110.00 ± 127.67	0.77	<i>W</i> = 65
Side of onset L / R / equal	19 / 18 / 2	1 / 2 / 0	1 <sup>b</sup>	$\chi^2 = 0.00^b$

Clinical characteristics (mean ± SD) are summarized in the observed groups. Between-group differences were analysed using Mann-Whitney U-test, Student's *t*-test or in the case of dichotomous variables by  $\chi^2$  test.

<sup>a</sup>Only 42 because one subject did not undergo both PET acquisitions.

<sup>b</sup>Direct comparison of side-of-onset right versus side of onset left group in both subtypes using an approximate binominal test.

AR = akinetic-rigid; L = left; LEDD<sub>A</sub> = Levodopa equivalent daily dose for dopamine agonists; R = right; TD = tremor-dominant.

Averaged PET images were co-registered to the subject's blood oxygen level-dependent (BOLD)-weighted MRI data, stereotactically normalized by non-linear registration to an established <sup>18</sup>F-FDG (Della Rosa *et al.*, 2014) or <sup>18</sup>F-DOPA-PET template (García-Gómez *et al.*, 2013) in Montreal Neurological Institute (MNI) standard space and spatially filtered with a 6 mm full-width at half-maximum (FWHM) Gaussian smoothing kernel using SPM12 (www.fil.ion.ucl.ac.uk/spm/software/spm12).

A group comparison of <sup>18</sup>F-DOPA scans was conducted in SPM12 using the voxel-wise two sample *t*-test with default parameters (threshold masking, proportional scaling), applying a family-wise error (FWE) corrected peak-level threshold of *P* < 0.05, to define the study-specific location of most severe dopamine depletion in Parkinson's disease patients. The resulting clusters were saved as binary masks to enable cross-modality comparisons. These masks were later imported into the Conn toolbox (Whitfield-Gabrieli and Nieto-Castanon, 2012) and used as seed region of interest for evaluating how resting state functional connectivity is affected by dopamine depletion in striatal regions in Parkinson's disease patients. To assess individual regional <sup>18</sup>F-DOPA uptake, mean values were exported from significant clusters using the ROI SPM toolbox MarsBaR (Brett *et al.*, 2002).

The same procedure was followed to evaluate group differences in <sup>18</sup>F-FDG uptake. Following a whole-brain two-sample

*t*-test, clusters where metabolism was significantly reduced in Parkinson's disease were saved as masks and normalized regional uptake values extracted for each subject and region of interest.

## Resting state functional MRI

Acquisition of MRI data was performed on a 3.0 T Siemens Magnetom Prisma using the software system syngo MR D13D (Siemens). Acquisition parameters for T<sub>1</sub>-weighted structural images were as follows: repetition time = 2300 ms, echo time = 2.32 ms, flip angle = 8°, field of view = 230 mm, slice thickness = 0.90 mm, voxel size = 0.9 × 0.9 × 0.9 mm, number of slices = 192. MRIs sensitive to changes in BOLD signal levels were obtained via a gradient-echo echo-planar imaging sequence (EPI) in interleaved acquisition mode. The slice thickness was 2 mm, field of view was 208 mm and the voxel size of functional data was 2.0 × 2.0 × 2.0 mm. Each brain volume comprised 72 axial slices, and each functional run contained 617 acquisition time points at a repetition time of 776 ms. Other technical parameters included echo time = 37.4 ms and flip angle = 55°.

All necessary preprocessing steps and resting state functional connectivity analysis of functional MRI data were performed using SPM12 and the SPM toolbox Conn v17 (Whitfield-

Gabrieli and Nieto-Castanon, 2017). The sequence of operations that was applied to co-registered structural and functional MRI data essentially followed the default preprocessing pipeline implemented in Conn. It included spatial realignment, outlier detection for correction of motion artefacts, direct segmentation and normalization to MNI space, spatial smoothing with a 5 mm FWHM 3D Gaussian filter, denoising [temporal band-pass filtering (0.01–0.1)], linear detrending and further reduction of physiological noise by anatomical component-based noise correction (aCompCor) (Behzadi *et al.*, 2007).

## Resting state functional connectivity analysis

In seed-based resting state functional connectivity analysis, correlation coefficients were calculated between the mean time course of a predefined seed region of interest and the time course of all other voxels (or predefined target regions of interest) in a first-level analysis using bivariate correlation (Whitfield-Gabrieli and Nieto-Castanon, 2012). In the second-level analysis, correlation coefficients obtained in the first-level analysis were converted into normally distributed scores using Fisher's transformation. Fisher transformed correlation coefficients were included as dependent variables to test for statistically significant correlations between the seed region of interest and other voxels within groups, as well as to identify significant differences in connectivity between groups by performing *t*-tests. The threshold for significance was set to  $P < 0.05$  FWE cluster-level corrected. In cortical regions where functional connectivity was altered in Parkinson's disease, individual seed-to-region of interest (ROI) correlation coefficients ( $\beta$ -values) were extracted for cross-modality analysis.

## Cross-modality correlation analysis

Statistical analyses of cross-modality correlations were performed using R [R-project (R Core Team, 2018)]. Correlations between normalized regional  $^{18}\text{F}$ -FDG and putaminal  $^{18}\text{F}$ -DOPA uptake, ROI-to-ROI  $\beta$ -values, as well as between imaging modalities and clinical variables, were calculated using Pearson correlation. For between-group analysis and cross-modality correlation analysis only subjects who underwent all imaging modalities were included (Table 1). As dopaminergic and glucose metabolism are known to critically depend on age and functional connectivity is influenced by dopaminergic medication (Tahmasian *et al.*, 2015a), even in the OFF state, age and LEDD were included as covariates in partial correlation analyses. Additionally, correlations with motor scores were corrected for MMSE and vice versa to separately assess the influence of motor and cognitive symptoms. We distinguished between tremor-dominant and non-tremor-dominant patients when performing correlations with UPDRS-III ratings and subscores. As indicated in corresponding figures, results were considered significant for  $P < 0.05$ .

## Data availability

The dataset generated and analysed during the present study will be made available from the corresponding author on reasonable request.

# Results

## Subject characteristics

In total, 42 patients with Parkinson's disease ( $67.24 \pm 7.94$  years old, 26 males) and 14 healthy controls ( $64.50 \pm 8.29$  years old, seven males) were available for all imaging modalities; hence only these were considered for clarifying associations between modalities (see Table 1 for clinical and demographic data). Only three of the patients with Parkinson's disease were classified as tremor-dominant. Tremor-dominant patients scored on average  $28.33 \pm 3.79$  on the UPDRS-III and the mean Hoehn and Yahr score was  $2.17 \pm 0.29$ . Non-tremor-dominant patients scored  $24.49 \pm 8.96$  on the UPDRS-III and the mean Hoehn and Yahr score was  $2.31 \pm 0.37$ . Left versus right side of onset was equally distributed in the present cohort. All participating Parkinson's disease patients received dopaminergic medication. Corresponding data for all subjects can be found in Supplementary Table 1.

## Nigral hypometabolism and concomitant putaminal dopamine depletion

Voxel-wise group comparison of cerebral  $^{18}\text{F}$ -FDG uptake in patients with Parkinson's disease and healthy controls revealed three clusters of regional hypometabolism in patients ( $P < 0.05$  FWE cluster-level corrected). Activity was reduced in a cortical cluster that primarily comprised parts of the bilateral occipital fusiform gyri, inferior lateral occipital cortex and superior lateral occipital cortex (MNI coordinates: 26, −90, −10,  $P < 0.001$  FWE cluster-level corrected; Fig. 1A and Table 2). On the left hemisphere, hypometabolism expanded into the posterior middle temporal gyrus (MNI coordinates: −66, −44, −4,  $P = 0.019$  FWE cluster-level corrected; Fig. 1A and Table 2).

Aside from regions mentioned in the Parkinson's disease-related pattern, Parkinson's disease patients also exhibited significantly reduced  $^{18}\text{F}$ -FDG metabolism in the midbrain (MNI coordinates: −10, −20, −20,  $P < 0.001$  FWE cluster-level corrected; Fig. 1A, B and Table 2), which has never been reported in another Parkinson's disease cohort. The midbrain cluster included the left lateral caudal SNpc as identified with a probabilistic human *in vivo* atlas (Pauli *et al.*, 2018). This finding was also mentioned in a separate study by our group, which analysed the same PET dataset in a different context (Glaab *et al.*, 2019).

Nigrostriatal fibre degeneration and consequential reduction of dopaminergic terminals typically first and most severely affect the posterior putamen in Parkinson's disease (Kish *et al.*, 1988). In terms of network degeneration, reduced dopaminergic transmission can be understood as the second stage at which the neurodegenerative process can be assessed by functional brain imaging.  $^{18}\text{F}$ -DOPA PET scans were used to determine the exact location and



## Hypometabolism and dopamine depletion in Parkinson's disease (Patients &lt; controls)

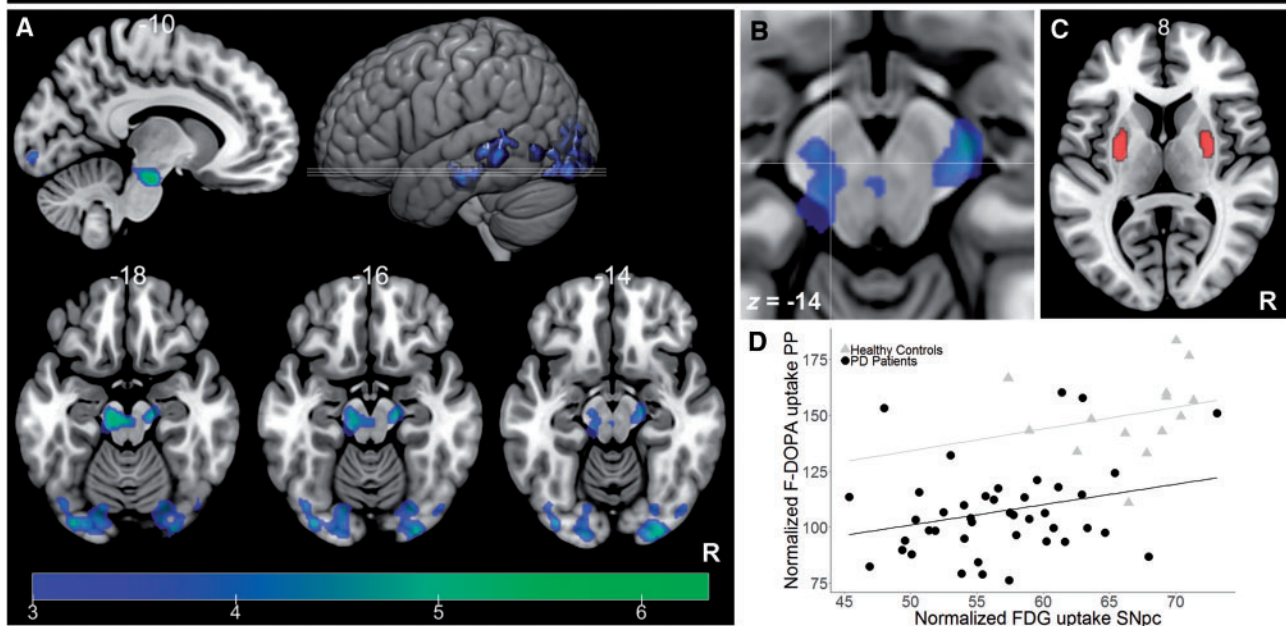


**Figure 1** Between-group differences in  $^{18}\text{F}$ -FDG metabolism and  $^{18}\text{F}$ -DOPA uptake. **(A)** Parkinson's disease patients exhibited a significantly reduced  $^{18}\text{F}$ -FDG metabolism in a midbrain cluster spanning the lateral caudal part of the SN as well as in the bilateral occipital and left temporal cortex (FWE cluster level-corrected  $P < 0.05$ ). Cortical regions that showed significant hypometabolism included the right and left occipital fusiform gyri (r OFusG, l OFusG), the right and left inferior occipital gyri (l iLOC, r iLOC) and the left middle temporal gyrus (pMTG). Colour bar indicates T-values and number on slices represent z-coordinates for axial slices or x-coordinates for sagittal slices. **(B)** Detailed display of the hypometabolic midbrain cluster, overlaid on anatomical MNI152 template. Crosshairs indicate the MNI coordinates: -10, -20, -14. **(C)** Spatial distribution of voxels exhibiting between-group differences in  $^{18}\text{F}$ -DOPA uptake overlaid on the MNI152 template. Parkinson's disease patients showed significantly reduced dopamine synthesis capacity in the bilateral posterior putamen (PP) (FWE-peak-level-corrected  $P < 0.001$ ). **(D)** Partial correlation analysis between nigral  $^{18}\text{F}$ -FDG metabolism (left) and ipsilateral putaminal  $^{18}\text{F}$ -DOPA uptake. A significant correlation was observed between normalized nigral metabolic activity (left) and ipsilateral, normalized putaminal  $^{18}\text{F}$ -DOPA uptake in patients (Pearson correlation:  $r = 0.31$ ,  $P = 0.041$  corrected for age and LEDD), but not in healthy controls ( $r = 0.25$ ,  $P = 0.383$ , corrected for age). PD = Parkinson's disease.

extent of reduced dopaminergic projections in the present cohort by whole-brain group comparison.  $^{18}\text{F}$ -DOPA uptake was significantly reduced in the bilateral putamen in Parkinson's disease patients (MNI coordinates: -30, -10, 0 and 28, -6, 2,  $P < 0.001$  FWE-peak-level corrected; Fig. 1C and Table 3). Both clusters were found to be mainly restricted to the posterior putamen when overlaid on an MNI152 structural template (Fig. 1C), using the anterior commissure as the antero-posterior border as suggested by Helmich *et al.* (2010). Dopamine depletion was asymmetrical in the current study cohort, with the left hemisphere being more affected (Table 3).

The relation between observed metabolic changes in the SNpc and putaminal dopamine depletion was analysed to verify the association between degenerative processes along the nigrostriatal pathway in patients with Parkinson's disease. Normalized  $^{18}\text{F}$ -FDG uptake values exported from the nigral cluster, where patients exhibited the most significantly reduced metabolism ( $P < 0.05$  FWE peak level correction), showed a significant positive correlation with normalized  $^{18}\text{F}$ -DOPA uptake values of putaminal peak

coordinates in patients with Parkinson's disease ( $r = 0.31$ ,  $P = 0.041$ ; Fig. 1D) when corrected for age and LEDD, but not in healthy controls ( $r = 0.25$ ,  $P = 0.383$ ; Fig. 1D). This linear relation between the most significant PET findings indicated that putaminal  $^{18}\text{F}$ -DOPA uptake drops with decreasing nigral  $^{18}\text{F}$ -FDG accumulation. Interestingly, both cerebral pathologies were primarily left-sided, with more profoundly reduced  $^{18}\text{F}$ -FDG uptake in the left mid-brain (Fig. 1B) and higher dopamine depletion in the left putamen (Fig. 1C and Table 3), suggesting a similarly asymmetrical pathology in SNpc and striatum.

Nigrostriatal pathway disruption was further analysed with ROI-to-ROI resting state functional connectivity between the midbrain cluster, in which patients with Parkinson's disease showed significantly reduced  $^{18}\text{F}$ -FDG metabolism and putaminal clusters where dopamine deficiency was most severe. Functional connectivity was significantly reduced between the hypometabolic SNpc cluster and the bilateral posterior putamen region of interest in patients compared to healthy controls [ $P = 0.043$  false-discovery-rate (FDR)-seed-level corrected; Supplementary

**Table 2 Hypometabolic clusters in Parkinson's disease patients (FWE cluster level  $P < 0.05$ )**

Region	Side	Size, voxel	x	y	z	T-value	FWE-corrected P-value
Brainstem	Left, right	455	−10	−20	−20	6.33	<0.001
OFusG	Left, right	2058	26	−90	−10	5.82	<0.001
iLOC	Left, right						
sLOC	Right						
pMTG	Left	188	−66	−44	−4	5.40	0.019

Height threshold = 3.25, extent threshold = 180 voxels

iLOC = inferior lateral occipital cortex; L = left; OFusG = occipital fusiform gyrus; pMTG = posterior middle temporal gyrus; R = right; sLOC = superior lateral occipital cortex.

**Table 3 Dopamine depleted clusters in patients with Parkinson's disease**

Region	Hemisphere	Size, voxels	x	y	z	T-value	FWE-corrected P-value
Putamen	Left	302	−30	−10	0	7.82	<0.001
Putamen	Right	204	28	−6	2	6.83	<0.001

Height threshold = 5.1

Characteristics of clusters in which patients exhibited significantly reduced putaminal  $^{18}\text{F}$ -DOPA uptake.

Table 2]. These findings were validated in the same cohort with atlas-defined regions of interest, using the putamen and brainstem masks included in the Conn toolbox (FSL Harvard-Oxford atlas). When the predefined brainstem region of interest was used as seed mask, significantly reduced connectivity was evident between the brainstem and the right putamen ( $P = 0.011$  FDR-seed-level corrected; Supplementary Table 2) as well as between the brainstem and both unilateral or bilateral cohort-specific posterior putaminal target regions of interest in patients compared to controls (posterior putamen left:  $P = 0.019$ , posterior putamen right:  $P = 0.003$ , posterior putamen bilateral:  $P = 0.003$ ; Supplementary Table 2).

## Putaminal resting state functional connectivity networks in healthy controls and Parkinson's disease patients

The study-specific bilateral posterior putamen cluster (Fig. 1C) was used as the seed region of interest for striatocortical functional connectivity analysis. Seed-to-voxel connectivity was first assessed separately in healthy controls and Parkinson's disease patients in a one sample  $t$ -test. In both groups, significant correlations of BOLD signal fluctuations were found between the bilateral putaminal seed region of interest and regions primarily belonging to the sensorimotor network, including the precentral gyrus, supplementary motor area, cerebellum, postcentral gyrus and parts of the parietal association cortex (Fig. 2 and Supplementary Tables 3 and 4). Visual comparison of patients' and controls' putaminal connectivity networks suggested several group differences (*cf.* Fig. 2A and B), e.g. functional correlation between the posterior putamen seed

region of interest and the precentral gyrus appeared lower in Parkinson's disease. Interestingly, the bilateral putaminal seed was functionally correlated with larger parts of the cerebellum, primarily the anterior cerebellar lobe, in Parkinson's disease patients (bilateral cerebellar lobules 4–6: patients: 1681 voxels; controls: 479 + 520 voxels; Fig. 2A, B and Supplementary Tables 3 and 4).

## Striatocortical hypoconnectivity is accompanied by reduced cortical metabolism

Between-group analysis of seed-to-voxel resting state functional connectivity networks was performed using bilateral or unilateral  $^{18}\text{F}$ -DOPA-defined seed regions of interest and a two-sample  $t$ -test (patients < controls,  $P < 0.05$  cluster-level FWE-corrected). Patients with Parkinson's disease exhibited significantly less functional connectivity between the dopamine depleted bilateral posterior putamen and several sensorimotor areas (Fig. 2C and Table 4). Cortical regions with reduced connectivity were identified using the Harvard-Oxford atlas. They primarily included the precentral gyrus, supplementary motor area, superior frontal gyrus and large clusters in the bilateral inferior parietal cortex (IPC), comprising the anterior and posterior part of the supramarginal gyrus as well as the neighbouring left and right opercular cortices (Fig. 2C and Table 4). Additionally, putaminal hypoconnectivity was detected in the bilateral precuneus, a central node of the DMN, and the brainstem. Interestingly, regardless of seed region of interest lateralization the most striking effects of reduced functional connectivity were located on the left cortical hemisphere and more severely when focusing on the left putamen (not shown). However, between-seed contrasts

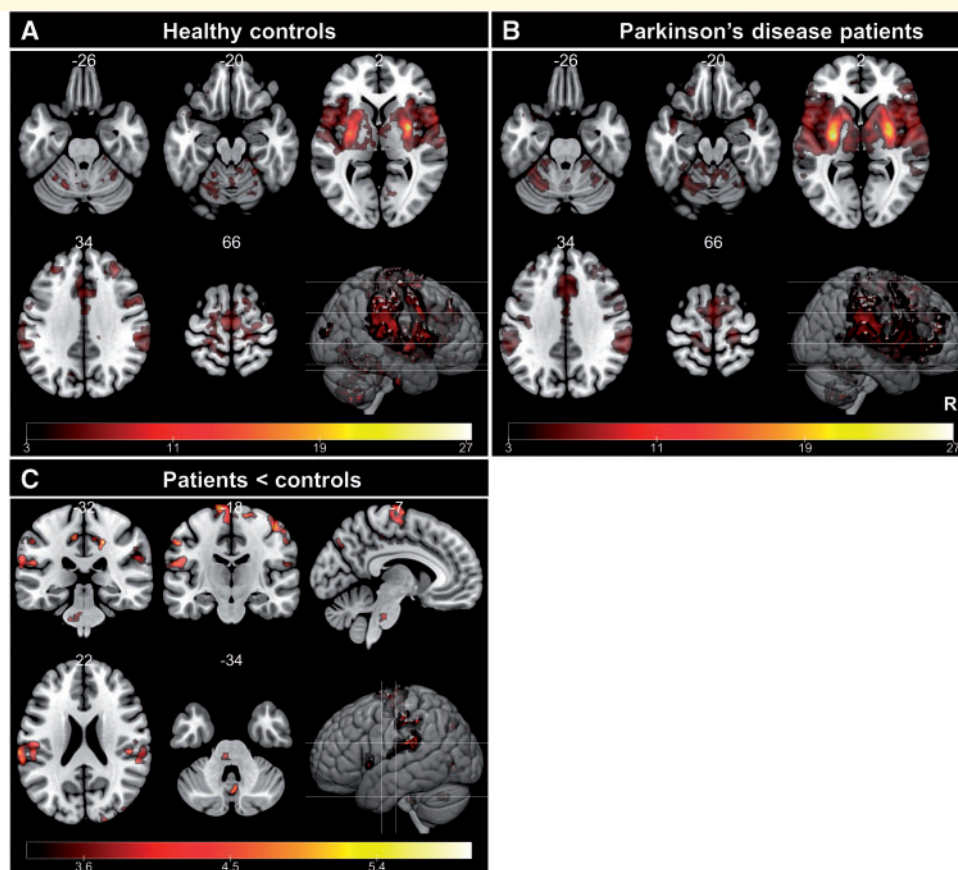


**Figure 2 Dopamine depleted putaminal regions exhibit reduced functional synchrony with the sensorimotor network in patients with Parkinson's disease.** Spatial distribution of clusters exhibiting significant correlations with the BOLD signal of the putaminal seed region of interest, in which dopamine depletion was most severe in Parkinson's disease patients, overlaid on T<sub>1</sub> MNI152 anatomical template. Red-yellow clusters indicate significant correlations with the BOLD signal of the posterior putamen (PP) in (A) healthy controls or (B) Parkinson's disease patients. (C) Spatial distribution of clusters in which patients exhibited a significantly reduced correlation with the posterior putamen seed region of interest compared to healthy controls. All results were corrected for multiple comparison, thresholded at  $P < 0.05$  FWE cluster-level correction. Colour bar indicates corresponding t-values. Slices and 3D display were constructed with MRICroGL, neurological display.

did not reveal statistically significant differences. A suspected increase in functional connectivity between the posterior putamen and the anterior cerebellar cortex did not reach significance when putaminal hyperconnectivity was analysed in a seed-to-voxel analysis. Similar cortical regions were found to exhibit putaminal hypoconnectivity when between-group contrasts were calculated between the total of 60 patients and 25 control subjects.

To analyse whether striatocortical connectivity disruption influences cortical metabolic activity, we exported functional connectivity values and normalized  $^{18}\text{F}$ -FDG uptake values from each cortical cluster, which exhibited reduced functional correlation with the bilateral posterior putamen seed region of interest in Parkinson's disease. Despite low spatial similarity between significantly hypometabolic regions and areas that were less functionally connected to the posterior putamen in patients with Parkinson's disease, significant associations were apparent between both imaging modalities (Fig. 3). Mean functional connectivity  $\beta$ -values

and  $^{18}\text{F}$ -FDG uptake in the right and the left IPC clusters showed a significant positive correlation in the Parkinson's disease group (IPC left:  $r = 0.35$ ,  $P = 0.021$ , IPC right:  $r = 0.36$ ,  $P = 0.018$ ; Fig. 3A and B, corrected for age and LEED), but not in controls, indicating concomitant changes in striatocortical functional connectivity and metabolic activity. In other clusters, which displayed significant hypoconnectivity to the posterior putamen in Parkinson's disease, no significant correlation between functional connectivity values and glucose metabolism was detected.

## Cerebral pathologies traced by multimodal imaging reflect clinical impairment

As an association between more severe motor symptoms and functional network alterations was hypothesized, correlation analyses were performed between imaging findings and motor scores in non-tremor dominant patients.

**Table 4** Between-group differences in putaminal functional connectivity (FWE-cluster-level corrected  $P < 0.05$ )

Region	Side	Size, voxel	x	y	z	T-value	FWE-corrected P-value
Precuneus	Right	135	20	–32	42	5.98	0.001
PC	Right						
PreCG	Left / right	840	–4	–10	72	5.54	<0.001
SFG	Left						
SMA	Left						
LG	Right	81	10	–76	–6	5.36	0.02
CO	Left	608	–68	–26	22	5.30	<0.001
PO	Left						
aSMG	Left						
PostCG	Left						
PreCG	Right	549	44	–18	56	5.28	<0.001
PostCG	Right						
PostCG	Left	306	–54	–20	40	5.23	<0.001
aSMG	Left						
PreCG	Right	92	4	–24	50	5.02	0.010
PO	Right	381	46	–26	22	4.82	<0.001
aSMG	Right						
PT	Right						
pSMG	Right						
OP	Right	200	22	–96	24	4.65	<0.001
sLOC	Right						
IFG oper	Left	83	–48	12	6	4.51	0.018
Precuneus	Left	104	–10	–72	38	4.49	0.005
Brainstem	Left / right	69	–2	–34	–32	4.47	0.044

All t-values were calculated using Conn in SPM12, significance was thresholded at  $P < 0.05$  FWE-corrected at cluster-level. Extent threshold  $k = 69$  voxels, height threshold  $T = 3.25$ . aSMG = anterior supramarginal gyrus; CO = central operculum cortex; IFG oper = inferior frontal gyrus pars opercularis; LG = lingual gyrus; OP = occipital pole; PC = cingulate gyrus; posterior; PO = parietal operculum cortex; PostCG = postcentral gyrus; PreCG = precentral gyrus; pSMG = posterior supramarginal gyrus; PT = planum temporale; SFG = superior frontal gyrus; sLOC = superior lateral occipital cortex; SMA = supplementary motor area.

Interestingly, the degree of side-specific akinetic-rigid symptoms, quantified by UPDRS-III right body non-tremor score, negatively correlated with metabolic activity in the left SNpc, suggesting a relation between decreasing  $^{18}\text{F}$ -FDG uptake in degenerating midbrain structures and akinesia-rigidity in Parkinson's disease (Fig. 4A,  $r = -0.40$ ,  $P = 0.010$ ). Focusing on disease duration, significantly reduced midbrain metabolism was observed in patients with a disease duration  $>7$  years compared to patients with a disease duration of  $\leq 7$  years ( $P = 0.016$ , Welch-test, one-sided). Predictably, right body akinesia and rigidity was accompanied by more severe dopaminergic deficits in the left putamen as quantified by  $^{18}\text{F}$ -DOPA-PET (Fig. 4B,  $r = -0.38$ ,  $P = 0.014$ ). Nigrostriatal functional connectivity between the midbrain and bilateral posterior putamen negatively correlated with non-tremor-dominant patients' total akinesia-rigidity scores (Fig. 4C,  $r = -0.49$ ,  $P = 0.0008$ ). Interestingly, a negative linear trend was observed between UPDRS-III right body scores and  $\beta$ -values quantifying the degree of connectivity between the left posterior putamen seed region of interest and the left IPC cluster (coordinates  $-68, -26, 22$ ), which was one of the cortical regions exhibiting less functional correlation with the posterior putamen in patients (Fig. 4D,  $r = -0.31$ ,

$P = 0.053$ , corrected for age, LEDD and MMSE). In other cortical clusters, including motor regions, which showed putaminal dysconnectivity, no significant correlation between functional connectivity values and motor impairment could be observed. In addition, the left hypoconnected IPC cluster was the only cortical region in which normalized  $^{18}\text{F}$ -FDG uptake exhibited a negative linear trend with contralateral motor impairment (Fig. 4E,  $r = -0.31$ ,  $P = 0.057$ , corrected for age, LEDD, MMSE and disease duration). Further, in the left IPC a positive correlation between total cognition MMSE score and striatocortical connectivity values was observed in patients with Parkinson's disease (Fig. 4E,  $r = 0.42$ ,  $P = 0.005$ , corrected for age, LEDD, and akinesia-rigidity-score).

## Discussion

The current study opens new perspectives by being the first to assess network degeneration in patients with Parkinson's disease by using a multimodal imaging approach in a large cohort of patients. Combining functional imaging methods has been a useful method to describe the vulnerability of distinct networks for neurodegenerative processes, but to



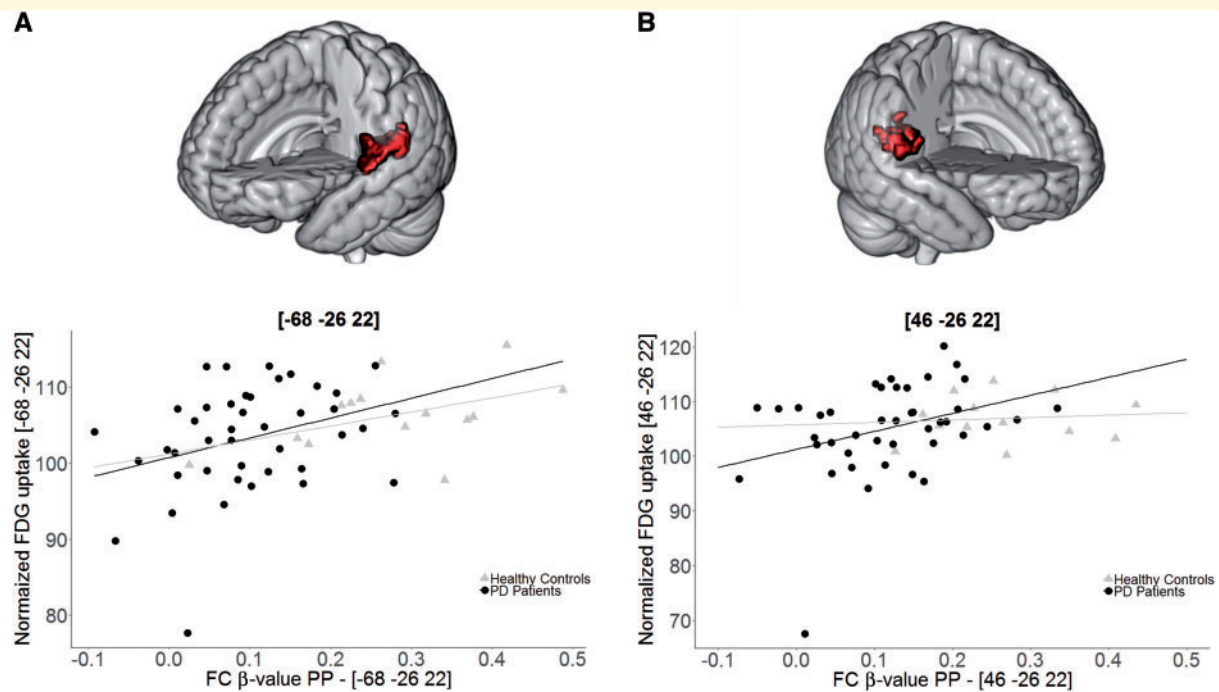


**Figure 3 Striatocortical connectivity  $\beta$ -values correlate with metabolic activity in the bilateral inferior parietal cortex in patients with Parkinson's disease.** Correlation analysis between subject-specific functional connectivity  $\beta$ -values, characterizing the connection between the posterior putamen (PP) seed region of interest and the (A) IPC left ( $r = 0.35$ ,  $P = 0.021$ ) or (B) IPC right ( $r = 0.36$ ,  $P = 0.018$ ) cluster, which were both less functionally correlated with the posterior putamen in Parkinson's disease patients, and normalized  $^{18}\text{F}$ -FDG-PET values exported from respective cortical clusters. In healthy controls both correlations revealed no significant results [IPC left ( $r = 0.47$ ,  $P = 0.079$ ), IPC right ( $r = 0.36$ ,  $P = 0.237$ )]. All correlation analyses were corrected for age and in patients also for LEDD. PD = Parkinson's disease.

date not for Parkinson's disease. In patients with Parkinson's disease, specific cortico-subcortical functional and metabolic changes have been described previously, but many studies were restricted to one or two imaging modalities, limiting cross-modality insights that could improve the understanding of disease pathology on a network level. We combined three functional imaging modalities, including  $^{18}\text{F}$ -DOPA-PET,  $^{18}\text{F}$ -FDG-PET and functional MRI to characterize functional consequences of cerebral pathologies and their regional association in patients with Parkinson's disease in comparison to healthy subjects. In summary, results support the hypothesis that degeneration of nigrostriatal connections and its neurochemical consequences in Parkinson's disease impair functional activity in specific cortical regions with strong association to motoric function. Using high-resolution PET data, we were the first to detect hypometabolism in the SNpc of patients with Parkinson's disease. This was accompanied by reduced nigrostriatal connectivity and dopamine depletion, which in turn appeared to cause a disruption in striatocortical resting state functional connectivity. Putaminal dysconnectivity in patients primarily affected the sensorimotor network and regions deploying the DMN. More severe functional desynchronization with the striatum was also accompanied by decreased global cognitive performance

and lower neural activity in the IPC in patients, suggesting that reduced input from the striatum leads to concomitant metabolic changes in the cerebral cortex and potentially cognitive decline.

### In vivo detection of nigrostriatal pathway disruption

The hypometabolic cortical areas observed in the current study stand in accordance with previous studies that reported reduced metabolic activity in parieto-occipital regions in Parkinson's disease (Eidelberg, 2009; Teune *et al.*, 2010; Granert *et al.*, 2015). The observed hypometabolic midbrain cluster overlapped in parts with the lateral and caudal SNpc, as confirmed by a high-resolution subcortical nuclei atlas (Pauli *et al.*, 2018), in correspondence with regions where nigral cell bodies are known to degenerate first. The significantly reduced metabolism observed in patients with Parkinson's disease might reflect an indirect correlate of severe loss of neural cell bodies which contribute to the nigrostriatal pathway, a major neuropathological hallmark of Parkinson's disease that has already been described *in vivo* in Parkinson's disease and rapid eye movement (REM) sleep behaviour disorder (RBD) patients using different MRI techniques (Ohtsuka *et al.*, 2013;

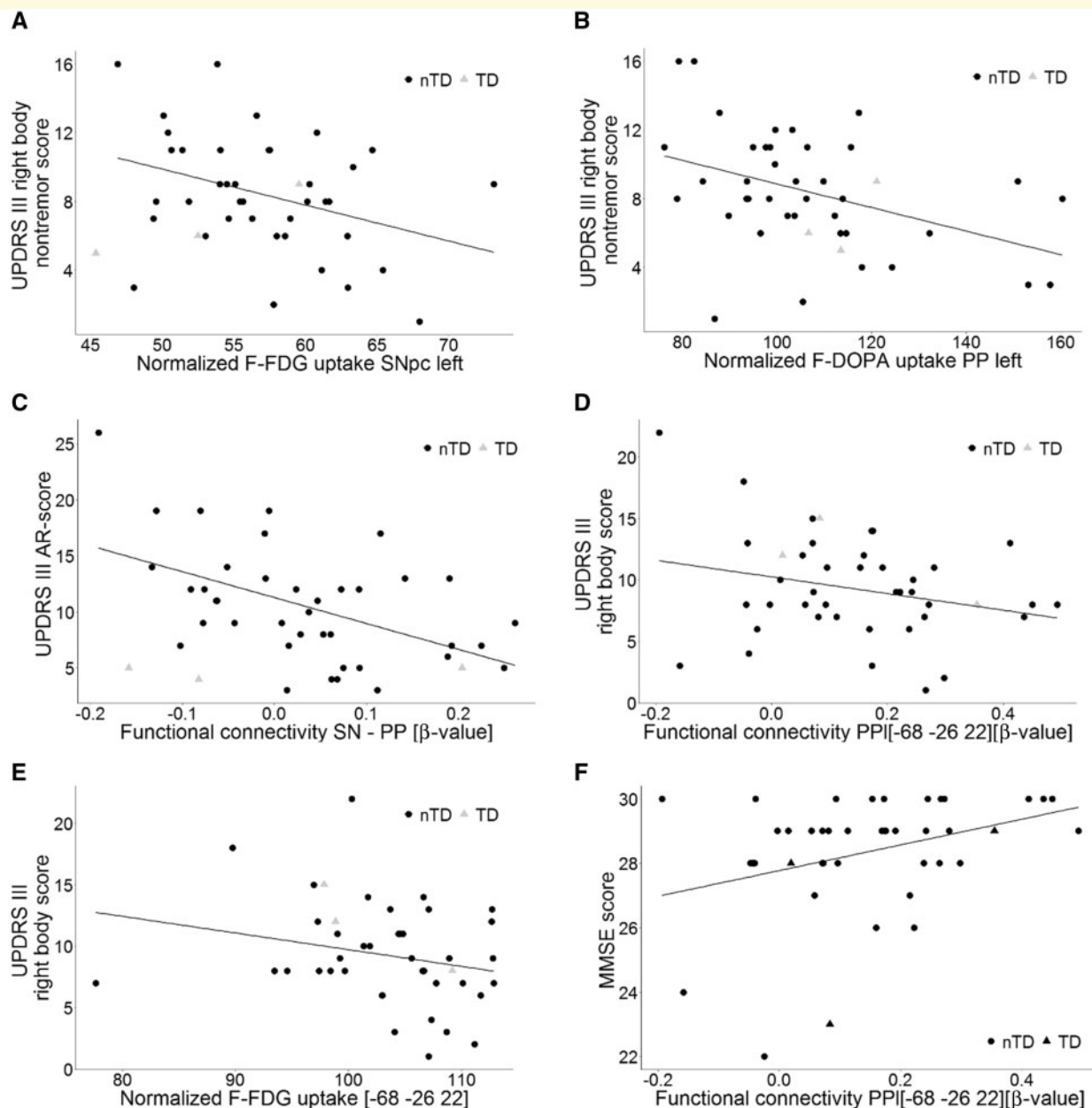


**Figure 4 Multimodally assessed nigrostriatal pathway integrity and functional alterations in the IPC correspond with motor and cognitive impairments in patients with Parkinson's disease.** Partial correlation analyses between subject-specific UPDRS-III right body non-tremor scores and (A) nigral metabolism (*left*) ( $r = -0.40$ ,  $P = 0.010$ ), (B) putaminal  $^{18}\text{F}$ -DOPA uptake (*left*) ( $r = -0.38$ ,  $P = 0.014$ ), (C) functional connectivity between SNpc and posterior putamen (PP) and UPDRS-III akinesia-rigidity score ( $r = -0.49$ ,  $P < 0.001$ ), UPDRS-III right body scores and (D)  $\beta$ -values quantifying functional connectivity between the posterior putamen left (PPI) seed and left IPC cluster (peak coordinates:  $-68, -26, 22$ ) ( $r = -0.31$ ,  $P = 0.053$ ), or (E) normalized  $^{18}\text{F}$ -FDG uptake in the left IPC cluster quantified by  $^{18}\text{F}$ -FDG-PET in non-tremor-dominant patients ( $r = -0.31$ ,  $P = 0.057$ ). (F) Global cognition score on MMSE and  $\beta$ -values quantifying functional connectivity between the PPI seed and left IPC cluster in all patients (peak coordinates:  $-68 -26 22$ ) ( $r = 0.42$ ,  $P = 0.005$ ). All correlations were corrected for age and LEDD and in the case of (D) MMSE, (E) MMSE, disease duration and (F) akinesia-rigidity (AR) scores were included as additional covariates. UPDRS-III right body non-tremor scores (maximum: 24), right body scores (maximum: 36) and akinesia-rigidity scores (maximum = 48) were calculated, as provided in the Supplementary material.

Pyatigorskaya *et al.*, 2017). Using neuromelanin-sensitive MRI, Ohtsuka *et al.* (2013) observed cell death-associated depigmentation in the lateral SNpc in Parkinson's disease, where hypometabolism was evident in our patients. Both

findings stand in accordance with topography of dopaminergic cell loss, most strongly affecting the caudal and mediolateral part of the SNpc, histopathologically described by Damier *et al.* (1999). Dopaminergic neurons in the SNpc

have been characterized as highly energy consuming neurons with numerous mitochondria, poor myelination, and long axonal processes, which makes them especially vulnerable to exhaustion (Braak *et al.*, 2006; Seibyl *et al.*, 2012). In consideration of the devastating decline of nigral neurons, which is already evident when first motor symptoms occur, the observed hypometabolic cluster is likely to reflect secondary metabolic changes due to the loss of high energy consuming neural populations. Despite this pathophysiological knowledge, nigral hypometabolism in human patients with Parkinson's disease has not been previously described, probably because resolution was lower than of the HRRT-PET scanner in the current study or because of smaller sample sizes.

To date, similar results were only reported in a 6-hydroxydopamine-lesioned rat model using high-resolution small-animal  $^{18}\text{F}$ -FDG-PET, where the strongest metabolic impairment was seen in the SNpc, attributable to dopaminergic cell loss (Jang *et al.*, 2012). Notably, we previously observed increased metabolic activity in the substantia nigra in an early-stage Parkinson's disease cohort of 10 patients (five unmedicated) with high resolution PET (Eggers *et al.*, 2009). In the latter study a different, region of interest-based approach was applied with nigral regions of interest drawn manually in native space. However, early-stage nigral hypermetabolism could reflect inflammatory processes, which may initially outweigh reduced neural metabolism due to neurodegeneration (Gerhard *et al.*, 2006; de Virgilio *et al.*, 2016). Evidence for a disease-stage dependent process is given in the linear relationship between midbrain metabolism and contralateral disease severity and the fact that stronger metabolic deficits in the midbrain were observed in patients with longer disease duration. It is noteworthy that several studies report an increased metabolism in pontine regions (Niethammer and Eidelberg, 2012; Granert *et al.*, 2015), which might 'blur over' reduced metabolism in the caudal midbrain on lower resolution scanners.

In the current study, a modest linear correlation between unilateral nigral  $^{18}\text{F}$ -FDG uptake and ipsilateral putaminal  $^{18}\text{F}$ -DOPA uptake was observed, suggesting a linear association between detected abnormalities identified along nigrostriatal connections. The correlation was relatively low, which may be due to a 'floor effect', meaning that in patients with more advanced degeneration, nigral  $^{18}\text{F}$ -FDG activity and/or fluorodopa uptake in the posterior putamen would have reached a minimum; or varying degrees of inflammatory activity between patients, which could not be distinguished from neural activity using  $^{18}\text{F}$ -FDG-PET. The description of concomitant changes was supported by resting state functional MRI findings, which implied that pathological changes are directly related to impaired functional coherence between the hypometabolic midbrain and dopamine depleted putamen, an observation underpinned by comparable studies (Sharman *et al.*, 2013). In conclusion, corresponding deficits along the nigrostriatal pathway were identified *in vivo* by measuring correlates of

neural dysfunction ( $^{18}\text{F}$ -FDG), dopaminergic activity ( $^{18}\text{F}$ -DOPA-PET) and functional synchrony (resting state functional MRI). Of note, cerebral pathologies identified along this pathway corresponded with contralateral akinetic-rigid symptoms, suggesting an involvement in motor impairment.

## Striatocortical functional network degeneration and metabolic consequences

In accordance with previous assumptions, the distribution of connectivity disruption in patients with Parkinson's disease converged with spatial patterns of putaminal functional connectivity networks in controls, indicating functional motor network disturbances in Parkinson's disease. These findings are consistent with anatomical studies pointing out parallel functional loops of different putaminal subregions in non-human primates (Alexander *et al.*, 1986) and functional imaging studies that emphasize functionally segregated striatocortical circuits in humans (Postuma and Dagher, 2006; Di Martino *et al.*, 2008; Helmich *et al.*, 2010). Although functional connectivity does not necessarily reflect direct anatomical connections, the current findings mostly overlap with structural putaminal connectivity networks and therefore are likely to reflect correlates of spatially organized direct connections and their reduced functional integrity in Parkinson's disease (Postuma and Dagher, 2006; Cacciola *et al.*, 2017). Of note, significantly reduced functional connectivity was detected between the bilateral putaminal seed region of interest, where dopamine depletion was most severe in the present cohort, and cortical regions of the sensorimotor network, suggesting a putative role of putaminal dopaminergic dysfunction as conjoining element, through which pathology enters the cerebral cortex. These findings are suggestive of pathologic processes that target predefined neural networks. More precisely, attenuation of nigrostriatal transmission leads to dysfunctions within the striatocortical loop responsible for sensorimotor processing by provoking an imbalanced functional coherence between areas that exhibit strong functional correlation in healthy controls. In line with these findings, a topographic overlap between predominant subcortical atrophy identified by deformation-based morphometry in Parkinson's disease and intrinsic connectivity networks in healthy controls was previously reported, and the observed patterns were suggestive of an SN-centred pathogenic epicentre (Zeighami *et al.*, 2015). Yau *et al.* (2018) described longitudinally that cortical thinning in Parkinson's disease primarily affects regions with high connectivity to a 'disease reservoir', a set of subcortical regions affected at baseline (Zeighami *et al.*, 2015). Those observations emphasize that vulnerability of affected cortical areas is determined by their functional connection to previously damaged subcortical areas, and along with the current findings support the hypothesis of network-dependent degeneration in Parkinson's disease.

In the current study, significantly reduced resting state functional connectivity was evident between the posterior putamen and mainly the bilateral precentral gyrus and postcentral gyrus, supplementary motor area but also the IPC in patients with Parkinson's disease (Fig. 2). In line with the current findings, Helmich *et al.* (2010) also reported similar findings regarding putaminal hypoconnectivity in Parkinson's disease and asymptomatic leucine-rich repeat kinase 2 (LRRK2) mutation carriers (Helmich *et al.*, 2015). Furthermore, a quantitative neuroimaging meta-analysis provided evidence for disturbed functional connectivity of the bilateral IPC in Parkinson's disease (Tahmasian *et al.*, 2017). Additionally, in the current study, normalized  $^{18}\text{F}$ -FDG uptake values exported from hypoconnected IPC clusters significantly correlated with  $\beta$ -values quantifying the degree of connectivity between the posterior putamen and the respective IPC cluster in patients (Fig. 3). Hypometabolism in the IPC has been reported as a promising predictive value for Parkinson's disease in a meta-analysis that examined sensitivity of  $^{18}\text{F}$ -FDG-PET and structural atrophy, albeit that this phenomenon was mainly attributed to cognitive symptoms (Albrecht *et al.*, 2019).

Interestingly, the IPC is thought to represent the conjoining element in sensory feedback processing during movement tasks (Mattingley *et al.*, 1998), which is of great interest facing the association between contralateral motor impairments and the connectivity between the posterior putamen and the left IPC (Fig. 4D) as well as concomitant changes in glucose metabolism (Fig. 4E). In line with the latter findings, an important role of the IPC in sensorimotor processing and integration has been postulated (Wang *et al.*, 2017). The IPC represents the intersection of several networks (DMN, ventral attention, frontoparietal control network, sensorimotor), rather than a component of a single network with specialized function. From a broader point of view, the IPC might represent the missing link between motor and cognitive deficits in Parkinson's disease. The identified IPC clusters encompass areas responsible for sensorimotor processing and default mode activity, according to functional subdivisions defined by Wang *et al.* (2017) and we observed a positive correlation between global cognition quantified by MMSE scores and the connectivity between the left IPC and posterior putamen. DMN dysfunction might arise secondarily to dopamine depletion (van Eimeren *et al.*, 2009; Wu *et al.*, 2012), more precisely in consequence of putaminal dysconnectivity of distinct DMN components, e.g. the IPC, which may provoke an impaired functional communication within the DMN and, eventually, cognitive decline. Additionally, cortical areas that exhibited putaminal dysconnectivity in patients could be related to non-motor symptoms as some of them, e.g. the superior frontal gyrus and fronto-insular network, were reported to be involved in impulsivity (Tahmasian *et al.*, 2015b; Schwartz *et al.*, 2019) and anosognosia in Parkinson's disease in previous studies (Maier *et al.*, 2016). Variability of the clinical course in different

subtypes might partially depend on which non-motor networks are impaired and thereby determine susceptibility to non-motor symptoms.

## Outlook and limitations

A relatively broad range of variability in medication and motor symptom severity is a typical limitation for a mild-to-moderately affected Parkinson's disease cohort.

As it has been suspected that levodopa attenuates radioligand binding (Politis, 2014), partially normalizes  $^{18}\text{F}$ -FDG activity (Asanuma *et al.*, 2006), and alters resting state functional connectivity (Tahmasian *et al.*, 2015a), all functional image acquisitions were performed in the OFF state. Dopamine replacement therapy has been assumed to normalize functional connectivity alterations within the sensorimotor network and longer lasting effects of dopaminergic therapy on resting state functional MRI have been suggested (Tahmasian *et al.*, 2015a). This issue was partly addressed by incorporating LEDD as covariate in correlation analyses. However, as similar changes in putaminal resting state functional connectivity have been described in drug-naïve patients with Parkinson's disease, it can be assumed that residual medication-related effects seen in the OFF state are fairly small (Luo *et al.*, 2014). Further analysis should also focus on large scale networks, in relation to non-motor symptoms and dopamine depletion.

In consideration of residual inter-subject variability, an accurate detection of small subcortical nuclei like the SNpc is always afflicted with some uncertainty. Nonetheless, the identification of the SNpc using a probabilistic atlas of subcortical nuclei suggests a metabolic deficit due to loss of nigral neurons. If this observation is consistently reproduced using high-resolution PET acquisitions examining different disease stages, it would have diagnostic importance as a metabolic parameter with clinical relevance. Nonetheless, one limitation here is the lower number of controls, which was limited by the Federal Bureau for Radiation.

Finally, only indirect correlates of neurodegeneration were assessed. However, multimodal approaches and prospective availability of specific  $\alpha$ -synuclein PET tracers may provide important additional insights into network degeneration and enable monitoring of disease progression. Measuring the degree of network degeneration at different stages, including subclinical network changes in prodromal subjects, could allow the identification of objectively definable disease stages.

## Conclusion

The present findings suggest that in consequence of cellular degeneration, affecting vulnerable dopaminergic neurons within the SNpc, sequential functional alterations are initiated in Parkinson's disease. Network degeneration



seems to spread beyond nigrostriatal dopaminergic projections into cortical areas belonging to the sensorimotor network, including the bilateral precentral gyrus, supplementary motor area and the IPC, which has outstanding functions in sensorimotor integration and might represent the link between basal ganglia dysfunction and DMN alterations. To our knowledge this is the first study that shows midbrain hypometabolism in Parkinson's disease and combines  $^{18}\text{F}$ -DOPA-PET,  $^{18}\text{F}$ -FDG-PET and functional MRI to examine spatial associations between multimodally assessed pathologies. The unique multimodal approach applied in the current study successfully detected cerebral pathologies from decline of midbrain nuclei through putaminal dopamine depletion to striatocortical motor circuit dysfunction, which stands in accordance with the degree of motor disability in the patients analysed, highlighting the capability of multimodal imaging protocols as biomarkers, which may be suitable for quantification of disease progression.

## Acknowledgements

We would like to thank all the participants who took part in the study and all of our colleagues who helped with data acquisition for their support in making the current research project possible.

## Funding

This study received funding by the the German Research Association (DFG) in context of the Clinical Research Group 219 (KFO 219, EG350/1–1).

## Competing interests

The authors report no competing interests.

## Supplementary material

Supplementary material is available at *Brain* online.

## References

- Albin RL, Young AB, Penney JB. The functional anatomy of basal ganglia disorders. *Trends Neurosci* 1989; 12: 366–75.
- Albrecht F, Ballarín T, Neumann J, Schroeter ML. FDG-PET hypometabolism is more sensitive than MRI atrophy in Parkinson's disease: a whole-brain multimodal imaging meta-analysis. *Neuroimage Clin* 2019; 21: 101594.
- Alexander GE, DeLong MR, Strick PL. Parallel organization of functionally segregated circuits linking basal ganglia and cortex. *Annu Rev Neurosci* 1986; 9: 357–81.
- Asanuma K, Tang C, Ma Y, Dhawan V, Mattis P, Edwards C, et al. Network modulation in the treatment of Parkinson's disease. *Brain* 2006; 129: 2667–78.
- Behzadi Y, Restom K, Liao J, Liu TT. A component based noise correction method (CompCor) for BOLD and perfusion based fMRI. *Neuroimage* 2007; 37: 90–101.
- Bischof GN, Ewers M, Franzmeier N, Grothe MJ, Hoenig M, Kocagoncu E, et al. Connectomics and molecular imaging in neurodegeneration. *Eur J Nucl Med Mol Imaging* 2019; 46: 2819–30.
- Bischof GN, Jessen F, Fliessbach K, Dronse J, Hammes J, Neumaier B, et al. Impact of tau and amyloid burden on glucose metabolism in Alzheimer's disease. *Ann Clin Transl Neurol* 2016; 3: 934–9.
- Braak H, Del Tredici K, Rüb U, de Vos R, Jansen Steur E, Braak E. Staging of brain pathology related to sporadic Parkinson's disease. *Neurobiol Aging* 2003; 24: 197–211.
- Braak H, Rüb U, Schultz C, Del Tredici K. Vulnerability of cortical neurons to Alzheimer's and Parkinson's diseases. *J Alzheimer's Dis* 2006; 9: 35–44.
- Brett M, Anton JL, Valabregue R, Poline J-B. Region of interest analysis using an SPM toolbox. In: Presented at the 8th International Conference on Functional Mapping of the Human Brain, Sendai, Japan. 2002. Available on CD-ROM in *NeuroImage*, Vol 16, No 2. [http://www.imm.dtu.dk/~fn/ps/Nielsen2002Translating\\_abstract.ps.gz](http://www.imm.dtu.dk/~fn/ps/Nielsen2002Translating_abstract.ps.gz).
- Buckner RL, Sepulcre J, Talukdar T, Krienen FM, Liu H, Hedden T, et al. Cortical hubs revealed by intrinsic functional connectivity: mapping, assessment of stability, and relation to Alzheimer's disease. *J Neurosci* 2009; 29: 1860–73.
- Buckner RL, Snyder AZ, Shannon BJ, LaRossa G, Sachs R, Fotenos AF, et al. Molecular, structural, and functional characterization of Alzheimer's disease: evidence for a relationship between default activity, amyloid, and memory. *J Neurosci* 2005; 25: 7709–17.
- Cacciola A, Calamuneri A, Milardi D, Mormina E, Chillemi G, Marino S, et al. A connectomic analysis of the human basal ganglia network. *Front Neuroanat* 2017; 11: 85.
- Cerasa A, Novellino F, Quattrone A. Connectivity changes in Parkinson's disease. *Curr Neurol Neurosci Rep* 2016; 16: 91.
- Cope TE, Rittman T, Borchert RJ, Jones PS, Vatansever D, Allinson K, et al. Tau burden and the functional connectome in Alzheimer's disease and progressive supranuclear palsy. *Brain* 2018; 141: 550–67.
- Damier P, Hirsch EC, Agid Y, Graybiel AM. The substantia nigra of the human brain. II. Patterns of loss of dopamine-containing neurons in Parkinson's disease. *Brain* 1999; 122 (Pt 8): 1437–48.
- Della Rosa PA, Cerami C, Gallivanone F, Prestia A, Caroli A, Castiglioni I, et al. A standardized 18F-FDG-PET template for spatial normalization in statistical parametric mapping of dementia. *Neuroinform* 2014; 12: 575–93.
- DeLong MR. Primate models of movement disorders of basal ganglia origin. *Trends Neurosci* 1990; 13: 281–5.
- Di Martino A, Scheres A, Margulies DS, Kelly AMC, Uddin LQ, Shehzad Z, et al. Functional connectivity of human striatum: a resting state FMRI study. *Cereb Cortex* 2008; 18: 2735–47.
- Dronse J, Fliessbach K, Bischof GN, von RB, Faber J, Hammes J, et al. In vivo patterns of tau pathology, amyloid- $\beta$  burden, and neuronal dysfunction in clinical variants of Alzheimer's disease. *J Alzheimers Dis* 2017; 55: 465–71.
- Drzezga A. The network degeneration hypothesis: spread of neurodegenerative patterns along neuronal brain networks. *J Nucl Med* 2018; 59: 1645–8.
- Drzezga A, Becker JA, van Dijk KRA, Sreenivasan A, Talukdar T, Sullivan C, et al. Neuronal dysfunction and disconnection of cortical hubs in non-demented subjects with elevated amyloid burden. *Brain* 2011; 134: 1635–46.
- Eggers C, Hilker R, Burghaus L, Schumacher B, Heiss WD. High resolution positron emission tomography demonstrates basal ganglia dysfunction in early Parkinson's disease. *J Neurol Sci* 2009; 276: 27–30.
- Eggers C, Kahraman D, Fink GR, Schmidt M, Timmermann L. Akinetic-rigid and tremor-dominant Parkinson's disease patients show different patterns of FP-CIT single photon emission computed tomography. *Mov Disord* 2011; 26: 416–23.

- Ehgoetz Martens KA, Hall JM, Georgiades MJ, Gilat M, Walton CC, Matar E, et al. The functional network signature of heterogeneity in freezing of gait. *Brain* 2018; 141: 1145–60.
- Eidelberg D. Metabolic brain networks in neurodegenerative disorders: a functional imaging approach. *Trends Neurosci* 2009; 32: 548–57.
- Emre M, Aarsland D, Brown R, Burn DJ, Duyckaerts C, Mizuno Y, et al. Clinical diagnostic criteria for dementia associated with Parkinson's disease. *Mov Disord* 2007; 22: 1689–707. quiz 1837.
- Fahn S, Elton RL. UPDRS development committee. The unified Parkinson's disease rating scale. In: Fahn S, Marsden CD, Calne DB, Goldstein M, editors. *Recent developments in Parkinson's disease*. 2nd edn. Florham Park, NJ: Macmillan Healthcare Information; 1987. p. 153–63. p. 293–304.
- Folstein MF, Folstein SE, McHugh PR. "Mini-mental state". *J Psychiatric Res* 1975; 12: 189–98.
- García-Gómez FJ, García-Solís D, Luis-Simón FJ, Marín-Oyaga VA, Carrillo F, Mir P, et al. Elaboración de una plantilla de SPM para la normalización de imágenes de SPECT con 123I-Ioflupano. *Rev Espanola Med Nucl Imagen Mol* 2013; 32: 350–6.
- Gerhard A, Pavese N, Hottot G, Turkheimer F, Es M, Hammers A, et al. In vivo imaging of microglial activation with 11C(R)-PK11195 PET in idiopathic Parkinson's disease. *Neurobiol Dis* 2006; 21: 404–12.
- Ghasemi M, Mahloojifar A. Disorganization of equilibrium directional interactions in the brain motor network of Parkinson's disease: new insight of resting state analysis using granger causality and graphical approach. *J Med Signals Sens* 2013; 3: 69–78.
- Glaab E, Trezzi J-P, Greuel A, Jäger C, Hodak Z, Drzezga A, et al. Integrative analysis of blood metabolomics and PET brain neuroimaging data for Parkinson's disease. *Neurobiol Dis* 2019; 124: 555–62.
- Granert O, Drzezga AE, Boecker H, Perneczky R, Kurz A, Götz J, et al. Metabolic topology of neurodegenerative disorders: influence of cognitive and motor deficits. *J Nucl Med* 2015; 56: 1916–21.
- Hacker CD, Perlmuter JS, Criswell SR, Ances BM, Snyder AZ. Resting state functional connectivity of the striatum in Parkinson's disease. *Brain* 2012; 135: 3699–711.
- Helmich RC, Derikx LC, Bakker M, Scheeringa R, Bloem BR, Toni I. Spatial remapping of cortico-striatal connectivity in Parkinson's disease. *Cereb Cortex* 2010; 20: 1175–86.
- Helmich RC, Thaler A, van Nuenen BFL, Gurevich T, Mirelman A, Marder KS, et al. Reorganization of corticostriatal circuits in healthy G2019S LRRK2 carriers. *Neurology* 2015; 84: 399–406.
- Hoehn MM, Yahr MD. Parkinsonism: onset, progression and mortality. *Neurology* 1967; 17: 427–42.
- Hoenig MC, Bischof GN, Seemiller J, Hammes J, Kukolja J, Onur ÖA, et al. Networks of tau distribution in Alzheimer's disease. *Brain* 2018; 141: 568–81.
- Jang DP, Min H-K, Lee S-Y, Kim IY, Park HW, Im YH, et al. Functional neuroimaging of the 6-OHDA lesion rat model of Parkinson's disease. *Neurosci Lett* 2012; 513: 187–92.
- Kish SJ, Shannak K, Hornykiewicz O. Uneven pattern of dopamine loss in the striatum of patients with idiopathic Parkinson's disease. *N Engl J Med* 1988; 318: 876–80.
- Langston JW, Widner H, Goetz CG, Brooks D, Fahn S, Freeman T, et al. Core assessment program for intracerebral transplantations (CAPIT). *Mov Disord* 1992; 7: 2–13.
- Luo C, Song W, Chen Q, Zheng Z, Chen K, Cao B, et al. Reduced functional connectivity in early-stage drug-naïve Parkinson's disease: a resting-state fMRI study. *Neurobiol Aging* 2014; 35: 431–41.
- Maier F, Williamson KL, Tahmasian M, Rochhausen L, Ellereit AL, Prigatano GP, et al. Behavioural and neuroimaging correlates of impaired self-awareness of hypo- and hyperkinesia in Parkinson's disease. *Cortex* 2016; 82: 35–47.
- Mattingley JB, Husain M, Rorden C, Kennard C, Driver J. Motor role of human inferior parietal lobe revealed in unilateral neglect patients. *Nature* 1998; 392: 179–82.
- Mohan A, Roberto AJ, Mohan A, Lorenzo A, Jones K, Lapidus KAB, et al. The Significance of the Default Mode Network (DMN) in neurological and neuropsychiatric disorders: a review. *Yale J Biol Med* 2016; 49–57.
- Niethammer M, Eidelberg D. Metabolic brain networks in translational neurology: concepts and applications. *Ann Neurol* 2012; 72: 635–47.
- Obeso JA, Stamelou M, Goetz CG, Poewe W, Lang AE, Weintraub D, et al. Past, present, and future of Parkinson's disease: a special essay on the 200th Anniversary of the Shaking Palsy. *Mov Disord* 2017; 32: 1264–310.
- Ohtsuka C, Sasaki M, Konno K, Koide M, Kato K, Takahashi J, et al. Changes in substantia nigra and locus coeruleus in patients with early-stage Parkinson's disease using neuromelanin-sensitive MR imaging. *Neurosci Lett* 2013; 541: 93–8.
- Pagano G, Niccolini F, Politis M. Imaging in Parkinson's disease. *Clin Med* 2016; 16: 371–5.
- Palop JJ, Chin J, Mucke L. A network dysfunction perspective on neurodegenerative diseases. *Nature* 2006; 443: 768–73.
- Pauli WM, Nili AN, Tyszka JM. A high-resolution probabilistic in vivo atlas of human subcortical brain nuclei. *Sci Data* 2018; 5: 180063.
- Politis M. Neuroimaging in Parkinson disease: from research setting to clinical practice. *Nat Rev Neurol* 2014; 10: 708–22.
- Postuma RB, Dagher A. Basal ganglia functional connectivity based on a meta-analysis of 126 positron emission tomography and functional magnetic resonance imaging publications. *Cereb Cortex* 2006; 16: 1508–21.
- Prodoehl J, Burciu RG, Vaillancourt DE. Resting state functional magnetic resonance imaging in Parkinson's disease. *Curr Neurol Neurosci Rep* 2014; 14: 448.
- Pyatigorskaya N, Gaurav R, Arnaldi D, Leu-Semenescu S, Yahia-Cherif L, Valabregue R, et al. Magnetic resonance imaging biomarkers to assess substantia nigra damage in idiopathic rapid eye movement sleep behavior disorder. *Sleep* 2017; 40. doi: 10.1093/sleep/zsx149.
- R Core Team. R: a language and environment for statistical computing. Vienna, Austria: R Foundation for Statistical Computing; 2018.
- Sawle GV, Playford ED, Burn DJ, Cunningham VJ, Brooks DJ. Separating Parkinson's disease from normality. *Arch Neurol* 1994; 51: 237–43.
- Schindlbeck KA, Eidelberg D. Network imaging biomarkers: insights and clinical applications in Parkinson's disease. *Lancet Neurol* 2018; 17: 629–40.
- Schwartz F, Tahmasian M, Maier F, Rochhausen L, Schnorrenberg KL, Samea F, et al. Overlapping and distinct neural metabolic patterns related to impulsivity and hypomania in Parkinson's disease. *Brain Imaging Behav* 2019; 13: 241–54.
- Seeley WW, Crawford RK, Zhou J, Miller BL, Greicius MD. Neurodegenerative diseases target large-scale human brain networks. *Neuron* 2009; 62: 42–52.
- Seibyl J, Russell D, Jennings D, Marek K. Neuroimaging over the course of Parkinson's disease: from early detection of the at-risk patient to improving pharmacotherapy of later-stage disease. *Semin Nucl Med* 2012; 42: 406–14.
- Sharman M, Valabregue R, Perlberg V, Marrakchi-Kacem L, Vidailhet M, Benali H, et al. Parkinson's disease patients show reduced cortical-subcortical sensorimotor connectivity. *Mov Disord* 2013; 28: 447–54.
- Tahmasian M, Bettray LM, van Eimeren T, Drzezga A, Timmermann L, Eickhoff CR, et al. A systematic review on the applications of resting-state fMRI in Parkinson's disease: does dopamine replacement therapy play a role? *Cortex* 2015a; 73: 80–105.
- Tahmasian M, Eickhoff SB, Giehl K, Schwartz F, Herz DM, Drzezga A, et al. Resting-state functional reorganization in Parkinson's disease: an activation likelihood estimation meta-analysis. *Cortex* 2017; 92: 119–38.

- Tahmasian M, Rochhausen L, Maier F, Williamson KL, Drzezga A, Timmermann L, et al. Impulsivity is associated with increased metabolism in the fronto-insular network in Parkinson's Disease. *Front Behav Neurosci* 2015b; 9: 317.
- Tahmasian M, Shao J, Meng C, Grimmer T, Diehl-Schmid J, Yousefi BH, et al. Based on the network degeneration hypothesis: separating individual patients with different neurodegenerative syndromes in a preliminary hybrid PET/MR Study. *J Nucl Med* 2016; 57: 410–5.
- Teune LK, Bartels AL, Jong BM, de Willemsen ATM, Eshuis SA, de Vries JJ, et al. Typical cerebral metabolic patterns in neurodegenerative brain diseases. *Mov Disord* 2010; 25: 2395–404.
- Tomlinson CL, Stowe R, Patel S, Rick C, Gray R, Clarke CE. Systematic review of levodopa dose equivalency reporting in Parkinson's disease. *Mov Disord* 2010; 25: 2649–53.
- van Eimeren T, Monchi O, Ballanger B, Strafella AP. Dysfunction of the default mode network in Parkinson disease: a functional magnetic resonance imaging study. *Arch Neurol* 2009; 66: 877–83.
- De Virgilio A, Greco A, Fabbrini G, Inghilleri M, Rizzo MI, Gallo A, et al. Parkinson's disease: autoimmunity and neuroinflammation. *Autoimmun Rev* 2016; 15: 1005–11.
- Vo A, Sako W, Fujita K, Peng S, Mattis PJ, Skidmore FM, et al. Parkinson's disease-related network topographies characterized with resting state functional MRI. *Hum Brain Mapp* 2017; 38: 617–30.
- Wang J, Xie S, Guo X, Becker B, Fox PT, Eickhoff SB, et al. Correspondent functional topography of the human left inferior parietal lobule at rest and under task revealed using resting-state fMRI and coactivation based parcellation. *Hum Brain Mapp* 2017; 38: 1659–75.
- Whitfield-Gabrieli S, Nieto-Castanon A. Conn: a functional connectivity toolbox for correlated and anticorrelated brain networks. *Brain Connect* 2012; 2: 125–41.
- Whitfield-Gabrieli S, Nieto-Castanon A. CONN - functional connectivity toolbox v17. 2017. <http://www.nitrc.org/projects/conn>.
- Wu T, Wang J, Wang C, Hallett M, Zang Y, Wu X, et al. Basal ganglia circuits changes in Parkinson's disease patients. *Neurosci Lett* 2012; 524: 55–9.
- Wu T, Wang L, Chen Y, Zhao C, Li K, Chan P. Changes of functional connectivity of the motor network in the resting state in Parkinson's disease. *Neurosci Lett* 2009; 460: 6–10.
- Yau Y, Zeighami Y, Baker TE, Larcher K, Vainik U, Dadar M, et al. Network connectivity determines cortical thinning in early Parkinson's disease progression. *Nat Commun* 2018; 9: 12.
- Zeighami Y, Ulla M, Iturria-Medina Y, Dadar M, Zhang Y, Larcher K-H, et al. Network structure of brain atrophy in de novo Parkinson's disease. *eLife* 2015; 4.
- Zhou J, Gennatas ED, Kramer JH, Miller BL, Seeley WW. Predicting regional neurodegeneration from the healthy brain functional connectome. *Neuron* 2012; 73: 1216–27.

6.2. Supplementary material

## Supplementary Material

### UPDRS III subscore calculation

To quantify the manifestation of akinesia and rigidity in a given subject, akinesia-rigidity (AR) scores for the whole body (AR-score) and for the left and right hemibody were calculated based on subsets of UPDRS-III items. Right body scores were calculated from the sum of UPDRS III items 20-26 for the right side (0 to a maximum of 36 points). Left body scores were calculated based on the sum of UPDRS III items 20-26 for the left side (0 to a maximum of 36 points). Hemibody non-tremor symptoms were quantified by subtracting items 20 and 21 from the previously described right and left body scores, leading to a maximum possible value of 24 points for each side. The bilateral akinesia-rigidity score is the sum of UPDRS items 18, 19, 22, 27-31 (0 to a maximum of 48 points), like described previously in Eggers et al. (2011). Subdivision of patients into tremor-dominant and non-tremor-dominant subtype was performed according to strictly defined criteria as previously described, which categorize patients as tremor-dominant if their tremor-score is at least twice their non-tremor-score (Eggers et al., 2011).

*Table 1: Subject characteristics and clinical data – all subjects*

Demographic and behavioral data – all subjects				
	Healthy controls	Parkinson's disease	p-value	Test statistic
No.	25	60	-	-
Gender male / female	12 / 13	41 / 19	0.08	$\chi^2 = 3.11$
Age [y]	63.52 ± 7.67	65.02 ± 9.82	0.46	$t = 0.75$
MMSE	28.92 ± 1.04	28.45 ± 1.73	0.39	$W = 664.5$
Clinical characteristics – Parkinson's disease patients by subtype				
	Non-TD Subtype	TD Subtype	p-value	Test statistic
No.	57	3	-	-
DD [y]	4.98 ± 3.57	3.17 ± 2.36	0.49	$W = 106$
UPDRS III off	24.14 ± 9.40	28.33 ± 3.79	0.17	$W = 45$
UPDRS III off AR-score	10.61 ± 5.06	4.67 ± 0.58	0.02	$W = 154.5$
UPDRS III off right body score off	9.02 ± 4.40	11.67 ± 3.51	0.20	$W = 47$
UPDRS III off left body score off	9.23 ± 4.47	13.00 ± 5.00	0.17	$W = 44.5$
UPDRS III off right body non-tremor score	8.00 ± 3.70	6.67 ± 2.08	0.44	$W = 108.5$
UPDRS III off left body non-tremor score	8.37 ± 3.85	10.00 ± 4.36	0.53	$W = 66.5$
Hoehn & Yahr	2.30 ± 0.45	2.17 ± 0.29	0.63	$W = 99$
LEDD [mg]	481.28 ± 284.26	401.67 ± 152.51	0.62	$W = 100.5$
LEDD <sub>A</sub> [mg]	148.87 ± 118.39	110.00 ± 127.67	0.61	$W = 101$
Side of onset L / R / equal	27 / 28 / 2	1 / 2 / 0	0.90*	$\chi^2 = 0.02^*$

This table summarizes clinical characteristics (mean ± SD) in the observed groups. Between-group differences were analyzed using Mann-Whitney-U-test, Welch's-test or in the case of dichotom variables by chi-squared test.

\*Direct comparison of side-of-onset right vs. side of onset left group in all patients using an approximate binominal test.

Abbreviations: DD = Disease duration, UPDRS-III = unified Parkinson's disease rating scale part III, LEDD = Levodopa equivalent daily dose, LEDD<sub>A</sub> = Levodopa equivalent daily dose for dopamine agonists, MMSE = Mini-Mental State Examination

Table 2: Midbrain-putamen ROI-to-ROI Hypoconnectivity in Parkinson's disease patients (patients < controls)

Region	Side	T-value	P-value (uncor.)	P-value (FDR-corr.)
<b>Seed</b>				
<b>Brain-stem</b>				
PP*	L R	3.74	0.0004	0.0027
PP*	R	3.61	0.0007	0.0027
putamen (atlas)	R	2.99	0.0042	0.0112
PP*	L	2.69	0.0095	0.0189
<b>Seed</b>				
<b>Substantia Nigra*</b>				
PP*	R	3.76	0.0004	0.0033
putamen (atlas)	R	2.57	0.0130	0.0427
PP*	L R	2.49	0.0160	0.0427

Statistics of ROI-to-ROI functional connectivity analysis between defined brain stem and putaminal ROIs. FDR-seed-level correction was applied to correct for multiple comparisons and number of seeds tested. Abbreviations: PP = posterior putamen, R = right, L = left.

\*indicates ROIs defined by group-contrasts in PET data

Table 3: Putaminal functional connectivity network in healthy controls

Region	Side	Size [voxel]	x	y	z	T-value	FWE-corrected p-value
PreCG Putamen aSMG IC CO pSMG PO PostCG Thalamus	R / L R / L R / L R / L R R / L R / L R / L	17160	30	-2	2	27.31	< 0.001
Vermis 8 9	R / L R / L	247	8	-58	-32	12.68	< 0.001
AC PreCG SMA PostCG SFG PC PaCiG	R / L R / L R / L R / L R / L R / L R / L	6249	-4	8	40	11.02	< 0.001
OP sLOC	L L	53	-38	-88	22	8.46	0.036
Cerebellum 6 45	L L	479	-18	-62	-26	8.29	< 0.001
pTFusC	R	61	38	-14	-40	8.20	< 0.017
Cerebellum 6 45	R	520	22	-32	-30	8.09	< 0.001
Brain stem	R / L	128	-10	-34	-40	7.84	< 0.001
Cerebellum 8 7	L L	402	22	-64	-54	7.81	< 0.001
FP MFG	R R	303	34	40	36	7.65	< 0.001
FP MFG	L L	337	-30	38	34	7.43	< 0.001
PreCG	L	86	-52	0	48	7.32	0.002
PreCG PostCG	L L	119	-30	-12	56	7.24	< 0.001
OP sLOC	R R	60	38	-90	14	6.79	0.019
FP FOrb	L	98	-24	38	-12	6.55	0.001
Cerebellum 8 9	L L	297	-22	-66	-54	6.41	< 0.001
Precuneus	R / L	85	-12	-70	36	5.40	0.002

Region	Side	Size [voxel]	x	y	z	T-value	FWE-corrected p-value
PreCG IC FP Putamen CO pSMG Thalamus IFG oper aSMG	R / L R / L R / L R / L R R / L R R / L	29151	-28	-10	2	26.94	< 0.001
AC SMA PaCiG PreCG SFG PostCG	R / L R / L R / L R / L R R / L	7152	10	12	40	9.22	< 0.001
Cerebellum 6 45 TOFusC	R / L R / L L	1681	-28	-54	-24	6.75	< 0.001
Cerebellum 8	R	352	30	-56	-54	6.81	< 0.001
Cerebellum 8	L	278	-18	-58	-60	6.75	< 0.001
FP FOrb	L L	145	-22	34	-20	5.29	< 0.001

Table 4: Putaminal functional connectivity network in Parkinson's disease patients

Statistics of seed-to-voxel functional connectivity analysis between the bilateral PP seed ROI, which reflected  $^{18}\text{F}$ -Dopa PET between-group contrast, and every other voxel throughout the whole brain.

Abbreviations: AC = anterior cingular cortex, a / pSMG = anterior / posterior supramarginal gyrus, CO = central operculum, FOrb = frontal orbital cortex, FP = frontal pole, IC = insular cortex, IFG oper = inferior frontal gyrus pars opercularis, L = left, MFG = middle frontal gyrus, OP = occipital pole, PaCiG = paracingular cortex, PC = posterior cingulate cortex, PO = parietal operculum cortex, PostCG = postcentral gyrus, PP = posterior putamen, PreCG = precentral gyrus, pTFusC = posterior temporal fusiform cortex, R = right, sLOC = superior lateral occipital cortex, SFG = superior frontal gyrus, SMA = supplementary motor area, TOFusC = temporal occipital fusiform cortex, Ver = Vermis. All *t*-values were calculated using *Conn* in SPM12, thresholded at  $p < 0.05$  FWE-cluster-level corrected.




## References

Eggers C, Kahraman D, Fink GR, Schmidt M, Timmermann L. Akinetic-rigid and tremor-dominant Parkinson's disease patients show different patterns of FP-CIT single photon emission computed tomography. *Movement disorders : official journal of the Movement Disorder Society* 2011; 26: 416–423.

6.3. The default mode network and cognition in Parkinson's disease: a multimodal resting-state network approach

## RESEARCH ARTICLE

# The default mode network and cognition in Parkinson's disease: A multimodal resting-state network approach

Marina C. Ruppert<sup>1,2</sup>  | Andrea Greuel<sup>1</sup> | Julia Freigang<sup>1,2</sup> | Masoud Tahmasian<sup>3</sup> | Franziska Maier<sup>4</sup> | Jochen Hammes<sup>5</sup> | Thilo van Eimeren<sup>5,6,9</sup> | Lars Timmermann<sup>1,2</sup> | Marc Tittgemeyer<sup>7,8</sup> | Alexander Drzezga<sup>5,9,10</sup> | Carsten Eggers<sup>1,2</sup>

<sup>1</sup>Department of Neurology, University Hospital of Marburg, Marburg, Germany

<sup>2</sup>Center for Mind, Brain, and Behavior—CMBB, Universities of Marburg and Gießen, Marburg, Germany

<sup>3</sup>Institute of Medical Science and Technology, Shahid Beheshti University, Tehran, Iran

<sup>4</sup>Medical Faculty, Department of Psychiatry, University Hospital Cologne, Cologne, Germany

<sup>5</sup>Multimodal Neuroimaging Group, Department of Nuclear Medicine, Medical Faculty and University Hospital Cologne, University Hospital Cologne, Cologne, Germany

<sup>6</sup>Department of Neurology, Medical Faculty and University Hospital Cologne, University Hospital Cologne, Cologne, Germany

<sup>7</sup>Max Planck Institute for Metabolism Research, Cologne, Germany

<sup>8</sup>Cluster of Excellence in Cellular Stress and Aging Associated Disease (CECAD), Cologne, Germany

<sup>9</sup>German Center for Neurodegenerative Diseases (DZNE), Bonn, Germany

<sup>10</sup>Cognitive Neuroscience, Institute of Neuroscience and Medicine (INM-2), Jülich, Germany

## Correspondence

Carsten Eggers, Department of Neurology, University Hospital of Giessen and Marburg, Baldingerstraße, 35033 Marburg, Germany. Email: carsten.eggers@uk-gm.de

## Funding information

Deutsche Forschungsgemeinschaft, Grant/Award Number: EG350/1-1

## Abstract

Involvement of the default mode network (DMN) in cognitive symptoms of Parkinson's disease (PD) has been reported by resting-state functional MRI (rsfMRI) studies. However, the relation to metabolic measures obtained by [18F]-fluorodeoxyglucose positron emission tomography (FDG-PET) is largely unknown. We applied multimodal resting-state network analysis to clarify the association between intrinsic metabolic and functional connectivity abnormalities within the DMN and their significance for cognitive symptoms in PD. PD patients were classified into normal cognition ( $n = 36$ ) and mild cognitive impairment (MCI;  $n = 12$ ). The DMN was identified by applying an independent component analysis to FDG-PET and rsfMRI data of a matched subset (16 controls and 16 PD patients) of the total cohort. Besides metabolic activity, metabolic and functional connectivity within the

**Abbreviations:** AGl, angular gyrus left; AGr, angular gyrus right; BDI-II, Beck's depression inventory version II; BNT, Boston naming test; DMN, default mode network; EPI, echo-planar imaging; FA, flip angle; FDG, Fluorodeoxyglucose; FDR, false discovery rate; FoV, field of view; fMRI, functional magnetic resonance imaging; H & Y, Hoehn and Yahr; HC, healthy controls; ICA, independent component analysis; IPL, inferior parietal lobe; LEDD, levodopa equivalent daily dose; MCI, mild cognitive impairment; NC, normal cognition; MNI, Montreal Neurological Institute; mPFC, medial prefrontal cortex; mWCST, modified Wisconsin card sorting test; PANDA, Parkinson neuropsychometric dementia assessment; ParaHL, parahippocampal cortex left; ParaHR, parahippocampal cortex right; PC, precuneus cortex; PCC, posterior cingulate cortex; PD, Parkinson's disease; PET, positron emission tomography; pSMGLs, posterior supramarginal gyrus left superior; pSMGL, posterior supramarginal gyrus left; pSMGLs, posterior supramarginal gyrus right superior; ROI, region of interest; SFGl, superior frontal gyrus left; MMSE, Mini-Mental Status Examination; midSFG, mid, superior frontal gyrus; rsfMRI, resting-state functional magnetic resonance imaging; SFGr, superior frontal gyrus right; sLOC, superior lateral occipital cortex left; sLOCr, superior lateral occipital cortex right; TE, echo time; TR, repetition time; UPDRS, unified Parkinson's disease rating scale; WMS, Wechsler memory scale.

This is an open access article under the terms of the Creative Commons Attribution-NonCommercial License, which permits use, distribution and reproduction in any medium, provided the original work is properly cited and is not used for commercial purposes.

© 2021 The Authors. *Human Brain Mapping* published by Wiley Periodicals LLC.

DMN were compared between the patients' groups and healthy controls ( $n = 16$ ). Glucose metabolism was significantly reduced in all DMN nodes in both patient groups compared to controls, with the lowest uptake in PD-MCI ( $p < .05$ ). Increased metabolic and functional connectivity along fronto-parietal connections was identified in PD-MCI patients compared to controls and unimpaired patients. Functional connectivity negatively correlated with cognitive composite z-scores in patients ( $r = -.43$ ,  $p = .005$ ). The current study clarifies the commonalities of metabolic and hemodynamic measures of brain network activity and their individual significance for cognitive symptoms in PD, highlighting the added value of multimodal resting-state network approaches for identifying prospective biomarkers.

#### KEYWORDS

[18F]-FDG-PET, default mode network, metabolic covariance, mild cognitive impairment, Parkinson's disease, resting-state fMRI

## 1 | INTRODUCTION

Mild cognitive impairment (MCI) is one of the most frequently observed nonmotor symptoms of Parkinson's disease (PD). Studies emphasize that up to 50% develop cognitive symptoms in the course of disease (Goldman et al., 2018) and the majority of PD patients with long disease duration will suffer from dementia (Hely, Reid, Adena, Halliday, & Morris, 2008). MCI may affect single or multiple cognitive domains and dramatically increases the risk for conversion to dementia (Hoogland et al., 2017). Dementia severely affects the ability to manage daily life, the patient's quality of life, mortality, and caregiver burden (Goldman, Williams-Gray, Barker, Duda, & Galvin, 2014; Levy et al., 2002). Besides enormous effort invested in the development of therapies to stop or delay cognitive decline, further research needs to be done to (a) understand neural substrates underlying cognitive impairment; (b) describe early indicators of prospective cognitive dysfunction; and (c) identify quantifiable abnormalities which could serve as objective markers to track symptom progression or the effect of interventional therapies.

Neural resting-state networks (RSNs) with importance for cognitive processing, have been examined thoroughly and reported consistently by resting-state functional MRI (rsfMRI) studies (Biswal et al., 2010). The default mode network (DMN), encompassing the precuneus cortex (PC), posterior cingulate cortex (PCC), medial prefrontal cortex (mPFC), parahippocampal cortex, and parts of the inferior parietal lobe (IPL; Raichle, MacLeod, Snyder, & Gordon, 2000), has been extensively studied in this context. Altered resting-state DMN functional connectivity has been described in neurodegenerative diseases and its prospective usefulness as imaging biomarker for cognitive dysfunction has been postulated (Hohenfeld, Werner, & Reetz, 2018). However, neurophysiological and metabolic basics of resting brain network activity and rsfMRI-derived functional connectivity remain largely unknown (Passow et al., 2015; Wehrl et al., 2013). Limited evidence suggests a close relation between resting-state functional connectivity and interregional covariance of

metabolic activity (Passow et al., 2015; Riedl et al., 2014) assessed by [18F]-fluorodeoxyglucose positron emission tomography (FDG-PET). A few recently published studies examined the topology of metabolic resting-state covariance patterns by conducting seed-based correlation or multivariate decomposition techniques such as independent component analysis (ICA) but revealed conflicting results. Particularly, some studies reported the identification of a component distinctly representing the DMN (Savio et al., 2017; Yakushev et al., 2013), whereas other studies reported weak or no metabolic correspondence of this network (Di & Biswal, 2012).

Although its basic underpinnings date back to 1984 (Clark & Stoessl, 1986; Horwitz, Grady, Schlageter, Duara, & Rapoport, 1987), the interregional analysis of metabolic activity still represents a new and rapidly evolving field. Recently, studies began to focus on metabolic connectivity—basically the interregional correlation of glucose consumption—as a marker of neuropathology and cognitive performance (Sala & Perani, 2019). Molecular FDG-PET images are likely to reveal more specific results about reflected processes, and therefore, might overcome the unspecificity of fMRI-derived functional connectivity metrics. Pioneering studies revealed characteristic changes in metabolic connectivity within defined resting-state networks in neurodegenerative diseases and its applicability as markers of cognitive dysfunction (Toussaint et al., 2012; Yakushev et al., 2013).

A large body of studies focused on resting-state networks and their prospective usefulness as imaging biomarkers of cognition in PD. Several studies reported altered resting-state functional connectivity of the DMN in PD patients with or without cognitive impairment and drew a relation to cognitive symptoms (Baggio et al., 2015; Karunanayaka et al., 2016; Lopes et al., 2017; Lucas-Jiménez et al., 2016; Tessitore et al., 2012), but findings delineating altered DMN connectivity based on rsfMRI were heterogeneous, and partly hinted at a predominant decrease or increase in functional connectivity (Amboni et al., 2015; Baggio et al., 2015; Karunanayaka et al., 2016; Krajcovicova, Mikl, Marecek, & Rektorova, 2012; Lopes et al., 2017; Tessitore et al., 2012; Zhan et al., 2018). Spetsieris

et al. (2015) concluded that DMN function is spared from pathological alterations in the early disease stage but followed by dopamine-responsive decreased metabolic connectivity in advanced stages. Using sparse-inverse covariance estimation and an interregional correlation approach, Sala et al. (2017) assessed altered metabolic connectivity in cognitively unimpaired PD patients and reported changes on multiple scales, including decreased frontal metabolic coupling in several important resting-state networks on one hand and enhanced coupling in the posterior cortex in comparison to age-matched controls on the other hand.

Given the plenty of studies which focus on single imaging modalities and fail to establish a robust marker, multimodal studies of resting-state networks are highly warranted to clarify the association between metabolic and hemodynamic network activity and its significance for cognitive dysfunction in PD. In a previous study, we reported reduced functional connectivity between the dopamine depleted putamen and DMN regions (IPL), and related metabolic changes in PD, which both were associated with global cognitive performance (Ruppert et al., 2020). No study has elaborated the correspondence between PD-associated changes in DMN metabolic network activity and functional connectivity by using FDG-PET and rsfMRI analyses in parallel. By applying a multivariate ICA-based approach followed by interregional correlation analysis to FDG-PET and rsfMRI data of healthy controls and PD patients with and without MCI, we describe consistency and differences in DMN abnormalities related to cognition in PD, obtained by cross-modal metrics in a well-characterized PD cohort.

## 2 | MATERIALS AND METHODS

### 2.1 | Subject inclusion

Twenty-five healthy controls (HC) and 60 PD patients diagnosed according to the UK Brain Bank criteria were enrolled into the study after having declared informed consent in conformation with the Declaration of Helsinki. The study was approved by the local Ethics Committee and permission was given by the Federal Office for Radiation Protection (Ethical clearance number: EK12-265). Recruitment of patients was performed via the neurological outpatient clinic at the University Hospital of Cologne and associated neurological practices. Healthy controls were recruited by word-of mouth advertising.

Subjects were excluded if one of the following exclusion criteria were met: Age < 40 years, any central nervous system diseases except for PD, and any safety concerns for MRI scanning. Particularly, patients were excluded if signs of atypical parkinsonian syndromes evolved or they had reached an advanced disease stage (i.e., Hoehn & Yahr stage >3). Dementia was excluded according to Movement Disorder Society criteria using a neuropsychological test battery with two tests for each of the five cognitive domains (Emre et al., 2007). Subjects were excluded if cognitive deficits were observed in more than one domain and severe enough to impair daily life (Emre et al., 2007).

As an additional measure of global cognitive screening, the Mini-Mental Status Examination (MMSE) was applied (Folstein, Folstein, & McHugh, 1975). In a neuropsychiatric assessment, subjects were screened for depressive symptoms by Beck's Depression Inventory version II (BDI-II; Beck, Steer, & Brown, 1996). Subjects were excluded if classified as having major depression. Participants were interviewed regarding a family history of PD or other neurodegenerative diseases. Subsets of the data analyzed in the present study were subject of previously published articles which analyzed the data in different contexts (Glaab et al., 2019; Greuel et al., 2020; Hammes et al., 2019; Ruppert et al., 2020).

### 2.2 | Clinical assessment

Clinical examinations were carried out at the University Hospital of Cologne, Department of Neurology. Disease severity was quantified by the Unified PD Rating Scale part III (UPDRS-III; Fahn, Elton, & UPDRS Program Members, 1987) and according to Hoehn & Yahr staging (H&Y; Hoehn & Yahr, 1967). Clinical examination and functional imaging were performed OFF-medication (12-hr [Langston et al., 1992] or 72 hr without medication in case of dopamine agonists), as it has been suggested previously (Tahmasian et al., 2015; Tahmasian et al., 2017). Levodopa-equivalent daily dose (LEDD) for total medication was calculated based on common standards (Tomlinson et al., 2010).

### 2.3 | Neuropsychological testing

The applied neuropsychological test battery comprised five domains: attention, memory, language, executive functions, and visuospatial abilities. At least two cognitive tests per domain were performed, including the MMSE subtests Pentagons and delayed recall, Wechsler Memory Scale (WMS) digit span test forwards and backwards (Härting & Wechsler, 2000), Parkinson Neuropsychometric Dementia Assessment (PANDA) subtests cubes and delayed recall (Kalbe et al., 2008), Regensburger verbal fluency task (alternating fluency sports-fruits, semantic fluency animals; Aschenbrenner, Tucha, & Lange, 2001), modified Wisconsin Card Sorting Test (mWCST) errors (Harris, 1990) and Boston Naming Test (BNT, (Kaplan, Googlass, & Weintraub, 1983). Individual test or subtest results were converted into standardized, age- and education-corrected domain-specific z-scores. All domain-specific z-scores were finally merged into a cognitive composite score.

Categorization of subjects into MCI and normal cognition (NC) was carried out according to Movement Disorder Society Level II criteria (Litvan et al., 2012) for all subjects who underwent both imaging modalities and complete neuropsychological assessment ( $n = 16$  HC;  $n = 48$  PD). Patients were diagnosed with MCI when a difference of  $\geq 1.5$  SD was observed in relation to age- and education-corrected norm means in at least two cognitive test results regardless of domain affiliation.

## 2.4 | Image acquisition and preprocessing

### 2.4.1 | FDG-PET

The acquisition of FDG-PET scans was conducted on an ECAT HRRT-PET-Scanner (CTI, Knoxville, TN) at the Max-Planck-Institute for Metabolism Research, Cologne. Measurements were carried out in the morning after overnight fasting and withdrawal of dopaminergic medication. Subjects were positioned along the kantho-meatal line under standardized conditions with dimmed lighting and shut eyes in a quiet room. After an initial transmission scan, 185 MBq of FDG were injected intravenously and tomographic images were dynamically acquired for 60 min. FDG-PET scans were corrected for attenuation and scattered radiation and reconstructed into one frame per 10 min with a  $256 \times 256$  matrix. Resulting FDG-PET scans consisted of 207 slices with 1.22 mm voxel size. Rigid-body transformation was conducted to realign the six frames and the last four frames were finally averaged into one image for further analysis. Mean FDG-PET images were co-registered to the subject's mean fMRI-image in SPM12 ([www.fil.ion.ucl.ac.uk/spm/software/spm12](http://www.fil.ion.ucl.ac.uk/spm/software/spm12)). Spatial normalization into Montreal Neurological Institute (MNI) space was performed by nonlinear registration to an established FDG-PET template (Della Rosa et al., 2014). Finally, FDG-PET scans were smoothed with a 6 mm full-width at half-maximum (FWHM) Gaussian kernel using SPM12.

### 2.4.2 | Intensity normalization

FDG-PET scans were intensity normalized using the reference cluster method, which proportionally scales each voxel with the corresponding value of a post-hoc defined reference region (Yakushev et al., 2009). In contrast to global mean normalization, it allows a more study-specific procedure to diminish inter-subject differences in intensity and has been shown to be better suited for the study of neurodegenerative diseases in which global mean differences are present (Borghammer et al., 2010; Win et al., 2019). This procedure included an initial group comparison of FDG-PET scans by voxel-wise two sample  $t$  test which was carried out in SPM12 with default parameters (threshold masking, proportional scaling). As mentioned elsewhere, a threshold of  $t > 2$  and  $p = .05$  uncorrected for multiple comparisons at voxel-level and a minimum spatial extent of 30 contiguous voxels were applied (Yakushev et al., 2009). Averaged normalized values were exported for all subjects from the cluster with the highest  $t$  value, in which patients exhibited an increased FDG uptake in comparison to healthy controls using the region of interest (ROI) SPM toolbox MarsBaR (Brett, Anton, Valabregue, & Poline, 2002; <http://marsbar.sourceforge.net/>, RRID:SCR\_009605). Subsequently, each subject's cluster value was multiplied with the subject-specific cerebral global mean value to obtain raw values for each subject in the observed cluster. Thereafter, intensity normalization was applied to each individual's FDG-PET scan by performing proportional scaling with respect to the cluster activity using the SPM imCalc tool.

### 2.4.3 | Resting-state functional magnetic resonance imaging

MRI data were acquired at the Max-Planck-Institute for Metabolism Research in Cologne on a 3.0 Tesla SIEMENS MAGNETOM Prisma using the software system syngo MR D13D (Siemens, Erlangen, Germany). T1-weighted structural images were obtained with the following parameters: repetition time [TR] = 2,300 ms, echo time [TE] = 2.32 ms, flip angle [FA] =  $8^\circ$ , field of view [FoV] = 230 mm, slice thickness = 0.90 mm, voxel size =  $0.9 \times 0.9 \times 0.9$  mm, number of slices = 192. Rs-fMRI images were acquired via a gradient-echo echo-planar imaging sequence (EPI) in interleaved acquisition mode. Acquisition parameters were as follows: slice thickness = 2 mm, FoV = 208 mm, voxel size =  $2.0 \times 2.0 \times 2.0$  mm, TR = 776 ms, TE = 37.4 ms and FA =  $55^\circ$ . Each brain volume covered 72 axial slices; 617 acquisition time points per subject were performed.

Structural and functional MRI preprocessing and ICA were performed using SPM12 and the SPM toolbox Conn v17 (<http://www.nitrc.org/projects/conn>, RRID: SCR\_009550). The default preprocessing pipeline implemented in Conn was applied, which included the following steps: functional realignment and unwarp, functional outlier detection for correction of motion artifacts (ART-based scrubbing, strict correction method according to Power, Schlaggar, and Petersen [2015]), functional and structural direct segmentation and normalization to MNI space, denoising (temporal band-pass filtering 0.01–0.1 Hz, linear detrending and further reduction of physiological noise by anatomical component-based noise correction [aCompCor; Behzadi, Restom, Liau, & Liu, 2007]) and functional smoothing (isotropic 5 mm FWHM).

### 2.4.4 | ICA

For the initial ICA-based identification of metabolic resting-state covariance patterns, 16 PD patients were selected from the total PD cohort for which FDG-PET and rsfMRI scans were available to match the group size of 16 HC with FDG-PET scans. This guarantees an evenly matched influence on the resulting covariance networks and improves the sensitivity for the subsequent between-group analysis (Figure 1). For ICA analysis, the single scans of 32 subjects were concatenated into one 4D file using SPM12. ICA was performed on the concatenated file using the Infomax algorithm implemented in the GIFT toolbox (<http://mialab.mrn.org/software/gift/>, RRID: SCR\_001953). The number of independent components was set to 5 (Yakushev et al., 2013).

The initial ICA-based identification of fMRI resting-state networks was performed on the fMRI-data from the same sample of 32 subjects mentioned above (Figure 1). ICA was conducted by applying the Infomax algorithm implemented in the Conn toolbox. The number of independent components was set to 5. The extent of spatial overlap between both modalities' components was quantified by dice coefficient of similarity, calculated as the overlapping volume of both binary masks divided by their mean volume (Zou et al., 2004).

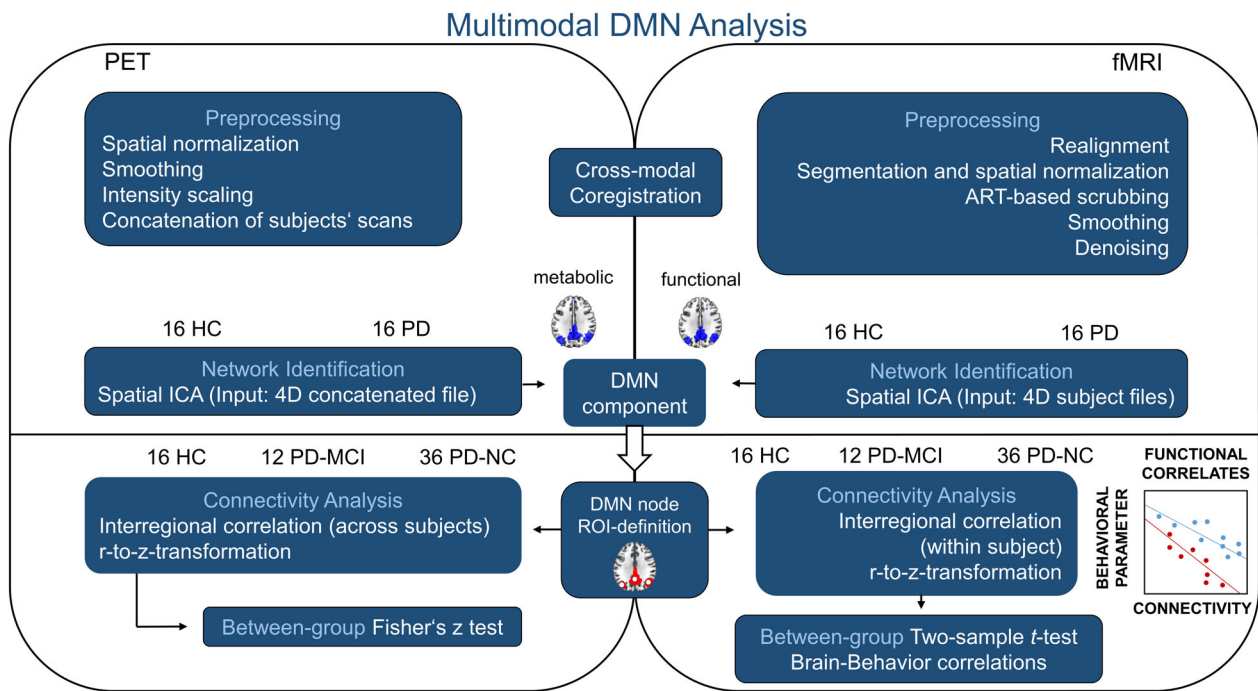


**FIGURE 1** Schematic representation of the processing pipeline applied during multimodal resting-state network analysis. fMRI and FDG-PET data were preprocessed according to standard pipelines except for the intensity normalization of FDG-PET scans which followed the recently described reference cluster method. Concatenated FDG-PET scans and single subject fMRI 4D files were fed into spatial ICA with the number of components set to 5. Fifteen spherical ROIs were defined based on the resulting DMN components and interregional correlation coefficients compared between the total sample of HC, PD-NC, and PD-MCI subjects. DMN, default mode network; HC, healthy controls; ICA, independent component analysis; MCI, mild cognitive impairment; NC, normal cognition; PD, Parkinson's disease; ROI, region of interest

Figures were created using MRICroGL (<http://www.mricro.com>, RRID: SCR\_002403).

#### 2.4.5 | Cross-modal region of interest analysis

In order to compare within-network connectivity between both modalities based on interregional temporal correlation of the BOLD signal (functional connectivity) and interregional metabolic correlation (metabolic connectivity), 15 ROIs were placed within the identified DMN components (Figure 1 and Table S1). Overlapping clusters of both DMN component masks were identified by visual inspection of superimposed binary masks in MRICroGL. Spherical ROIs covering the overlapping volumes were created in MarsBaR and their position was checked by visually controlling the overlap with DMN masks. Since we were also interested in frontal DMN regions and the parahippocampal gyri have been assigned to the DMN in literature, spherical ROIs were placed in the bilateral superior frontal gyrus (SFG), mPFC, and parahippocampal clusters although they were only part of the functional component (Table S1).

Correlation coefficients for fMRI-based connectivity were obtained via conducting Pearson correlation on the mean BOLD time course of each pair of ROIs. Corresponding metabolic measures were obtained by calculating Spearman's rank correlation coefficients between the mean normalized FDG uptake of both ROIs. Extraction

of mean normalized uptake values was performed using MarsBaR. Resulting interregional correlation coefficients were z-transformed and subsequently compared between controls and PD-NC or PD-MCI patients by conducting *t*-tests in Conn (rsfMRI) or Fisher's *z* test (FDG-PET) in R (<https://www.r-project.org>).

#### 2.5 | Statistical analyses

Statistical analyses of clinical, demographic, behavioral data, and ROI-based uptake values were performed using R. Normal distribution of numeric variables was verified by Shapiro-Wilk test. Differences between controls and the total PD group were assessed by Mann-Whitney *U* test or *t* test; differences between more than two groups by analysis of variance (ANOVA) or Kruskal-Wallis test. Post-hoc statistical analysis was carried out by performing pairwise Mann-Whitney *U* tests or *t*-tests with Bonferroni-Holm correction for multiple comparisons. Significant downward trends of FDG uptake with stronger cognitive impairment were tested one-sided by nonparametric Jonckheere-Terpstra test. An exploratory correlation analysis between imaging findings and cognition z-scores was performed in SPSS (IBM Corp. Released 2020. IBM SPSS Statistics for Windows, Version 27.0. Armonk, NY: IBM Corp) using age, sex, LEDD, UPDRS-III, disease duration, and BDI-II performance as covariates. Modulatory effects of clinical parameters on imaging results were



investigated by performing analyses of covariance (ANCOVA), including UPDRS-III, LEDD and disease duration as covariates.

## 2.6 | Data availability

The data set analyzed in the present study will be made available by the corresponding author upon reasonable request.

## 3 | RESULTS

### 3.1 | Subject characteristics

In total, 60 PD patients ( $65.02 \pm 9.82$  years; 19 female) and 25 healthy controls ( $63.52 \pm 7.67$  years; 13 female) were analyzed with fMRI in the current study. FDG-PET scans were available for 51 ( $66.45 \pm 8.53$  years; 18 female) of the analyzed patients and 16 healthy controls ( $64.63 \pm 8.33$  years; nine female) who underwent fMRI (Table S2). Characteristics of the 16 controls who underwent both modalities and 16 PD patients whose scans were fed into the ICA analyses are shown in Table S3.

Among the patients who underwent fMRI and FDG-PET scanning and completed neuropsychological testing, 12 patients were classified as having MCI and 36 exhibited normal cognition according to level II criteria (Litvan et al., 2012; Table 1). Six out of 36 PD-NC patients reported a family history of PD and one of the 12 PD-MCI patients mentioned a relative with PD. None of the healthy controls were categorized as having MCI and three reported a family history of PD. None of the subjects reported a family history of another

neurodegenerative disorder, aside from one PD-NC patient reporting a relative with multisystem atrophy. Demographic, clinical, and behavioral data of all subgroups are listed in Table 1. No significant differences were found among the healthy control group and patients' groups for age and gender, but for education years, BDI-II and global cognition (MMSE; Table 1). Significant differences between both patient groups were observed for MMSE, but not for education years and BDI-II. As expected, patients with MCI scored fewer points on the MMSE than PD-NC patients and healthy controls (Table 1). No significant between-group differences regarding demographic variables, motor severity and clinical measures were found between the PD-NC and PD-MCI group.

In addition, the groups differed significantly in the cognitive composite z-score and all five domain-specific z-scores (Table 2). PD-NC patients showed significantly reduced z-scores in the attention and executive domains and the cognitive composite score in comparison to controls. PD-MCI patients exhibited significantly reduced z-scores in comparison to controls and PD-NC patients in the cognitive composite score and all domains except for the language and executive domains, in which they only differed from controls (Table 2). Detailed results for all neuropsychological tests per domain and group can be found in Table 2.

### 3.2 | Metabolic and functional DMN components

The ICA-based analyses of concatenated FDG-PET data and fMRI data of 32 subjects revealed distinctly definable resting-state networks in both modalities. When the number of components per modality was set to 5, the DMN was the clearest visually

	FDG-PET and fMRI			
Groups	HC (n = 16)	PD-NC (n = 36)	PD-MCI (n = 12)	p value
Demographic and clinical variables				
Age, years	64.63 ± 8.33	66.69 ± 7.77	68.92 ± 8.77	.385
Gender, F/M	9/7	10 / 26	7 / 5	.060
Education, years	16.44 ± 2.06 <sup>b,c</sup>	14.44 ± 2.77 <sup>a</sup>	13.82 ± 2.75 <sup>a</sup>	.018*
DD, years	–	4.61 ± 3.68	4.13 ± 2.20	.838
UPDRS III total	–	24.67 ± 9.13	23.25 ± 7.00	.943
H & Y, stage (n)	–	2 (22) 2.5 (9) 3 (5)	2 (6) 2.5 (5) 3 (1)	.530
LEDD	–	410.48 ± 231.81	519.63 ± 181.62	.107
MMSE	28.94 ± 1.00 <sup>c</sup>	29.03 ± 0.88 <sup>c</sup>	26.50 ± 2.47 <sup>a,b</sup>	.001***
BDI-II	3.47 ± 6.00 <sup>b,c</sup>	8.86 ± 5.70 <sup>a</sup>	9.83 ± 7.61 <sup>a</sup>	<.001***

Note: Between-group differences were analyzed by ANOVA, Kruskal–Wallis test, Student's t-test or Mann–Whitney U test, and for dichotomous variables by Chi-square test. Significant post-hoc test results in comparison to a = HC, b = PD-NC, or c = PD-MCI are indicated by superscripts.

Abbreviations: BDI-II, Beck's depression inventory; DD, disease duration; H&Y, Hoehn and Yahr; HC, healthy controls; LEDD, Levodopa equivalent daily dose; PD-MCI, PD patients with mild cognitive impairment; PD-NC, PD patients with normal cognition; MMSE, mini-mental status examination.

\* $p < .05$ ; \*\* $p < .01$ ; \*\*\* $p < .001$ .

**TABLE 1** Demographic, clinical, and behavioral characteristics of PD patients with and without cognitive impairment and controls included in the multimodal cohort



**TABLE 2** Neuropsychological characteristics of PD patients with and without cognitive impairment and controls included in the multimodal cohort

	FDG-PET and fMRI			
Groups	HC (n = 16)	PD-NC (n = 36)	PD-MCI (n = 12)	p value
Scores for individual neuropsychological subtests				
Visuospatial				
MMSE pentagons	0.26 ± 0.00 <sup>c</sup>	0.04 ± 0.91 <sup>c</sup>	−2.69 ± 1.78 <sup>a,b</sup>	<.001***
PANDA cubes	0.09 ± 1.14	0.15 ± 1.02 <sup>c</sup>	−0.68 ± 1.04 <sup>b</sup>	.044*
Language				
Semantic fluency	1.20 ± 0.54 <sup>b,c</sup>	0.45 ± 0.85 <sup>a</sup>	0.18 ± 0.91 <sup>a</sup>	.002**
Boston naming test	0.19 ± 0.35	0.04 ± 0.47	−0.07 ± 0.53	.359
Executive function				
mWCST errors	0.22 ± 0.74 <sup>b,c</sup>	−0.59 ± 0.50 <sup>a,c</sup>	−1.03 ± 0.73 <sup>a,b</sup>	<.001***
Alternating fluency	1.04 ± 0.95 <sup>b,c</sup>	0.37 ± 0.83 <sup>a</sup>	0.13 ± 1.19 <sup>a</sup>	.025*
Attention				
Digit span forwards	1.03 ± 0.76 <sup>b,c</sup>	−0.14 ± 0.97 <sup>a</sup>	−0.40 ± 1.13 <sup>a</sup>	<.001***
Digit span backwards	0.28 ± 1.18 <sup>c</sup>	−0.18 ± 0.81	−0.65 ± 0.87 <sup>a</sup>	.039*
Memory				
Delayed recall PANDA	−0.04 ± 1.12 <sup>c</sup>	−0.60 ± 1.43	−2.20 ± 2.56 <sup>a</sup>	.024*
Delayed recall MMSE	0.28 ± 0.95	0.40 ± 0.83	−0.31 ± 1.05	.097
Neuropsychological z-scores				
Cognitive composite score	0.46 ± 0.32 <sup>b,c</sup>	−0.01 ± 0.30 <sup>a,c</sup>	−0.80 ± 0.35 <sup>a,b</sup>	<.001***
Visuospatial	0.18 ± 0.57 <sup>c</sup>	0.10 ± 0.74 <sup>c</sup>	−1.69 ± 0.87 <sup>a,b</sup>	<.001***
Language	0.70 ± 0.32 <sup>c</sup>	0.29 ± 0.65	0.01 ± 0.68 <sup>a</sup>	.010*
Executive function	0.63 ± 0.58 <sup>b,c</sup>	−0.11 ± 0.53 <sup>a</sup>	−0.45 ± 0.75 <sup>a</sup>	<.001***
Attention	0.65 ± 0.87 <sup>b,c</sup>	−0.14 ± 0.71 <sup>a,c</sup>	−0.53 ± 0.90 <sup>a,b</sup>	<.001***
Memory	0.12 ± 0.85 <sup>c</sup>	−0.10 ± 0.89 <sup>c</sup>	−1.26 ± 1.44 <sup>a,b</sup>	.010*

Note: Between-group differences were analyzed by ANOVA or Kruskal–Wallis test; pairwise Student's *t* test or Mann–Whitney *U* tests were performed for post-hoc comparisons. Significant post-hoc test results in comparison to *a* = HC, *b* = PD-NC, or *c* = PD-MCI are indicated by superscripts.

Abbreviations: HC, healthy controls; MMSE, Mini-Mental Status Examination; mWCST, modified Wisconsin Card Sorting Test; PANDA, Parkinson Neuropsychometric Dementia Assessment, PD-MCI, PD patients with mild cognitive impairment; PD-NC, PD patients with normal cognition.

\**p* < .05; \*\**p* < .01; \*\*\**p* < .001.

recognizable resting-state network in both modalities. In the fMRI data set, the other four components represented either the visual, fronto-parietal, dorsal-attention, or sensorimotor network. In the FDG-PET data set, a sensorimotor component with subcortical contribution, an auditory network, a midline cingulate cortex component with parietal clusters (Di & Biswal, 2012) and one noise component representing CSF noise were identified. The spatial correspondence between the metabolic and the fMRI DMN component was fair (dice coefficient = 0.25). But, especially for posterior DMN regions including the PC, PCC, and the bilateral superior lateral occipital cortex (sLOC) higher correspondence was observed (dice coefficient = 0.27; Figure 2). Nevertheless, some regions were found to be part of the functional DMN component, but not of the metabolic one or vice versa. The most striking differences were found in the frontal cortex, where frontal areas involving the frontal pole, frontal medial cortex, paracingulate gyrus, and subcallosal cortex were found to be part of the fMRI component but absent in the FDG-PET component (Figure 2). Further, clusters in the SFG which extended into the

juxtapositional lobule were found in both modalities, but only in the metabolic component additional clusters in the anterior cingulate gyrus and paracingulate gyrus were found to be part of the network. Additionally, the bilateral parahippocampal gyri were part of the functional network but not reported in the corresponding metabolic pattern. Parts of the cerebellar cortex were obtained in the metabolic covariance pattern but not in the functional component, and the parietal cluster extended into the cuneal cortex and occipital pole in the metabolic component (Figure 2). Similar findings were observed when ICA was performed on the fMRI data of 25 controls and 25 patients (Figure S1).

### 3.3 | Metabolic DMN activity is decreased in PD-NC patients and further decreases with MCI

When normalized FDG uptake values were exported from 15 ROIs placed within the identified DMN components and compared

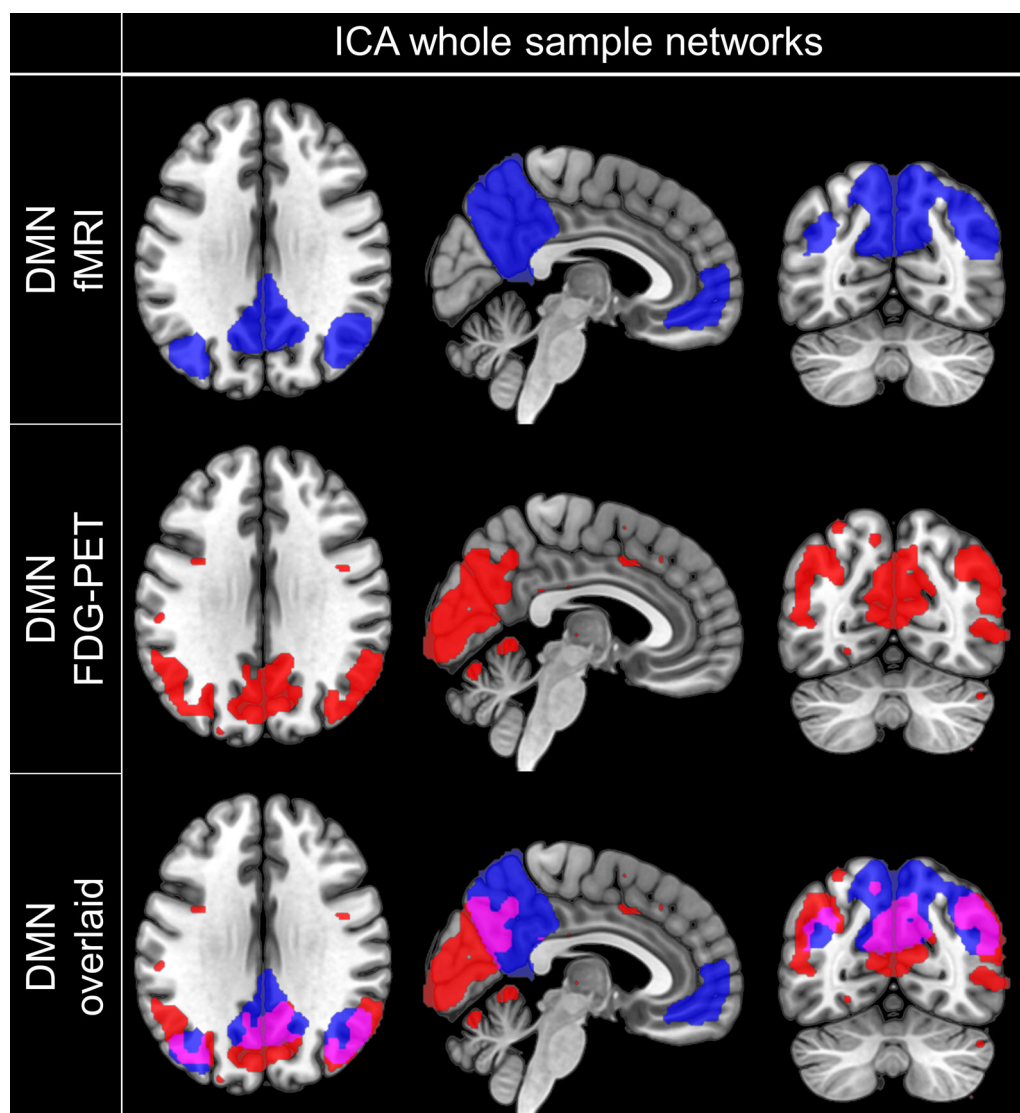


**FIGURE 2** Spatial coincidence of ICA-derived metabolic and functional DMN. Spatial distribution of components representing the DMN obtained by fMRI (first row) or FDG-PET (second row) and their spatial correspondence (third row). Masks were created by thresholding the component-specific group maps at  $z = 2$  and overlaid on a T1-weighted MNI template for visualization. Neurological view. DMN, default mode network; ICA, independent component analysis; FDG-PET, Fluorodeoxyglucose positron emission tomography

between healthy controls, cognitively normal patients and patients with MCI, significant differences in metabolic activity were identified between the groups for all ROIs (Figure 3, Kruskal-Wallis test,  $p < .05$ , Table S4). For all DMN regions, a significant trend towards an increment of metabolic deficits from healthy controls via unimpaired patients to patients with MCI was identified (Figure 3, Jonckheere-Terpstra test;  $p < .01$ , Table S4). The identified trend, which indicated stronger metabolic deficits with increasing cognitive impairment remained significant after controlling for UPDRS-III scores, disease duration and LEDD in patients (Table S4). The most profound metabolic deficits between both patient groups and healthy controls were found in the PC (pairwise Wilcoxon test; HC vs. PD-NC difference in location: 0.17 [0.10; 0.25]  $p < .001$  (all  $p$  values Bonferroni-Holm adjusted); HC versus PD-MCI: 0.24 [0.17; 0.36]  $p < .0001$ , the right

posterior superior supramarginal gyrus (pSMGr; HC vs. PD-NC: 0.20 [0.10; 0.27]  $p < .0001$ ; HC vs. PD-MCI: 0.22 [0.10; 0.34]  $p = .001$ ) and right superior lateral occipital cortex (sLOC; HC vs. PD-NC: 0.16 [0.09; 0.23]  $p < .0001$ ; HC vs. PD-MCI: 0.22 [0.15; 0.31]  $p < .0001$ ) as well as the right angular gyrus (AGr; HC vs. PD-NC: 0.18 [0.09; 0.27]  $p < .001$ ; HC vs. PD-MCI: 0.26 [0.16; 0.38]  $p < .001$ ). Although the decreasing trend was significant, visual inspection of mean FDG uptake values revealed that for some regions only minor between-group differences were found between cognitively unimpaired and impaired patients, especially for ROIs that were exclusively found to be part of the network in the fMRI analysis but not the FDG-PET component (mPFC, parahippocampal cortex left [ParaHL], parahippocampal cortex right [ParaHR], and superior frontal gyrus right [SFGr]).

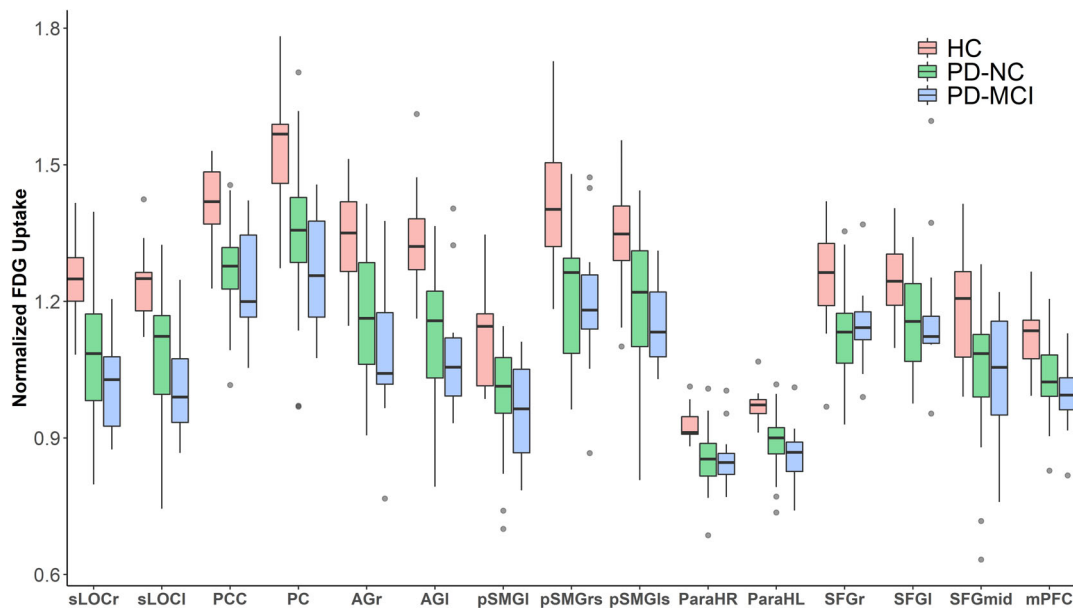


**FIGURE 3** Metabolic DMN activity in HC ( $n = 16$ ), PD-NC ( $n = 36$ ), and PD patients with MCI ( $n = 12$ ). In PD patients, normalized regional FDG uptake was significantly reduced in all DMN nodes when compared to healthy controls. For all ROIs, a significant trend towards a progressive metabolic deficit from healthy controls via cognitively unimpaired patients to MCI patients was observed (Jonckheere–Terpstra test  $p < .01$ ). Grey colored dots indicate outliers (defined as  $>1.5$  times the interquartile distance range). AGI, angular gyrus left; AGr, angular gyrus right; HC, healthy controls; mPFC, medial prefrontal cortex; ParaHL, parahippocampal cortex left; ParaHR, parahippocampal cortex right; PC, precuneus cortex; PCC, posterior cingulate cortex; PD-MCI, PD patients with mild cognitive impairment; PD-NC, PD patients with normal cognition; pSMGI, posterior supramarginal gyrus left; pSMGLs, posterior supramarginal gyrus left superior; pSMGrs, posterior supramarginal gyrus right superior; SFGI, superior frontal gyrus left; SFG mid, superior frontal gyrus mid; SFGGr, superior frontal gyrus right; sLOCI, superior lateral occipital cortex left; sLOCr, superior lateral occipital cortex right

### 3.4 | Metabolic connectivity is altered in PD-NC and changes proceed in PD-MCI

An exploratory analysis of interregional metabolic connectivity between DMN ROIs revealed gradually changing differences in network coherency between healthy controls and the groups of cognitively unimpaired and impaired PD patients. Patients with normal cognition exhibited an increased metabolic connectivity between the SFGGr and posterior DMN regions, especially the AGr ( $z = 2.61$ ,  $p$  value = .009; Figure 4a). These changes were also found in patients with MCI compared to HC and the reported differences were of stronger magnitude in this patient group, especially for the AGr ( $z = -3.56$ ,  $p$  value  $<.001$ ), the posterior division of the left superior supramarginal gyrus (pSMGLs;  $z = -2.13$ ,  $p$  value = .033), and the left superior occipital cortex (sLOCI;  $z = -2.03$ ,  $p$  value = .043; Figure 4b). Patients with MCI further showed a significantly higher correlation between the SFGGr and the PC ( $z = -2.13$ ,  $p$  value = .033) compared to unimpaired patients (Figure 4c). In addition to this increase along fronto-parietal connections, an increased correlation of regional metabolic activity was observed between posterior DMN regions in both patient groups compared to healthy controls (Figure 4a,b). Cognitively normal and impaired patients showed a trend towards an increased metabolic connectivity between the AGr and the sLOCr compared to controls (PD-NC:  $z = -3.02$ ,  $p = .003$ ; PD-MCI:  $z = -1.57$ ,  $p = .116$ );

patients with MCI additionally between the PC and sLOCr ( $z = -2.02$ ,  $p$  value = .043; Figure 4a,b). In addition, patients without cognitive impairment exhibited a significantly increased metabolic connectivity between the ParaHL and posterior DMN regions, especially the left posterior supramarginal gyrus (pSMGI;  $z = 2.57$ ,  $p$  value = .010) and sLOCI ( $z = 2.42$ ,  $p$  value = .015). The latter observations were not observed in patients with MCI (Figure 4a,b). By contrast, in patients with MCI decreased metabolic connectivity was found between the ParaHR and mostly posterior DMN regions, including the pSMGI ( $z = 2.48$ ,  $p$  value = .013) and left angular gyrus (AGI;  $z = 2.01$ ,  $p$  value = .045), in comparison to cognitively unimpaired patients (Figure 4c).

### 3.5 | Posterior and fronto-parietal functional hyperconnectivity proceeds in PD-MCI

A comparison of interregional hemodynamic correlations among 15 ICA-derived DMN ROIs between the three groups revealed primarily an increase of functional connectivity along fronto-parietal connections in cognitively impaired patients compared to unimpaired patients and healthy controls. In patients without MCI, an increased functional connectivity between the PC and the sLOCI was observed in comparison to controls (Figure 5a-1,  $p_{\text{uncorr}} = .041$ ). Patients with

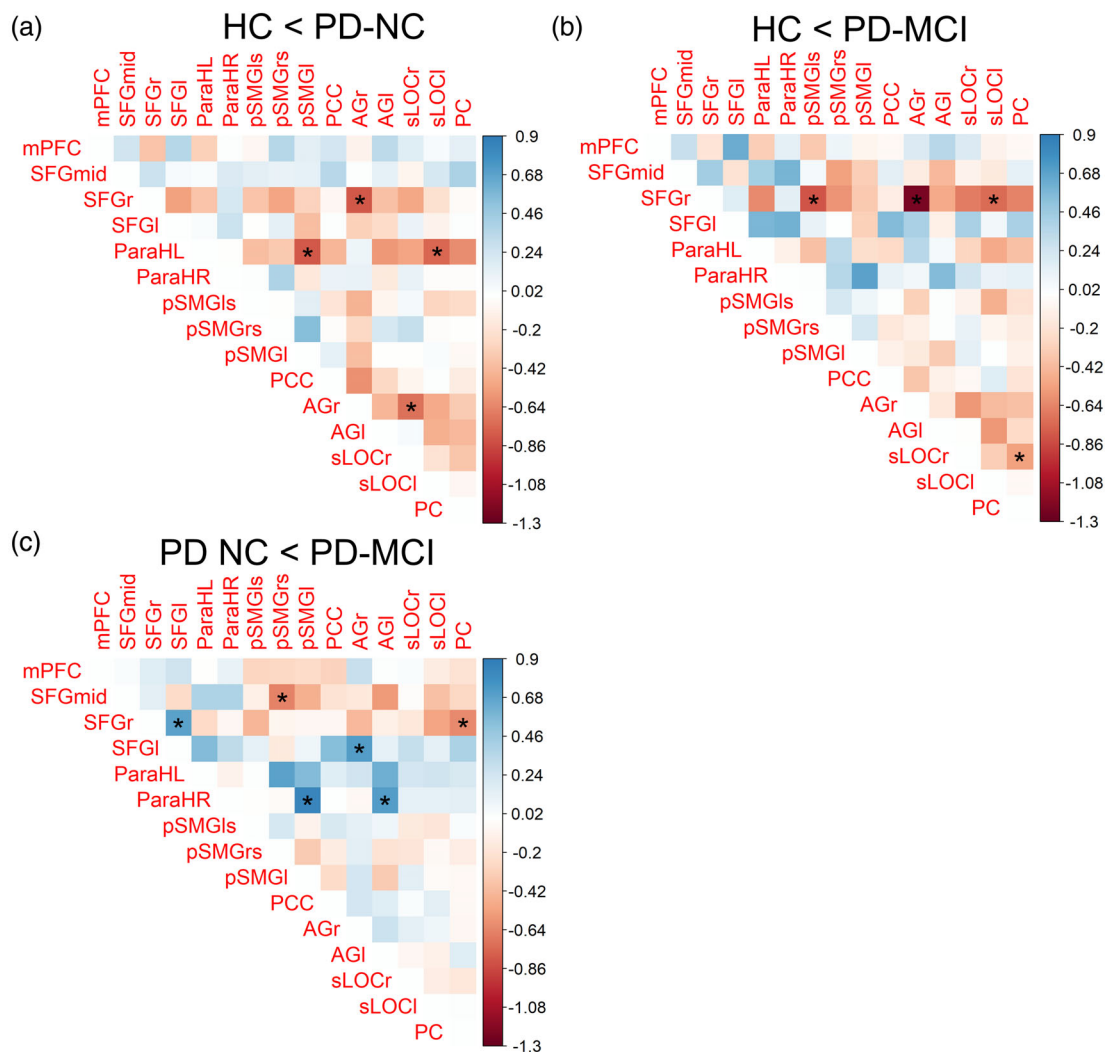


**FIGURE 4** Group differences in metabolic connectivity of DMN ROIs between healthy controls and cognitively impaired (PD-MCI) or unimpaired (PD-NC) PD patients. Color scale indicates the difference in correlation coefficients between the groups. Correlation coefficients were compared by Fisher's z test; \*significant at  $p < .05$ . AGl, angular gyrus left; AGr, angular gyrus right; mPFC, medial prefrontal cortex; ParaHL, parahippocampal cortex left; ParaHR, parahippocampal cortex right; PC, precuneus cortex; PCC, posterior cingulate cortex; PD-MCI, PD patients with mild cognitive impairment; PD-NC, PD patients with normal cognition; pSMGI, posterior supramarginal gyrus left; pSMGls, posterior supramarginal gyrus left superior; pSMGrs, posterior supramarginal gyrus right superior; SFGl, superior frontal gyrus left; SFG mid, superior frontal gyrus mid; SFGr, superior frontal gyrus right; sLOCl, superior lateral occipital cortex left; sLOCr, superior lateral occipital cortex right

normal cognition further showed decreased functional connectivity of the AGr and the PCC ( $p_{FDR} = 0.013$ ), ParaHL and the left superior frontal gyrus (SFGl;  $p_{uncorr} = .024$ ), and between both the AGl ( $p_{uncorr} = 0.046$ ) and the pSMGrs ( $p_{uncorr} = .043$ ) and the ParaHR compared to controls (Figure 5a-1 and Table 3). In addition, functional connectivity between the SFGr and both, the PCC ( $p_{uncorr} = .011$ ) and AGr ( $p_{FDR} = .047$ ) was reduced in PD-NC patients compared to controls. In patients with cognitive impairment, increased functional connectivity was additionally found between the SFGl and the PC ( $p_{uncorr} = .043$ ) and between the pSMGls and SFGr ( $p_{uncorr} = .005$ ) as well as between the mPFC and both the AGr and SFGl compared to controls (Figure 5a-2,  $p_{uncorr} < .05$ ). Reductions of functional connectivity were found in PD-MCI patients compared to controls between the pSMGrs and SFGl ( $p_{uncorr} = .033$ ).

A direct comparison of DMN ROI-based connectivity among both patient groups revealed an increased functional connectivity in MCI patients between each of the following ROIs: PC, right AG, and PCC (Figure 5a-3 and Table 3). In addition, the PC was correlated stronger with the ParaHL ( $p_{uncorr} = .013$ ), the PCC with the mPFC ( $p_{uncorr} = .021$ ) and the AGr with the SFGl ( $p_{FDR} = .030$ ) in patients with MCI (Figure 5a-3 and Table 3). The reported differences among both patient groups remained significant after controlling for UPDRS-III, disease duration and LEDD (Figure S3). No significant decreases of functional connectivity were observed in patients with MCI compared to patients with normal cognition among DMN regions. Similar findings were observed when group differences were analyzed in a larger rsfMRI sample which had not undergone FDG-PET scanning (Figure S2).

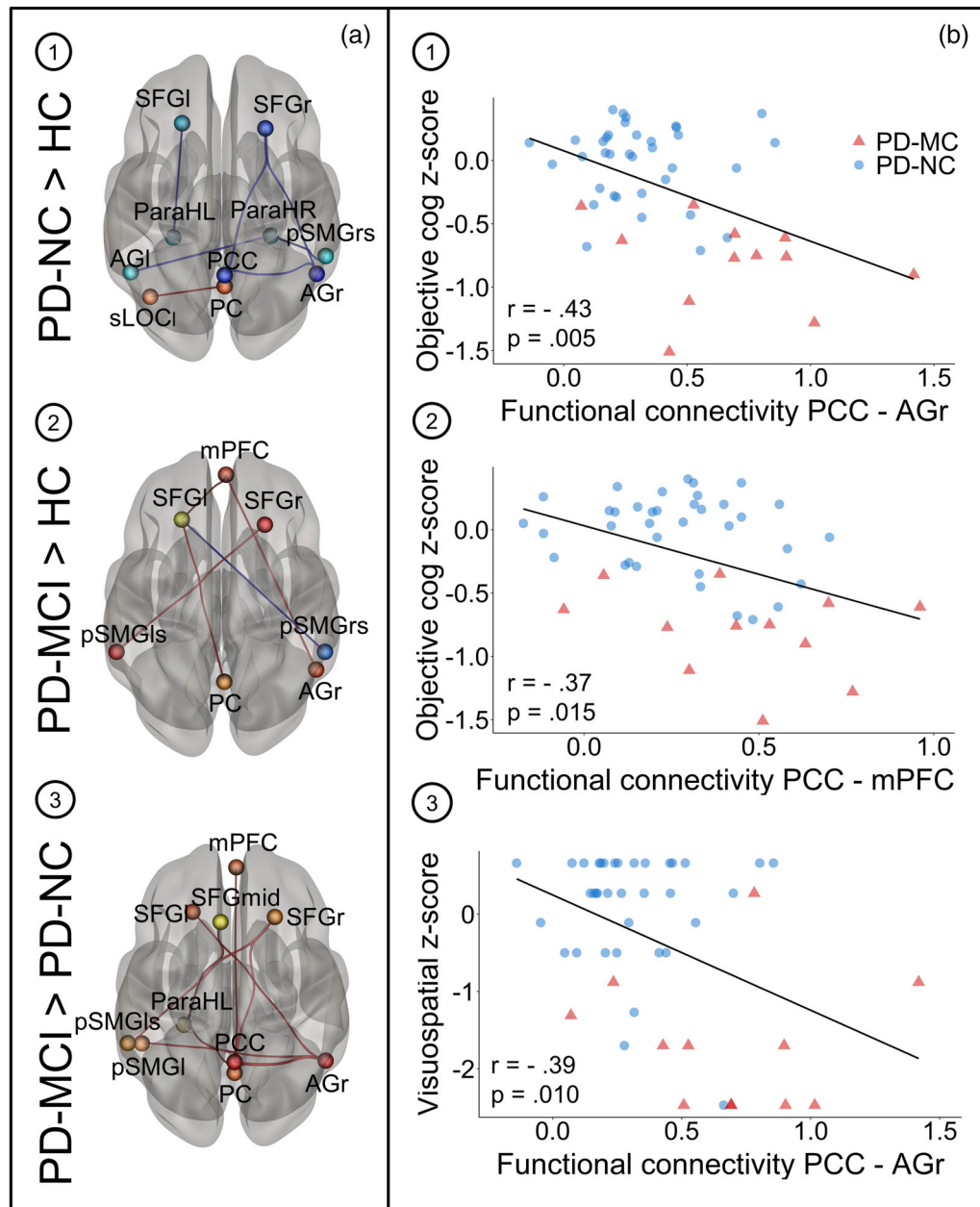


**FIGURE 5** (a) Group differences in functional connectivity of DMN ROIs between healthy controls ( $n = 16$ ) and cognitively impaired ( $n = 13$ ) and unimpaired ( $n = 36$ ) PD patients. Between-group differences were tested two-sided with threshold set at  $p$  uncorrected or FDR-corrected  $< .05$ . Connections shown in red represent increased connectivity strength, blue connections refer to the opposite contrast. ROIs' sizes do not indicate the actual ROI diameters. Results are shown in 3D view from superior perspective. Neurological view. (b) Correlation plots showing significant negative correlations between functional connectivity and cognitive z-scores in PD patients for the following connections and z-scores: (1) PCC-AGr and cognitive composite z-scores, (2) PCC-mPFC and cognitive composite z-scores and (3) PCC-AGr and visuospatial z-scores. Pearson's correlation coefficients and  $p$  values are shown on the bottom left in each plot. AGI, angular gyrus left; AGr, angular gyrus right; mPFC, medial prefrontal cortex; ParaHL, parahippocampal cortex left; ParaHR, parahippocampal cortex right; PC, precuneus cortex; PCC, posterior cingulate cortex; PD-MCI, PD patients with mild cognitive impairment; PD-NC, PD patients with normal cognition; pSMGI, posterior supramarginal gyrus left; pSMGls, posterior supramarginal gyrus left superior; pSMGrs, posterior supramarginal gyrus right superior; SFGI, superior frontal gyrus left; SFG mid, superior frontal gyrus mid; SFGGr, superior frontal gyrus right; sLOCi, superior lateral occipital cortex right

### 3.6 | DMN hyperconnectivity is associated with cognitive impairment in PD patients

An exploratory partial correlation analysis between domain-specific cognitive z-scores, metabolic activity and functional connectivity

revealed significant negative associations between DMN functional connectivity and cognitive composite z-scores as well as positive associations between DMN metabolic activity and cognitive composite z-scores in patients. Cognitive composite z-scores correlated significantly with functional connectivity between the (a) PCC and AGr

**TABLE 3** Statistics of ROI-based functional connectivity analysis between healthy controls ( $n = 16$ ) and cognitively impaired ( $n = 12$ ) and unimpaired PD patients ( $n = 36$ )

Contrast and regions	tstatistic	$p_{uncorr}$	$p_{FDR}$
PD-MCI > PD-NC			
Seed AGr			
PCC	4.27	.0001	.0013
SFGI	3.00	.0043	.0301
PC	2.47	.0172	.0725
pSMGI	2.40	.0207	.0725
Seed PCC			
AGr	4.27	.0001	.0013
PC	2.89	.0059	.0411
SFGr	2.53	.0149	.0696
mPFC	2.39	.0210	.0733
Seed PC			
PCC	2.89	.0059	.0803
ParaHL	2.58	.0131	.0803
AGr	2.47	.0172	.0803
Seed mPFC			
PCC	2.39	.0210	.2934
Seed SFGI			
AGr	3.00	.0043	.0603
Seed SFGr			
PCC	2.53	.0149	.1868
pSMGls	2.29	.0267	.1868
Seed pSMGls			
SFGr	2.29	.0267	.3736
ParaHL			
PC	2.58	.0131	.1838
SFGmid	2.13	.0386	.2699
Seed pSMGI			
AGr	2.40	.0207	.2899
Seed SFG mid			
ParaHL	2.13	.0386	.5399
PD-NC > HC			
Seed AGr			
PCC	-3.51	.0010	.0134
SFGr	-3.08	.0034	.0237
Seed SFGI			
ParaHL	-2.33	.0237	.3320
Seed PC			
sLOCI	2.10	.0411	.5366
Seed PCC			
AGr	-3.51	.0010	.0134
SFGr	-2.63	.0113	.0791
Seed SFGr			
AGr	-3.08	.0034	.0474
PCC	-2.63	.0113	.0791



**TABLE 3** (Continued)

Contrast and regions	tstatistic	<i>p</i> <sub>uncorr</sub>	<i>p</i> <sub>FDR</sub>
Seed ParaHL			
SFGl	−2.33	.0237	.2725
Seed AGl			
ParaHR	−2.05	.0457	.6404
Seed sLOCl			
PC	2.10	.0411	.4504
Seed ParaHR			
pSMGrS	−2.07	.0434	.3202
AGl	−2.05	.0457	.3202
PD-MCI > HC			
Seed AGr			
mPFC	2.23	.0349	.3307
Seed pSMGls			
SFGr	3.08	.0048	.0678
Seed SFGl			
mPFC	2.46	.0208	.2005
PC	2.13	.0430	.2005
pSMGrS	−2.25	.0334	.2005
Seed SFGr			
pSMGls	3.08	.0048	.0678
Seed PC			
SFGl	2.13	.0430	.4733
Seed mPFC			
SFGl	2.46	.0208	.2445
AGr	2.23	.0349	.2445
Seed pSMGrS			
SFGl	−2.25	.0334	.4680

Abbreviations: AGl, angular gyrus left; AGr, angular gyrus right; FDR, false discovery rate; mPFC, medial prefrontal cortex; ParaHL, parahippocampal cortex left; ParaHR, parahippocampal cortex right; PC, precuneus cortex; PCC, posterior cingulate cortex; PD-MCI, PD patients with mild cognitive impairment; PD-NC, PD patients with normal cognition; pSMGl, posterior supramarginal gyrus left; pSMGls, posterior supramarginal gyrus left superior; pSMGrS, posterior supramarginal gyrus right superior; SFGl, superior frontal gyrus left; SFG mid, superior frontal gyrus mid; SFGr, superior frontal gyrus right; sLOCl, superior lateral occipital cortex left; sLOCr, superior lateral occipital cortex right.

( $r = -.43$ ,  $p = .005$ , Figure 5b-1), (b) PCC and mPFC ( $r = -.37$ ,  $p = .015$ , Figure 5b-2), and (c) AGr and SFGl ( $r = -.32$ ,  $p = .040$ ) when controlling for age, sex, LEDD, UPDRS-III, disease duration, and BDI-II. Visuo-spatial z-scores also showed a significant linear association with the functional connectivity between the AGr and PCC ( $r = -.39$ ,  $p = .010$ , Figure 5b-3) and the connectivity between the AGr and SFGl ( $r = -.33$ ,  $p = .032$ ). A negative association was identified between the attention domain z-scores and the functional connections PC-PCC ( $r = -.32$ ,  $p = .037$ ) and ParaHL-PC ( $r = -.33$ ,  $p = 0.034$ ). By contrast, only the executive domain z-scores correlated positively with metabolic activity, especially in the sLOCl ( $r = .50$ ,  $p = .001$ ), sLOCr ( $r = .33$ ,  $p = .031$ ), PC ( $r = .36$ ,  $p = .019$ ), SFGl ( $r = .36$ ,  $p = .019$ ), pSMGls ( $r = .55$ ,  $p < .001$ ), and AGl ( $r = .31$ ,  $p = .042$ ). No significant correlation was observed between functional connectivity and UPDRS-III scores, LEDD or disease duration. In posterior DMN regions (pSMGrS, AGl,

AGr, pSMGls, and sLOCr) and SFGl metabolic activity negatively correlated with disease severity, quantified by UPDRS-III, LEDD, and disease duration.

## 4 | DISCUSSION

In the current study, we applied a multivariate ICA approach on both fMRI and FDG-PET data of healthy controls and PD patients with and without MCI to study consistency and differences in DMN abnormalities related to cognitive symptoms in PD. Post-hoc ROI-based analyses were performed to unravel the relation between local glucose consumption, interregional metabolic and functional connectivity in controls and a well-characterized PD cohort. Particularly, we opened new perspectives by clarifying if disease related changes in functional

connectivity within the DMN are accompanied by similar changes in metabolic connectivity and associated with metabolic deficits in PD patients with and without MCI. In contrast to previous analysis in this cohort, we focused on the comprehensive neuropsychological data, methodologically applied a completely data-driven ICA approach to FDG-PET and rsMRI data to obtain study-specific DMN components and performed interregional metabolic analyses.

In line with PETMRI hybrid studies in healthy controls, we found a fair spatial correspondence of the DMN in resting-state FDG-PET and fMRI data in the analyzed subjects, with higher spatial convergence in parieto-occipital regions. Focusing on DMN metabolic activity, we encountered a gradual metabolic decline in all DMN ROIs, with strongest metabolic deficits in the posterior DMN in PD-MCI. By integrating both modalities, we provide first evidence for a predominant increase in hemodynamic and metabolic network coherency between posterior DMN regions, including the PC, AG, and the sLOC and the frontal cortex in cognitively impaired patients compared to unimpaired patients and healthy controls. Fronto-parietal interregional correlations revealed by both modalities were elevated in unimpaired patients and proceeded (i.e., further increased) in cognitively impaired patients, while reduced connectivity of the parahippocampal gyri in PD-MCI was exclusively observed in the PET modality. Increased functional connectivity along fronto-parietal connections and in the posterior DMN was significantly associated with worse cognitive functions in PD patients.

The present study partly continues, and answers questions raised in response to our previous study, which hinted at an involvement of DMN regions in cognitive symptoms of PD and a relation between functional network degeneration and metabolic activity (Ruppert et al., 2020). The current study for the first time clarifies the commonalities of both measures of brain network activity and their individual significance for cognitive symptoms in PD. Our results highlight how multimodal resting-state studies can provide new insights into the (patho-)physiological network organization of brain activity by confirming insights obtained with one modality but also how multimodal approaches can deepen our understanding of disease processes.

#### 4.1 | Spatial convergence of metabolic and hemodynamic DMN

In the current study, fair spatial correspondence was detected between metabolic covariance across subjects and coherent hemodynamic fluctuations within the DMN in a subset of 16 healthy controls and 16 PD patients. These observations stand in accordance with a previous hybrid scanner study which reported a moderate spatial convergence between metabolic covariance and fMRI-derived DMN patterns in simultaneously acquired data sets of 22 healthy, mid-aged subjects (Savio et al., 2017). Interestingly, Savio et al. (2017) found similar differences between the FDG-PET- and fMRI-derived DMN: prefrontal clusters were smaller in the FDG-PET modality but included more medial frontal regions, and parts of the cerebellar cortex were only found with FDG-PET (Figure 2). In line with the present findings,

Di and Biswal (2012) described only posterior DMN regions in an FDG-PET ICA, while the medial prefrontal cortex was included in the corresponding fMRI DMN component. In contrast, by conducting a comparable ICA (GIFT, five components) in 35 mid-aged healthy subjects, Yakushev et al. (2013) observed the typical DMN topology in FDG-PET data with extensive involvement of the prefrontal cortex. The fact that a similar spatial overlap can be identified in independently or simultaneously acquired images and across different age ranges supports the hypothesis that metabolic networks, characterized by common covariance across subjects, can robustly be detected in the resting human brain. This underscores the assumption that, at least in posterior parts of the DMN, synchronous hemodynamic fluctuations at rest are a result of coherent neural activity. Residual differences in network distribution between both modalities might be related to the overall different methodology of network identification by using static FDG-PET data (one image per subject) or fMRI-data (image timeseries per subject). The selection of included FDG-PET frames and further parameters of the acquisition protocol (e.g., time spent after radioligand injection) might also have a critical influence on network analysis and might provoke discrepancies among different studies.

#### 4.2 | Reduced FDG uptake in DMN ROIs is associated with network-level changes in PD

Here, we report significantly reduced FDG uptake in all DMN regions in patients with normal cognition and a significant trend towards a progressive decline in PD-MCI patients. The observation of frontal and occipito-parietal hypometabolism in PD-MCI compared to patients with normal cognition stands in accordance with previous studies emphasizing parietal, occipital, temporal and frontal metabolic decreases as classical features observed in PD-MCI (Hosokai et al., 2009; Huang et al., 2008; Lyoo, Jeong, Ryu, Rinne, & Lee, 2010; Pappatà et al., 2011), which further progress in PD dementia (Garcia-Garcia et al., 2012) and are independent from medicative status (Pappatà et al., 2011). In addition, comparable studies report similar but limited metabolic changes in patients with normal cognition compared to healthy controls (Garcia-Garcia et al., 2012; Hosokai et al., 2009; Huang et al., 2008; Pappatà et al., 2011).

Interestingly, regions in which the strongest metabolic deficits and gradual decline were observed in comparison to controls (PC, sLOCr, AGr, and pSMGr), mainly including the posterior DMN, also showed the strongest increases in both metabolic and functional connectivity, indicating a link between degenerative processes on one hand and network reorganization on the other hand. All these regions were found to be part of both the metabolic covariance pattern and the fMRI component. By contrast, in regions which showed only a minor difference in glucose metabolism between patient groups (e.g., ParaHR), a reduced metabolic connectivity was found in patients with MCI compared to both healthy controls and unimpaired patients. Further, the latter regions were also not identified as parts of the metabolic DMN component.



### 4.3 | Metabolic and functional network alterations in the posterior DMN in PD with and without cognitive impairment

When functional and metabolic connectivity within the DMN were compared between healthy controls and both groups of PD patients, several similarities between both measures of coherent network activity were identified. In both modalities, PD patients with and without MCI in their OFF-state exhibited an increased correlation between frontal and posterior DMN regions in comparison to controls. Increased functional connectivity, for example, between the SFG and pSMGs, was accompanied by similar changes in metabolic connectivity in PD-MCI compared to controls. By contrast, decreased metabolic correlation was observed between the PC and the left SFG, but functional connectivity was increased in PD-MCI compared to controls. Although significantly increased functional connectivity was observed between the AGr and PCC in PD-MCI compared to PD-NC, no increased metabolic correlation was detected between these regions. On the other hand, while strikingly decreased metabolic covariance of the ParaHR with the pSMG and AGI was observed in PD-MCI compared to PD-NC, no decreased functional connectivity was noticed.

The increased interregional metabolic correlations in posterior DMN regions in PD patients detected here stand in accordance with observations from Sala et al. (2017) who reported enhanced metabolic coupling in the posterior cortex in PD patients with normal cognition compared to age-matched controls. Additionally, Baggio et al. (2015) revealed an increased functional correlation between the DMN and posterior cortical regions, including the bilateral dorsal precuneus, posterior cingulate gyrus, and superior occipital areas involving the occipito-parietal junctions in PD patients with and without cognitive impairment compared to controls. Of note, the authors found a significant negative association between these functional connectivity alterations and visuospatial performance in PD (Baggio et al., 2015). In the current study, we observed a significant increase in functional connectivity along fronto-parietal connections in PD-MCI compared to PD-NC and healthy controls and a comparable association between the functional connectivity of the PC, PCC, and mPFC and objective cognition in PD patients. Similarly, Zhan et al. (2018) reported an increased functional connectivity between the PCC and the bilateral mid frontal gyri, middle temporal gyrus, left precuneus, and posterior cerebellum in cognitively impaired PD patients compared to unimpaired patients. An rsfMRI study of early PD patients by Caso et al. (2013) also revealed an increased connectivity within DMN regions, including the temporal gyri, hippocampus and parahippocampus, precuneus, and the cingulate cortices in comparison to healthy controls. The latter findings seem to contradict previous rsfMRI studies, which report decreased functional connectivity of DMN regions, for example, the IPL, medial-temporal lobe and precuneus, but contrary to our study, most of the studies which reported decreased DMN functional connectivity in PD-MCI analyzed patients in their ON-state (Amboni et al., 2015; Lucas-Jiménez et al., 2016). Dopaminergic impact on DMN activity has been reported by previous studies (Krajcovicova et al., 2012) and a few studies

hinted at a modulatory role of dopamine which contributes to decreases in DMN connectivity (Conio et al., 2020). Further, the decreased metabolic connectivity between frontal regions belonging to the DMN component observed in our study is in line with findings by Sala et al. (2017), who revealed reduced frontal metabolic coupling in several important resting-state networks in PD.

By integrating both measures of network coherency and local glucose metabolism, it becomes clear that DMN dysfunction—characterized by increased connectivity between frontal and parietal regions—and concurrent local metabolic deficits represent a PD-related phenomenon occurring in the absence of cognitive impairment. The occurrence of MCI is not solely explained by more profound local metabolic changes but accompanied by additional alterations in network parameters. In particular, strongly decreased metabolic connectivity is evident between the parahippocampal areas and the parietal cortex, and stronger fronto-parietal synchronization is identified with both modalities at this stage. Previous studies suggested that decreased metabolic connectivity in the frontal cortex and occipital hyperconnectivity might have compensatory effects in cognitively unimpaired PD patients (Sala et al., 2017). By contrast, functional connectivity within the posterior DMN and fronto-parietal synchronization further increased with worse cognitive functioning in PD-MCI in the present cohort. It could thus be speculated that increased posterior synchronization represents a contributor for cognitive impairment rather than a compensatory mechanism for cognitive function in PD patients. In support of this hypothesis, Gardini et al. (2015) speculated that an increased functional connectivity between the PCC and the medio-temporal lobe, which they observed in MCI patients, might represent a maladaptive response to neurodegenerative processes, for example, atrophy.

This corresponds with recently published longitudinal studies of cortical thinning in PD, which report reduced cortical thickness in occipital and parietal lobes in PD patients with normal cognition and additional thinning of frontotemporal regions in cognitively impaired patients (Filippi et al., 2020; Gorges et al., 2020). In PD patients with conversion to MCI, cortical thinning was observed in the precuneus and posterior cingulum, medial and superior frontal gyri, and supramarginal gyri (Filippi et al., 2020), key regions of the DMN for which dysregulated network connectivity was observed in the present study. In line with the first appearance of hippocampal metabolic dysconnectivity and increasing frontoparietal connectivity alterations at the MCI stage reported here, Filippi et al. (2020) highlight structural changes of the hippocampus and fronto-temporo-parietal regions as key drivers of cognitive impairment. Gorges et al. (2020) provide evidence of cortical thinning in anterior DMN regions in baseline MRI scans of PD patients who developed cognitive impairment compared to patients who remained cognitively stable. Cortical thinning confined to the anterior cingulate cortex was associated with cognitive performance and may be an early predictor of future cognitive impairment (Gorges et al., 2020) and the aforementioned functional imbalance in PD. At some point, the imbalance induced by fronto-parietal synchronization and parahippocampal desynchronization proceeds and normal cognition can no longer be maintained. The increased

coherent DMN activity in PD patients in the OFF-state reported in the current study may be related to the inability to deactivate during cognitive tasks described by previous studies (Ibarretxe-Bilbao et al., 2011; van Eimeren, Monchi, Ballanger, & Strafella, 2009), which has also been linked to poor cognitive performance (Gardini et al., 2015).

Further studies including patients with PD dementia are required to resolve whether hyperconnectivity represents a phenomenon contributing to cognitive decline (Baggio et al., 2015) or maintaining cognitive function. In line with the increased metabolic connectivity within posterior cortical regions reported in the present study, including the SMG, sLOC and AG, Toussaint et al. (2012) also reported an increase in correlated metabolic activity between parietal and temporal hypometabolic regions in MCI patients with conversion to AD compared to controls. Another similarity between both studies is the increased correlation between frontal and parietal regions which was more pronounced in PD-MCI or MCI converters. Toussaint et al. (2012) found this alteration to break down during transition from MCI to AD. Another study reported increased metabolic correlation strength in the dorsal DMN in older subjects and less elevated measures in ApoE  $\epsilon$ 4 carriers or amyloid positive subjects with higher risk of suffering from AD (Arnemann, Stöber, Narayan, Rabinovici, & Jagust, 2018). Together with the current findings, it can be speculated that decreased metabolic activity and reorganization towards an increased coherent activity within posterior DMN regions might precede the clinical manifestation of MCI.

It is still an open question if there is a relation between cortical hypometabolism, network alterations, and PD pathology. For example, dopaminergic imaging studies reveal evidence for an involvement of striato-frontal pathway degeneration in frontal dysfunction (Hammes et al., 2019; Polito et al., 2012). Additionally, there might be a possible link between posterior cortical dysfunction and the degeneration of cholinergic pathways (Hilker et al., 2005; Klein et al., 2010). Particularly, volumetric studies of longitudinally obtained t1-weighted MRI scans revealed evidence for a role of basal forebrain cholinergic nuclei in the development of cognitive decline in PD (Ray et al., 2018). Since preliminary findings show a modulatory role of the basal forebrain for DMN activity (Nair et al., 2018), there might be a possible link to DMN dysregulation reported in the current study. Future studies, combining comprehensive analyses of multiple neurotransmitter systems, are highly warranted to complete our knowledge about network dysfunction in the PD spectrum.

#### 4.4 | Limitations and future directions

A limitation of the current study is the low number of controls which may restrain the identification of more significant differences between healthy controls and patients. Another critical point represents the fact that metabolic covariance studies focusing on static FDG-PET images are restricted to group-level analysis, resulting in one correlation measure per group in contrast to fMRI analysis, where interregional correlations can be assessed on a subject level. Since FDG-PET connectivity

measures are therefore quite rough and critically depend on the cohorts' homogeneity in image acquisition and preprocessing, the good spatial correspondence of multimodally obtained resting-state networks is remarkable. Further studies should combine dynamic FDG-PET acquisitions with fMRI to assess within-subject glucose dynamics. Recent investigations in animal models have shown the usefulness of constant infusion protocols in this context (Amend et al., 2019). Additionally, decreased metabolic connectivity in frontal regions of patients might have contributed to the fact that not all frontal regions were represented in the PET-DMN component. However, including only one group in the initial pattern derivation would have introduced bias for subsequent analysis. The patient groups examined in the current study did not differ in disease duration, motor impairment, LEDD and mood status. Therefore, it can be assumed that differences in cognitive performance were also not substantially driven by depressive mood. Finally, simultaneous acquisition of both modalities using hybrid PETMRI scanners would enable a more direct comparison of metabolic and functional resting brain activity. However, the adherence of standard conventions regarding subject instruction, scanner environment and cross-modal registration in the current study enabled a sufficient intra- and inter-subject comparability. Since there is mounting evidence that impairment of posterior cortical regions precedes cognitive symptoms (Williams-Gray et al., 2009), the present findings should be confirmed in longitudinal studies.

## 5 | CONCLUSION

To date, comprehensive studies that compare both functional and metabolic resting-state connectivity across subjects within the same PD cohort were still lacking, although combining modalities could complement the insights obtained with one modality and provide greater diagnostic accuracy. By performing interregional analysis in two modalities, we describe a spatial association between patterns of altered functional and metabolic DMN connectivity in PD patients with distinctly defined cognitive profiles in comparison to controls. While univariate FDG uptake was gradually reduced in PD patients, with PD-MCI patients showing the lowest metabolism in all DMN nodes, increased interregional metabolic and functional connectivity along fronto-parietal connections was found in PD-MCI compared to controls and unimpaired patients. Therefore, the data are suggestive of a relation between hypometabolism and network reorganization in cognitive decline, since they provide evidence for proceeding metabolic deficits and network synchrony within the DMN, associated with poorer cognitive performance. The current study for the first time clarifies the commonalities of both measures of brain network activity and their individual significance for cognitive symptoms in PD, highlighting the added value of multimodal resting-state network approaches for identifying prospective biomarkers.

## ACKNOWLEDGMENTS

This study received funding by the Deutsche Forschungsgemeinschaft (DFG) in context of the Clinical Research Group 219 (KFO

219, EG350/1-1). The authors would like to thank all participants who made the current work possible and colleagues who were involved in data acquisition. Open Access funding enabled and organized by Projekt DEAL.

## CONFLICT OF INTEREST

The authors declare no conflicts of interest.

## ETHICS STATEMENT

The study was approved by the local Ethics Committee of the University of Cologne and permission was given by the Federal Office for Radiation Protection (Ethical clearance number: EK12-265).

## DATA AVAILABILITY STATEMENT

The data set analysed in the present study will be made available by the corresponding author upon reasonable request.

## ORCID

Marina C. Ruppert  <https://orcid.org/0000-0002-9025-7058>

## REFERENCES

- Amboni, M., Tessitore, A., Esposito, F., Santangelo, G., Picillo, M., Vitale, C., ... Barone, P. (2015). Resting-state functional connectivity associated with mild cognitive impairment in Parkinson's disease. *Journal of Neurology*, 262(2), 425–434. <https://doi.org/10.1007/s00415-014-7591-5>
- Amend, M., Ionescu, T. M., Di, X., Pichler, B. J., Biswal, B. B., & Wehrl, H. F. (2019). Functional resting-state brain connectivity is accompanied by dynamic correlations of application-dependent 18FFDG PET-tracer fluctuations. *NeuroImage*, 196, 161–172. <https://doi.org/10.1016/j.neuroimage.2019.04.034>
- Arnemann, K. L., Stöber, F., Narayan, S., Rabinovici, G. D., & Jagust, W. J. (2018). Metabolic brain networks in aging and preclinical Alzheimer's disease. *NeuroImage Clinical*, 17, 987–999. <https://doi.org/10.1016/j.nicl.2017.12.037>
- Aschenbrenner, S., Tucha, O., & Lange, K. W. (2001). *RWT Regensburger Wortflüssigkeitstest*. Göttingen: Hogrefe Verlag für Psychologie.
- Baggio, H.-C., Segura, B., Sala-Llonch, R., Martí, M.-J., Valdeorola, F., Compta, Y., ... Junqué, C. (2015). Cognitive impairment and resting-state network connectivity in Parkinson's disease. *Human Brain Mapping*, 36(1), 199–212. <https://doi.org/10.1002/hbm.22622>
- Beck, A. T., Steer, R. A., & Brown, G. K. (1996). *Manual for the beck depression inventory-II*. San Antonio, TX: Psychological Corporation.
- Behzadi, Y., Restom, K., Liu, J., & Liu, T. T. (2007). A component based noise correction method (CompCor) for BOLD and perfusion based fMRI. *NeuroImage*, 37, 90–101.
- Biswal, B. B., Mennes, M., Zuo, X.-N., Gohel, S., Kelly, C., Smith, S. M., ... Milham, M. P. (2010). Toward discovery science of human brain function. *Proceedings of the National Academy of Sciences of the United States of America*, 107(10), 4734–4739. <https://doi.org/10.1073/pnas.0911855107>
- Borghammer, P., Chakravarty, M., Jonsdottir, K. Y., Sato, N., Matsuda, H., Ito, K., ... Gjedde, A. (2010). Cortical hypometabolism and hypoperfusion in Parkinson's disease is extensive: Probably even at early disease stages. *Brain Structure & Function*, 214(4), 303–317. <https://doi.org/10.1007/s00429-010-0246-0>
- Brett, M., Anton, J. L., Valabregue, R., & Poline, J.-B. (2002, June). Region of interest analysis using an SPM toolbox [abstract]. Presented at the 8th International Conference on Functional Mapping of the Human Brain, (Vol. 16, No. 2), Sendai, Japan. Available on CD-ROM in NeuroImage.
- Caso, F., Agosta, F., Inuggi, A., Tomic, A., Stankovic, I., Canu, E., ... Filippi, M. (2013). Dysfunction of the default mode network in early Parkinson's disease: A resting state fMRI study (P06.081). *Neurology*, 80(Suppl. 7), P06.081.
- Clark, C. M., & Stoessl, A. J. (1986). Glucose use correlations: A matter of inference. *Journal of Cerebral Blood Flow & Metabolism*, 6(4), 511–512. <https://doi.org/10.1038/jcbfm.1986.87>
- Conio, B., Martino, M., Magioncalda, P., Escelsior, A., Inglese, M., Amore, M., & Northoff, G. (2020). Opposite effects of dopamine and serotonin on resting-state networks: Review and implications for psychiatric disorders. *Molecular Psychiatry*, 25(1), 82–93. <https://doi.org/10.1038/s41380-019-0406-4>
- Della Rosa, P. A., Cerami, C., Gallivanone, F., Prestia, A., Caroli, A., Castiglioni, I., ... Perani, D. (2014). A standardized 18F-FDG-PET template for spatial normalization in statistical parametric mapping of dementia. *Neuroinformatics*, 12(4), 575–593. <https://doi.org/10.1007/s12021-014-9235-4>
- Di, X., & Biswal, B. B. (2012). Metabolic brain covariant networks as revealed by FDG-PET with reference to resting-state fMRI networks. *Brain Connectivity*, 2(5), 275–283. <https://doi.org/10.1089/brain.2012.0086>
- Emre, M., Aarsland, D., Brown, R., Burn, D. J., Duyckaerts, C., Mizuno, Y., ... Dubois, B. (2007). Clinical diagnostic criteria for dementia associated with Parkinson's disease. *Movement Disorders: Official Journal of the Movement Disorder Society*, 22(12), 1689–1707; quiz 1837. <https://doi.org/10.1002/mds.21507>
- Fahn, S., Elton, R. L., & UPDRS Program Members (1987). Unified Parkinson's disease rating scale. In S. Fahn, C. D. Marsden, M. Goldstein, & D. B. Calne (Eds.), *Recent developments in Parkinson's disease* (Vol. 2, pp. 153–163). Florham Park, NJ: Macmillan Health Care Information.
- Filippi, M., Canu, E., Donzuso, G., Stojkovic, T., Basaia, S., Stankovic, I., ... Agosta, F. (2020). Tracking cortical changes throughout cognitive decline in Parkinson's disease. *Movement Disorders: Official Journal of the Movement Disorder Society*, 35(11), 1987–1998. <https://doi.org/10.1002/mds.28228>
- Folstein, M. F., Folstein, S. E., & McHugh, P. R. (1975). Mini-mental state. *Journal of Psychiatric Research*, 12(3), 189–198. [https://doi.org/10.1016/0022-3956\(75\)90026-6](https://doi.org/10.1016/0022-3956(75)90026-6)
- García-García, D., Clavero, P., Gasca Salas, C., Lamet, I., Arbizu, J., Gonzalez-Redondo, R., ... Rodriguez-Oroz, M. C. (2012). Posterior parietooccipital hypometabolism may differentiate mild cognitive impairment from dementia in Parkinson's disease. *European Journal of Nuclear Medicine and Molecular Imaging*, 39(11), 1767–1777. <https://doi.org/10.1007/s00259-012-2198-5>
- Gardini, S., Venneri, A., Sambataro, F., Cuetos, F., Fasano, F., Marchi, M., ... Caffarra, P. (2015). Increased functional connectivity in the default mode network in mild cognitive impairment: A maladaptive compensatory mechanism associated with poor semantic memory performance. *Journal of Alzheimer's Disease*, 45(2), 457–470. <https://doi.org/10.3233/JAD-142547>
- Glaab, E., Trezzi, J.-P., Greuel, A., Jäger, C., Hodak, Z., Drzezga, A., ... Eggers, C. (2019). Integrative analysis of blood metabolomics and PET brain neuroimaging data for Parkinson's disease. *Neurobiology of Disease*, 124, 555–562. <https://doi.org/10.1016/j.nbd.2019.01.003>
- Goldman, J. G., Williams-Gray, C., Barker, R. A., Duda, J. E., & Galvin, J. E. (2014). The spectrum of cognitive impairment in Lewy body diseases. *Movement Disorders: Official Journal of the Movement Disorder Society*, 29(5), 608–621. <https://doi.org/10.1002/mds.25866>
- Goldman, J. G., Vernaleo, B. A., Camicioli, R., Dahodwala, N., Dobkin, R. D., Ellis, T., ... Simmonds, D. (2018). Cognitive impairment in Parkinson's disease: A report from a multidisciplinary symposium on unmet needs and future directions to maintain cognitive health. *NPJ Parkinson's Disease*, 4, 19. <https://doi.org/10.1038/s41531-018-0055-3>

- Gorges, M., Kunz, M. S., Müller, H.-P., Liepelt-Scarfone, I., Storch, A., Dodel, R., ... Kassubek, J. (2020). Longitudinal brain atrophy distribution in advanced Parkinson's disease: What makes the difference in "cognitive status" converters? *Human Brain Mapping*, 41(6), 1416–1434. <https://doi.org/10.1002/hbm.24884>
- Greuel, A., Trezzi, J.-P., Glaab, E., Ruppert, M. C., Maier, F., Jäger, C., ... Eggers, C. (2020). GBA variants in Parkinson's disease: Clinical, metabolomic, and multimodal neuroimaging phenotypes. *Movement Disorders: Official Journal of the Movement Disorder Society*, 35, 2201–2210. <https://doi.org/10.1002/mds.28225>
- Hammes, J., Theis, H., Giehl, K., Hoenig, M. C., Greuel, A., Tittgemeyer, M., ... van Eimeren, T. (2019). Dopamine metabolism of the nucleus accumbens and fronto-striatal connectivity modulate impulse control. *Brain: A Journal of Neurology*, 142(3), 733–743. <https://doi.org/10.1093/brain/awz007>
- Harris, M. E. (1990). *Wisconsin card sorting test computer version*. Odessa, FL: Psychological Assessment Resources.
- Härting, C., & Wechsler, D. (Eds.). (2000). *Wechsler-Gedächtnistest: revidierte Fassung—WMS-R; Manual; deutsche Adaptation der revidierten Fassung der Wechsler Memory scale* (1st ed.). Bern: Huber.
- Hely, M. A., Reid, W. G. J., Adena, M. A., Halliday, G. M., & Morris, J. G. L. (2008). The Sydney multicenter study of Parkinson's disease: The inevitability of dementia at 20 years. *Movement Disorders: Official Journal of the Movement Disorder Society*, 23(6), 837–844. <https://doi.org/10.1002/mds.21956>
- Hilker, R., Thomas, A. V., Klein, J. C., Weisenbach, S., Kalbe, E., Burghaus, L., ... Heiss, W. D. (2005). Dementia in Parkinson disease: Functional imaging of cholinergic and dopaminergic pathways. *Neurology*, 65(11), 1716–1722. <https://doi.org/10.1212/01.wnl.0000191154.78131.f6>
- Hoehn, M. M., & Yahr, M. D. (1967). Parkinsonism: Onset, progression and mortality. *Neurology*, 17(5), 427–442.
- Hohenfeld, C., Werner, C. J., & Reetz, K. (2018). Resting-state connectivity in neurodegenerative disorders: Is there potential for an imaging biomarker? *NeuroImage Clinical*, 18, 849–870. <https://doi.org/10.1016/j.nicl.2018.03.013>
- Hoogland, J., Boel, J. A., de Bie, R. M. A., Geskus, R. B., Schmand, B. A., Dalrymple-Alford, J. C., ... Geurtsen, G. J. (2017). Mild cognitive impairment as a risk factor for Parkinson's disease dementia. *Movement Disorders: Official Journal of the Movement Disorder Society*, 32(7), 1056–1065. <https://doi.org/10.1002/mds.27002>
- Horwitz, B., Grady, C. L., Schlageter, N. L., Duara, R., & Rapoport, S. I. (1987). Interrelations of regional cerebral glucose metabolic rates in Alzheimer's disease. *Brain Research*, 407(2), 294–306. [https://doi.org/10.1016/0006-8993\(87\)91107-3](https://doi.org/10.1016/0006-8993(87)91107-3)
- Hosokai, Y., Nishio, Y., Hirayama, K., Takeda, A., Ishioka, T., Sawada, Y., ... Mori, E. (2009). Distinct patterns of regional cerebral glucose metabolism in Parkinson's disease with and without mild cognitive impairment. *Movement Disorders: Official Journal of the Movement Disorder Society*, 24(6), 854–862. <https://doi.org/10.1002/mds.22444>
- Huang, C., Mattis, P., Perrine, K., Brown, N., Dhawan, V., & Eidelberg, D. (2008). Metabolic abnormalities associated with mild cognitive impairment in Parkinson disease. *Neurology*, 70(16 Pt 2), 1470–1477. <https://doi.org/10.1212/01.wnl.0000304050.05332.9c>
- Ibarretxe-Bilbao, N., Zarei, M., Junque, C., Marti, M. J., Segura, B., Vendrell, P., ... Tolosa, E. (2011). Dysfunctions of cerebral networks precede recognition memory deficits in early Parkinson's disease. *NeuroImage*, 57(2), 589–597. <https://doi.org/10.1016/j.neuroimage.2011.04.049>
- Kalbe, E., Calabrese, P., Kohn, N., Hilker, R., Riedel, O., Wittchen, H.-U., ... Kessler, J. (2008). Screening for cognitive deficits in Parkinson's disease with the Parkinson neuropsychometric dementia assessment (PANDA) instrument. *Parkinsonism & Related Disorders*, 14(2), 93–101. <https://doi.org/10.1016/j.parkreldis.2007.06.008>
- Kaplan, E. F., Googlass, H., & Weintraub, S. (1983). *The Boston naming test* (2nd ed.). Philadelphia: Lea & Febiger.
- Karunanayaka, P. R., Lee, E.-Y., Lewis, M. M., Sen, S., Eslinger, P. J., Yang, Q. X., & Huang, X. (2016). Default mode network differences between rigidity- and tremor-predominant Parkinson's disease. *Cortex: A Journal Devoted to the Study of the Nervous System and Behavior*, 81, 239–250. <https://doi.org/10.1016/j.cortex.2016.04.021>
- Klein, J. C., Eggers, C., Kalbe, E., Weisenbach, S., Hohmann, C., Vollmar, S., ... Hilker, R. (2010). Neurotransmitter changes in dementia with Lewy bodies and Parkinson disease dementia in vivo. *Neurology*, 74(11), 885–892. <https://doi.org/10.1212/WNL.0b013e3181d55f61>
- Krajcovicova, L., Mikl, M., Marecek, R., & Rektorova, I. (2012). The default mode network integrity in patients with Parkinson's disease is levodopa equivalent dose-dependent. *Journal of Neural Transmission (Vienna, Austria: 1996)*, 119(4), 443–454. <https://doi.org/10.1007/s00702-011-0723-5>
- Langston, J. W., Widner, H., Goetz, C. G., Brooks, D., Fahn, S., Freeman, T., & Watts, R. (1992). Core assessment program for intracerebral transplantations (CAPIT). *Movement Disorders: Official Journal of the Movement Disorder Society*, 7(1), 2–13. <https://doi.org/10.1002/mds.870070103>
- Levy, G., Tang, M.-X., Louis, E. D., Côté, L. J., Alfaró, B., Mejia, H., ... Marder, K. (2002). The association of incident dementia with mortality in PD. *Neurology*, 59(11), 1708–1713. <https://doi.org/10.1212/01.WNL.0000036610.36834.E0>
- Litvan, I., Goldman, J. G., Tröster, A. I., Schmand, B. A., Weintraub, D., Petersen, R. C., ... Emre, M. (2012). Diagnostic criteria for mild cognitive impairment in Parkinson's disease: Movement Disorder Society task force guidelines. *Movement Disorders: Official Journal of the Movement Disorder Society*, 27(3), 349–356. <https://doi.org/10.1002/mds.24893>
- Lopes, R., Delmaire, C., Defebvre, L., Moonen, A. J., Duits, A. A., Hofman, P., ... Dujardin, K. (2017). Cognitive phenotypes in parkinson's disease differ in terms of brain-network organization and connectivity. *Human Brain Mapping*, 38(3), 1604–1621. <https://doi.org/10.1002/hbm.23474>
- Lucas-Jiménez, O., Ojeda, N., Peña, J., Díez-Cirarda, M., Cabrera-Zubizarreta, A., Gómez-Esteban, J. C., ... Ibarretxe-Bilbao, N. (2016). Altered functional connectivity in the default mode network is associated with cognitive impairment and brain anatomical changes in Parkinson's disease. *Parkinsonism & Related Disorders*, 33, 58–64. <https://doi.org/10.1016/j.parkreldis.2016.09.012>
- Lyoo, C. H., Jeong, Y., Ryu, Y. H., Rinne, J. O., & Lee, M. S. (2010). Cerebral glucose metabolism of Parkinson's disease patients with mild cognitive impairment. *European Neurology*, 64(2), 65–73. <https://doi.org/10.1159/000315036>
- Nair, J., Klaassen, A.-L., Arato, J., Vyssotski, A. L., Harvey, M., & Rainer, G. (2018). Basal forebrain contributes to default mode network regulation. *Proceedings of the National Academy of Sciences of the United States of America*, 115(6), 1352–1357. <https://doi.org/10.1073/pnas.1712431115>
- Pappatà, S., Santangelo, G., Aarsland, D., Viciomini, C., Longo, K., Bronnick, K., ... Barone, P. (2011). Mild cognitive impairment in drug-naïve patients with PD is associated with cerebral hypometabolism. *Neurology*, 77(14), 1357–1362. <https://doi.org/10.1212/WNL.0b013e3182315259>
- Passow, S., Specht, K., Adamsen, T. C., Biermann, M., Brekke, N., Craven, A. R., ... Hugdahl, K. (2015). Default-mode network functional connectivity is closely related to metabolic activity. *Human Brain Mapping*, 36(6), 2027–2038. <https://doi.org/10.1002/hbm.22753>
- Polito, C., Berti, V., Ramat, S., Vanzi, E., de Cristofaro, M. T., Pellicanò, G., ... Pupi, A. (2012). Interaction of caudate dopamine depletion and brain metabolic changes with cognitive dysfunction in early Parkinson's disease. *Neurobiology of Aging*, 33(1), 206.e29–206.e39. <https://doi.org/10.1016/j.neurobiolaging.2010.09.004>



- Power, J. D., Schlaggar, B. L., & Petersen, S. E. (2015). Recent progress and outstanding issues in motion correction in resting state fMRI. *NeuroImage*, 105, 536–551. <https://doi.org/10.1016/j.neuroimage.2014.10.044>
- Raichle, M. E., MacLeod, A. M., Snyder, A. Z., ... Gordon, L. (2000). A default mode of brain function. *Proceedings of the National Academy of Sciences of the United States of America*, 98(2), 676–682.
- Ray, N. J., Bradburn, S., Murgatroyd, C., Toseeb, U., Mir, P., Kountouriotis, G. K., ... Grothe, M. J. (2018). In vivo cholinergic basal forebrain atrophy predicts cognitive decline in de novo Parkinson's disease. *Brain: A Journal of Neurology*, 141(1), 165–176. <https://doi.org/10.1093/brain/awx310>
- Riedl, V., Bienkowska, K., Strobel, C., Tahmasian, M., Grimmer, T., Förster, S., ... Drzezga, A. (2014). Local activity determines functional connectivity in the resting human brain: A simultaneous FDG-PET/fMRI study. *The Journal of Neuroscience: The Official Journal of the Society for Neuroscience*, 34(18), 6260–6266. <https://doi.org/10.1523/JNEUROSCI.0492-14.2014>
- Ruppert, M. C., Greuel, A., Tahmasian, M., Schwartz, F., Stürmer, S., Maier, F., ... Eggers, C. (2020). Network degeneration in Parkinson's disease: Multimodal imaging of nigro-striato-cortical dysfunction. *Brain: A Journal of Neurology*, 143(3), 944–959. <https://doi.org/10.1093/brain/awaa019>
- Sala, A., & Perani, D. (2019). Brain molecular connectivity in neurodegenerative diseases: Recent advances and new perspectives using positron emission tomography. *Frontiers in Neuroscience*, 13, 617. <https://doi.org/10.3389/fnins.2019.00617>
- Sala, A., Caminiti, S. P., Presotto, L., Premi, E., Pilotto, A., Turrone, R., ... Perani, D. (2017). Altered brain metabolic connectivity at multiscale level in early Parkinson's disease. *Scientific Reports*, 7(1), 4256. <https://doi.org/10.1038/s41598-017-04102-z>
- Savio, A., Fänger, S., Tahmasian, M., Rachakonda, S., Manoliu, A., Sorg, C., ... Yakushev, I. (2017). Resting-state networks as simultaneously measured with functional MRI and PET. *Journal of Nuclear Medicine: Official Publication, Society of Nuclear Medicine*, 58(8), 1314–1317. <https://doi.org/10.2967/jnumed.116.185835>
- Spetsieris, P. G., Ko, J. H., Tang, C. C., Nazem, A., Sako, W., Peng, S., ... Eidelberg, D. (2015). Metabolic resting-state brain networks in health and disease. *Proceedings of the National Academy of Sciences of the United States of America*, 112(8), 2563–2568. <https://doi.org/10.1073/pnas.1411011112>
- Tahmasian, M., Bettray, L. M., van Eimeren, T., Drzezga, A., Timmermann, L., Eickhoff, C. R., ... Eggers, C. (2015). A systematic review on the applications of resting-state fMRI in Parkinson's disease: Does dopamine replacement therapy play a role? *Cortex; A Journal Devoted to the Study of the Nervous System and Behavior*, 73, 80–105. <https://doi.org/10.1016/j.cortex.2015.08.005>
- Tahmasian, M., Eickhoff, S. B., Giehl, K., Schwartz, F., Herz, D. M., Drzezga, A., ... Eickhoff, C. R. (2017). Resting-state functional reorganization in Parkinson's disease: An activation likelihood estimation meta-analysis. *Cortex; A Journal Devoted to the Study of the Nervous System and Behavior*, 92, 119–138. <https://doi.org/10.1016/j.cortex.2017.03.016>
- Tessitore, A., Esposito, F., Vitale, C., Santangelo, G., Amboni, M., Russo, A., ... Tedeschi, G. (2012). Default-mode network connectivity in cognitively unimpaired patients with Parkinson disease. *Neurology*, 79(23), 2226–2232. <https://doi.org/10.1212/WNL.0b013e31827689d6>
- Tomlinson, C. L., Stowe, R., Patel, S., Rick, C., Gray, R., & Clarke, C. E. (2010). Systematic review of levodopa dose equivalency reporting in Parkinson's disease. *Movement Disorders: Official Journal of the Movement Disorder Society*, 25(15), 2649–2653. <https://doi.org/10.1002/mds.23429>
- Toussaint, P.-J., Perlberg, V., Bellec, P., Desarnaud, S., Lacomblez, L., Doyon, J., ... Benali, H. (2012). Resting state FDG-PET functional connectivity as an early biomarker of Alzheimer's disease using conjoint univariate and independent component analyses. *NeuroImage*, 63(2), 936–946. <https://doi.org/10.1016/j.neuroimage.2012.03.091>
- van Eimeren, T., Monchi, O., Ballanger, B., & Strafella, A. P. (2009). Dysfunction of the default mode network in Parkinson disease: A functional magnetic resonance imaging study. *Archives of Neurology*, 66(7), 877–883. <https://doi.org/10.1001/archneurol.2009.97>
- Wehrl, H. F., Hossain, M., Lankes, K., Liu, C.-C., Bezrukov, I., Martirosian, P., ... Pichler, B. J. (2013). Simultaneous PET-MRI reveals brain function in activated and resting state on metabolic, hemodynamic and multiple temporal scales. *Nature Medicine*, 19(9), 1184–1189. <https://doi.org/10.1038/nm.3290>
- Williams-Gray, C. H., Evans, J. R., Goris, A., Foltynie, T., Ban, M., Robbins, T. W., ... Barker, R. A. (2009). The distinct cognitive syndromes of Parkinson's disease: 5 year follow-up of the CamPaIGN cohort. *Brain: A Journal of Neurology*, 132(Pt 11), 2958–2969. <https://doi.org/10.1093/brain/awp245>
- Win, T. P., Hosokai, Y., Minagawa, T., Muroi, K., Miwa, K., Maruyama, A., ... Saito, H. (2019). Comparison of count normalization methods for statistical parametric mapping analysis using a digital brain phantom obtained from Fluorodeoxyglucose-positron emission tomography. *Asia Oceania Journal of Nuclear Medicine & Biology*, 7(1), 58–70. <https://doi.org/10.22038/AOJNMB.2018.11745>
- Yakushev, I., Hammers, A., Fellgiebel, A., Schmidtman, I., Scheurich, A., Buchholz, H.-G., ... Schreckenberger, M. (2009). Spm-based count normalization provides excellent discrimination of mild Alzheimer's disease and amnesic mild cognitive impairment from healthy aging. *NeuroImage*, 44(1), 43–50. <https://doi.org/10.1016/j.neuroimage.2008.07.015>
- Yakushev, I., Chételat, G., Fischer, F. U., Landeau, B., Bastin, C., Scheurich, A., ... Salmon, E. (2013). Metabolic and structural connectivity within the default mode network relates to working memory performance in young healthy adults. *NeuroImage*, 79, 184–190. <https://doi.org/10.1016/j.neuroimage.2013.04.069>
- Zhan, Z.-W., Lin, L.-Z., Yu, E.-H., Xin, J.-W., Lin, L., Lin, H.-L., ... Pan, X.-D. (2018). Abnormal resting-state functional connectivity in posterior cingulate cortex of Parkinson's disease with mild cognitive impairment and dementia. *CNS Neuroscience & Therapeutics*, 24(10), 897–905. <https://doi.org/10.1111/cns.12838>
- Zou, K. H., Warfield, S. K., Bharatha, A., Tempany, C. M. C., Kaus, M. R., Haker, S. J., ... Kikinis, R. (2004). Statistical validation of image segmentation quality based on a spatial overlap index1. *Academic Radiology*, 11(2), 178–189. [https://doi.org/10.1016/S1076-6332\(03\)00671-8](https://doi.org/10.1016/S1076-6332(03)00671-8)

## SUPPORTING INFORMATION

Additional supporting information may be found online in the Supporting Information section at the end of this article.

**How to cite this article:** Ruppert MC, Greuel A, Freigang J, et al. The default mode network and cognition in Parkinson's disease: A multimodal resting-state network approach. *Hum Brain Mapp*. 2021;42:2623–2641. <https://doi.org/10.1002/hbm.25393>

7.4. Supplementary material

## Supplementary material

MNI coordinates	Regions of interest (radius in mm)	MNI coordinates	Regions of interest (radius in mm)
<b>3 51 -9</b>	<b>mPFC</b> medial prefrontal cortex (10 mm)	<b>-59 -47 35</b>	<b>pSMGls</b> Supramarginal gyrus posterior division left superior (5 mm)
<b>-22 28 42</b>	<b>SFGI</b> middle frontal gyrus, frontal pole (5 mm)	<b>59 -47 35</b>	<b>pSMGrs</b> Supramarginal gyrus posterior division right superior (5 mm)
<b>2 15 40</b>	<b>SFGmid</b> Paracingulate cortex, cingulate gyrus anterior division	<b>-51 -56 25</b>	<b>AGl</b> Angular gyrus left (5 mm)
<b>25 25 5</b>	<b>SFGr</b> superior frontal gyrus, middle temporal gyrus (5 mm)	<b>54 -57 26</b>	<b>AGr</b> Angular gyrus right (5 mm)
<b>-40 -70 32</b>	<b>sLOCi</b> lateral occipital cortex superior division left (10 mm)	<b>-27 -36 -15</b>	<b>ParaHL</b> Parahippocampal gyrus left (5 mm)
<b>40 -70 32</b>	<b>sLOCr</b> lateral occipital cortex superior division right (10 mm)	<b>28 -35 -15</b>	<b>ParaHR</b> Parahippocampal gyrus right (5 mm)
<b>2 64 23</b>	<b>PC</b> precuneous cortex (10 mm)	<b>2 -42 32</b>	<b>PCC</b> Cingulate cortex posterior division (10 mm)
<b>-51 -47 16</b>	<b>pSMGI</b> posterior supramarginal gyrus (5 mm)		

Table S1: Regions of interest (ROIs) within the identified DMN components. Spherical ROIs centered at the indicated MNI coordinates (left column) were defined in MarsBaR (Brett, Anton, Valabregue, & Poline, 2002) based on overlapping volumes of binary DMN masks obtained with both modalities. Included anatomical regions (right column) were evaluated with respect to Harvard-Oxford atlas. Prefrontal and parahippocampal ROIs were defined based on the rsfMRI component only.

Groups	FDG-PET and fMRI		p-value	fMRI		p-value
	HC (n = 16)	PD (n = 51)		HC (n = 25)	PD (n = 60)	
Age, years	64.63 ± 8.33	66.45 ± 8.53	0.455	63.52 ± 7.67	65.02 ± 9.82	0.455
Gender, F/M	9 / 7	18 / 33	0.231	13 / 12	19 / 41	0.129
Education, years	16.44 ± 2.06	14.20 ± 2.73	<b>0.004**</b>	16.50 ± 2.04	14.54 ± 2.80	<b>0.004**</b>
DD, years	-	4.56 ± 3.29	-	-	4.89 ± 3.53	-
UPDRS III total	-	25.10 ± 9.54	-	-	24.35 ± 9.23	-
H & Y, stage (n)	-	-	-	-	1 (1)	-
		2 (30)			2 (32)	
		2.5 (14)			2.5 (19)	
		3 (6)			3 (7)	
		4 (1)			4 (1)	
LEDD	-	453.88 ± 244.72	-	-	477.30 ± 278.91	-
MMSE	28.94 ± 1.00	28.37 ± 1.82	0.392	28.92 ± 1.04	28.45 ± 1.73	0.394

Table S2: Demographic, clinical and behavioural characteristics of the FDG-PET or fMRI cohort including all PD patients and healthy controls. Abbreviations: DD = disease duration; H&Y = Hoehn and Yahr; HC = healthy controls; Levodopa equivalent daily dose; PD = Parkinson's disease; MMSE = Mini-Mental Status Examination. \*\* p < 0.01

Groups	FDG-PET and fMRI		p-value
	HC (n = 16)	PD (n = 16)	
Demographic and clinical variables			
Age, years	64.63 ± 8.33	69.69 ± 9.45	0.118
Gender, F/M	9 / 7	6 / 10	0.479
Education, years	16.44 ± 2.06	13.44 ± 2.99	0.005**
DD, years	-	5.63 ± 3.44	-
UPDRS III total	-	23.06 ± 6.69	-
H & Y, stage (n)	-	2 (8) 2.5 (5) 3 (3)	-
LEDD	-	533.03 ± 262.31	-
MMSE	28.94 ± 1.00	28.25 ± 2.11	0.550
MCI status (yes • no)	0 • 16	6 • 10	0.024*

Table S3: Demographic, clinical and behavioural characteristics of the subset of subjects whose scans were fed into ICA analysis, including 16 PD patients and 16 healthy controls who underwent FDG-PET and fMRI. Abbreviations: DD = disease duration; H&Y = Hoehn and Yahr; HC = healthy controls; Levodopa equivalent daily dose; PD = Parkinson's disease; MCI = mild cognitive impairment (according to Movement Disorder Society Level II diagnostic criteria); MMSE = Mini-Mental Status Examination. \* $<0.05$ ; \*\*  $p < 0.01$



## ICA whole sample networks

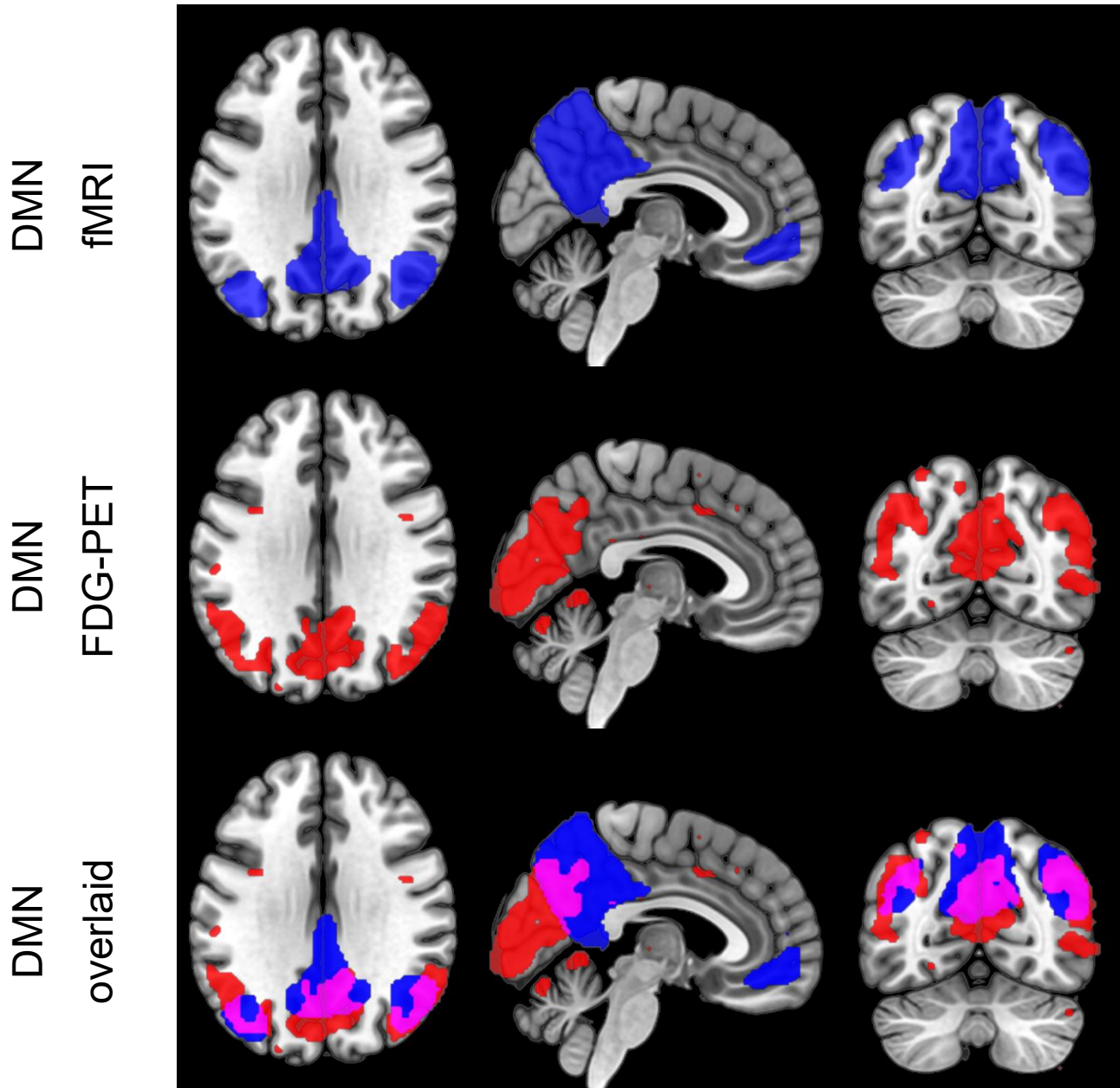


Figure S1: Spatial coincidence of ICA-derived metabolic and functional DMN. A) Spatial distribution of components representing the DMN obtained by fMRI (first row) or FDG-PET (second row) and their spatial correspondence (third row). Masks were created by thresholding the component-specific group maps at  $z = 2$  and overlaid on a T1-weighted MNI template for visualisation. Abbreviations: DMN = default mode network.

Region	ANOVA	PD-NC-HC	PD-MCI-HC	PD-MCI-PD-NC	JT-test
mPFC	Kruskal-Wallis chi-squared = 19.58, df = 2, p < 0.0001	-0.10 [-0.14; -0.06] p < 0.001	0.13 [0.07; 0.19] p < 0.001	0.03 [-0.02; 0.08] p = 0.206	JT = 270 (120), p < 0.00001
PC	Kruskal-Wallis chi-squared = 21.07, df = 2, p < 0.0001	0.17 [0.10; 0.25] p < 0.001	-0.24 [-0.36; -0.17] p < 0.0001	-0.09 [-0.19; -0.001] p = 0.049	JT = 246 (133), p < 0.000001
sLOCi	Kruskal-Wallis chi-squared = 22.47, df = 2, p < 0.0001	0.13 [0.08; 0.21] p < 0.0001	0.25 [0.15; 0.31] p < 0.0001	-0.09 [-0.17; 0.002] p = 0.054	JT = 233 (92), p < 0.000001
sLOCr	Kruskal-Wallis chi-squared = 23.18, df = 2, p < 0.0001	0.16 [0.09; 0.23] p < 0.0001	0.22 [0.15; 0.31] p < 0.0001	0.07 [-0.01; 0.15] p = 0.098	JT = 236 (127), p < 0.000001
AGl	Kruskal-Wallis chi-squared = 23.67, df = 2, p < 0.00001	0.19 [0.11; 0.27] p < 0.00001	0.27 [0.18; 0.34] p < 0.001	0.07 [-0.04; 0.15] p = 0.173	JT = 235 (158), p < 0.000001
AGr	Kruskal-Wallis chi-squared = 18.01, df = 2, p < 0.001	0.18 [0.09; 0.27] p < 0.001	0.26 [0.16; 0.38] p < 0.001	0.08 [-0.04; 0.20] p = 0.181	JT = 281 (159), p < 0.00001
PCC	Kruskal-Wallis chi-squared = 19.95, df = 2, p < 0.0001	0.14 [0.08; 0.19] p < 0.0001	0.18 [0.08; 0.27] p < 0.001	0.05 [-0.04; 0.11] p = 0.352	JT = 276 (170), p < 0.00001
pSMGI	Kruskal-Wallis chi-squared = 16.02, df = 2, p < 0.001	0.12 [0.05; 0.19] p < 0.001	0.17 [0.07; 0.27] p < 0.001	0.04 [-0.02; 0.11] p = 0.223	JT = 300 (227), p < 0.0001
pSMGrs	Kruskal-Wallis chi-squared = 18.52, df = 2, p < 0.0001	0.20 [0.10; 0.27] p < 0.0001	0.22 [0.10; 0.34] p = 0.001	-0.04 [-0.13; 0.08] p = 0.390	JT = 289 (254), p = 0.0001
pSMGls	Kruskal-Wallis chi-squared = 14.75, df = 2, p < 0.001	-0.11 [-0.20; -0.04] p = 0.005	-0.19 [-0.28; -0.09] p < 0.001	-0.07 [-0.16; 0.01] p = 0.098	JT = 305 (231), p = 0.0001
ParaHR	Kruskal-Wallis chi-squared = 20.44, df = 2, p < 0.0001	-0.07 [-0.10; -0.04] p < 0.00001	-0.08 [-0.12; -0.05] p = 0.002	-0.01 [-0.04; 0.04] p = 0.630	JT = 288 (217), p = 0.0001
ParaHL	Kruskal-Wallis chi-squared = 23.35, df = 2, p < 0.00001	-0.07 [-0.09; -0.05] p < 0.0001	-0.11 [-0.15; -0.07] p < 0.001	-0.03 [-0.07; 0.003] p = 0.068	JT = 226 (112), p = 0.000001
SFGl	Kruskal-Wallis chi-squared = 7.23, df = 2, p = 0.027	-0.08 [-0.14; -0.03] p = 0.026	-0.09 [-0.17; 0.003] p = 0.106	-0.02 [-0.10; 0.07] 0.787	JT = 415 (405), p = 0.008 (p = 0.005)
SFGGr	Kruskal-Wallis chi-squared = 13.79, df = 2, p = 0.001	-0.13 [-0.19; -0.06] p < 0.001	-0.12 [-0.20; -0.04] p = 0.014	0.01 [-0.04; 0.07] p = 0.630	JT = 383 (341), p = 0.002 (p < 0.001)
SFGmid	Kruskal-Wallis chi-squared = 8.97, df = 2, p = 0.011	-0.11 [-0.20; -0.03] p = 0.022	-0.15 [-0.26; -0.03] p = 0.022	-0.03 [-0.12; 0.06] p = 0.533	JT = 384 (268), p = 0.002 (p < 0.001)

Table S4: Statistical comparisons of normalised FDG-Uptake values exported from 15 DMN regions. Test statistic and p-values in brackets represent the adjusted statistics obtained using estimated means, corrected for UPDRS-III, disease duration and LEDD in patients.

Abbreviations: AGl = angular gyrus left; AGr = angular gyrus right; HC = healthy controls; mPFC = medial prefrontal cortex; ParaHL = parahippocampal cortex left; ParaHR = parahippocampal cortex right; PC = precuneus cortex; PCC = posterior cingular cortex; pSMGI = posterior supramarginal gyrus; pSMGls = posterior supramarginal gyrus left superior; pSMGrs = posterior supramarginal gyrus right superior; SFGl = superior frontal gyrus left; SFG mid = superior frontal gyrus mid; SFGGr = superior frontal gyrus right; sLOCi = superior lateral occipital cortex left; sLOCr = superior lateral occipital cortex right. JT: Jonckheere terpsita test statistic; PD = Parkinson's disease; PD-NC = PD patients with normal cognition; PD-MCI = PD patients with mild cognitive impairment

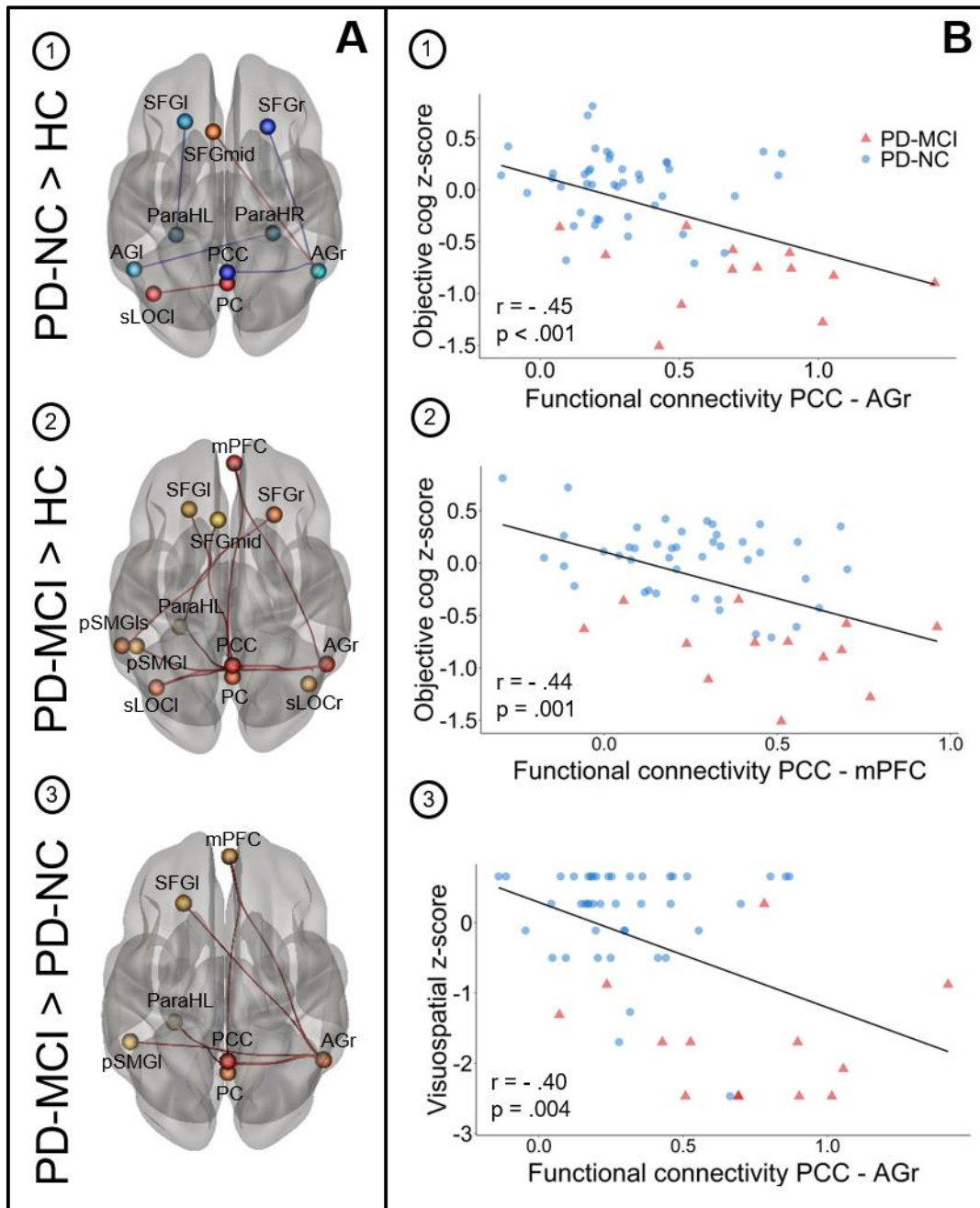


Figure S2: A) Group differences in functional connectivity of DMN ROIs between healthy controls ( $n = 24$ ) and cognitively impaired ( $n = 13$ ) and unimpaired ( $n = 43$ ) PD patients of the rsfMRI cohort. A1-A2 uncorrected, A3 FDR-corrected two-sided  $p < .05$ . Connections shown in red represent increased connectivity strength, blue connections refer to the opposite contrast. ROIs' sizes do not indicate the actual ROI diameters. Results are shown in 3D view from superior perspective. B) Correlation plots showing significant negative correlations between functional connectivity and cognitive z-scores in PD for the following connections and z-scores: 1) PCC-AGr and cognitive composite z-scores, 2) PCC-mPFC and cognitive composite z-scores and 3) PCC-AGr and visuospatial z-scores. Pearson's correlation coefficients and p-values are shown on the bottom left in each plot.

Abbreviations: AGl = angular gyrus left; AGr = angular gyrus right; mPFC = medial prefrontal cortex; ParaHL = parahippocampal cortex left; ParaHR = parahippocampal cortex right; PC = precuneus cortex; PCC = posterior cingular cortex; pSMGI = supramarginal gyrus left; pSMGls

= posterior supramarginal gyrus left superior; pSMGrS = posterior supramarginal gyrus right superior; SFGl = superior frontal gyrus left; SFG mid = superior frontal gyrus mid; SFGr = superior frontal gyrus right; sLOCl = superior lateral occipital cortex left; sLOCr = superior lateral occipital cortex right.

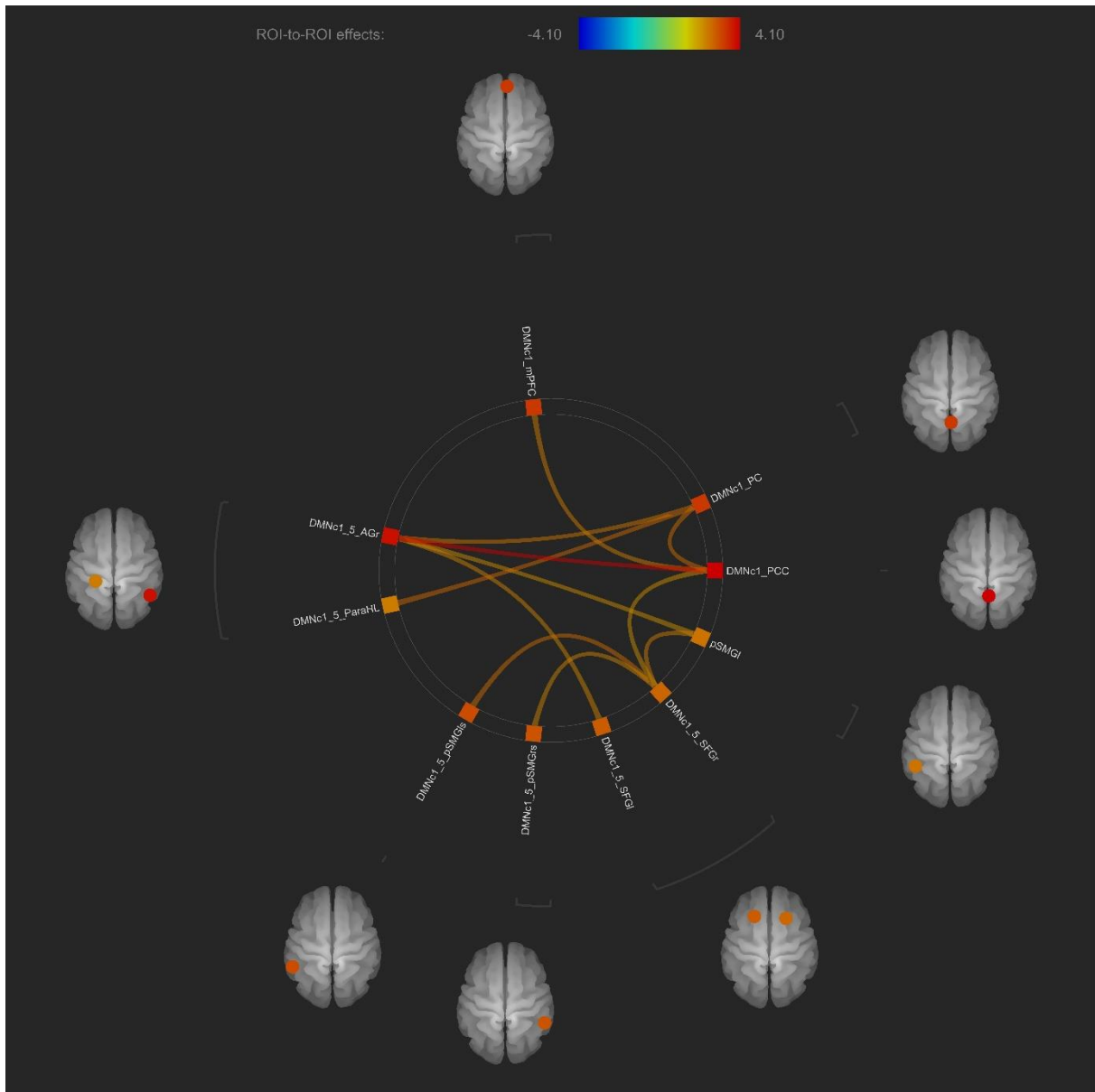


Figure S3: Group differences in functional connectivity of DMN ROIs between PD-MCI (n = 12) and cognitively unimpaired (n = 36) PD patients with covariates UPDRS-III, disease duration and LEDD. Connections shown in red represent increased connectivity strength, blue connections refer to the opposite contrast. ROIs' sizes do not indicate the actual ROI diameters.

Abbreviations: AGl = angular gyrus left; AGr = angular gyrus right; mPFC = medial prefrontal cortex; ParaHL = parahippocampal cortex left; ParaHR = parahippocampal cortex right; PC = precuneus cortex; PCC = posterior cingulate cortex; pSMGI = supramarginal gyrus left; pSMGrS = posterior supramarginal gyrus left superior; pSMGrL = posterior supramarginal gyrus left lateral; SFGl = superior frontal gyrus left; SFG mid = superior frontal gyrus mid; SFGr = superior frontal gyrus right; sLOCl = superior lateral occipital cortex left; sLOCr = superior lateral occipital cortex right.

## References

Brett, M., Anton, J. L., Valabregue, R., & Poline, J.-B. (2002). Region of interest analysis using an SPM toolbox.  
*Presented at the 8th International Conference on Functional.*

7.5. Lebenslauf



7.6. Publikationsverzeichnis



Poster/Abstracts

1.7. Verzeichnis der akademischen Lehrer\*innen

Philipps-Universität Marburg:

Adhikary, Till, PD Dr.  
Bacher, Michael, Prof. Dr.  
Baranovski, Sergei, Prof. Dr.  
Bauer, Stefan, Prof. Dr.  
Bauer, Uta Maria, Prof. Dr.  
Behrendt, Marc, Dr.  
Bertoune, Mirjam, Dr.  
Bökel, Christian, Prof. Dr.  
Bopp, Miriam, PD Dr.  
Borchers, Annette, Prof. Dr.  
Brandt, Dominique, Dr.  
Brehm, Alexander, Prof. Dr.  
Bremmer, Frank, Prof. Dr.  
Bünemann, Moritz, Prof. Dr.  
Chung, Ho Ryun, Prof. Dr.  
Conrad Matthias, Dr.  
Culmsee, Carsten, Prof. Dr.  
Decher, Niels, Prof. Dr.  
Del Rey, Adriana, Prof. Dr.  
Dodel, Richard, Prof. Dr.  
Eggers, Carsten, Prof. Dr.  
Elsässer, Hans-Peter, Prof. Dr.  
Endres, Dominik, Prof. Dr.  
Feuser, Beate, Dr.  
Fritz, Barbara, PD Dr.  
Ganjam, Goutham K., Dr.  
Greene, Brandon, Dr.  
Guthoff, Philipp, Dr.  
Halaszovich, Christian, Dr.  
Höbenreich, Sabrina, Dr.  
Hobiger, Kirstin, Dr.  
Homburg, Uwe, Prof. Dr.  
Huber, Magdalena, Prof. Dr.  
Jacob, Ralf, Prof. Dr.

Jänsch, Heinz J., Prof. Dr.  
Jansen, Andreas, Prof. Dr.  
Kiper, Aytug, Dr.  
Kircher, Thilo, Prof. Dr.  
Kleinschnitz, Eva-Maria, Dr.  
Kronimus, Yannick, Dr.  
Leitner, Michael, Dr.  
Lill, Roland, Prof. Dr.  
Maisner, Andrea, Prof. Dr.  
Matschke, Lina, Dr.  
Milani, Wiebke, Dr.  
Moll, Roland, Prof. Dr.  
Mühlenhoff, Ulrich, Prof. Dr.  
Müller, Rolf, Prof. Dr.  
Müller-Brüsselbach, Sabine, PD Dr.  
Nieweg, Katja, Prof. Dr.  
Oberwinkler, Johannes, Prof. Dr.  
Oehrn, Carina, Dr.  
Oliver, Dominik, Prof. Dr.  
Pagenstecher, Axel, Prof. Dr.  
Peper, Martin, Prof. Dr. Dr.  
Plant, Timothy D., Prof. Dr.  
Preisig-Müller, Regina, PD Dr.  
Pütz, Michael, Dr.  
Reiß, Philipp, Dr.  
Rinné, Susanne, PD Dr.  
Rust, Marco, Prof. Dr.  
Schachtner, Joachim, Prof. Dr.  
Schäfer, Martin, Dr.  
Schmidt, Ansgar, Dr.  
Schnare, Markus, Prof. Dr.  
Schu, Ulrich, Dr.  
Schubö, Anna, Prof. Dr.  
Schütz, Burkhard, Prof. Dr.  
Schwaringer, Mathias, Prof. Dr.  
Schwaring, Rainer, Prof. Dr.  
Sommer, Jens, Dr.

Stehling, Oliver, Dr.

Steinhoff, Ulrich, Prof. Dr.

Straube, Benjamin, Prof. Dr.

Strauer, Dorothea, Dr.

Suske, Guntram, Prof. Dr.

Tackenberg, Björn, Prof. Dr.

Thieme, Kati, Prof. Dr.

Thorwart, Anna, Dr.

Timmermann, Lars, Prof. Dr.

Vidovic, Natascha, Dr.

Weber, Immo, Dr.

Weihe, Eberhard, Prof. Dr.

Westermann, Reiner, PD Dr.

Wrocklage, Christian, Dr.

### 1.8. Danksagung

Ich danke an dieser Stelle meinen Eltern und meiner Familie, die mich während meines gesamten Studiums bedingungslos und liebevoll unterstützt haben. Mein ganz besonderer Dank gilt meinem Ehemann Johannes für die unzähligen Gespräche und die Zusprüche, die es geschafft haben, mich stets immer wieder zu motivieren. Des Weiteren danke ich Prof. Dr. Carsten Eggers für die Unterstützung, das entgegengebrachte Vertrauen und die konstruktive Kritik während der Planung und Umsetzung der gemeinsamen Projekte. Mein aufrichtiger Dank geht an Herrn PD Dr. Pedrosa, der sich meiner Betreuung vor Ort gewidmet hat und mich bei der Umsetzung der Projekte und allen damit verbundenen Hürden unterstützt hat und dabei immer ein offenes Ohr für mich hatte. Ganz besonders danke ich darüber hinaus meinen Kolleginnen Andrea Greuel, Vanessa Heinecke sowie Herrn Dr. Kenan Steidel für die Unterstützung bei der Planung und Umsetzung der Projekte. Des Weiteren gilt mein herzlicher Dank allen Kooperationspartnern, vor allem der Abteilung für Nuklearmedizin des Universitätsklinikums Marburg und Gießen (Standort Marburg), Prof. A. Jansen, Dr. Jens Sommer, Rita Werner und Mechthild Wallnig der Core Facility Brain Imaging sowie dem Team des Max-Planck-Instituts für Stoffwechselforschung in Köln und Herrn Prof. Drzezga für die Unterstützung bei der Datenakquise und der Projektumsetzung.

Abschließend möchte ich meinen Dank an Herrn Prof. Timmermann sowie an die Kolleg\*innen der Klinik für Neurologie, das Team der Arbeitsgruppe Bewegungsstörungen und Neuromodulation, und allem voran Stefanie Spriewald, richten, die mir ein Umfeld schafften, in dem das Promotionsprojekt umgesetzt werden konnte. Mein größter Dank gilt jedoch den Studienteilnehmer\*innen, die durch ihre Teilnahme die Umsetzung des vorliegenden Projekts erst möglich gemacht haben.

1.9. Ehrenwörtliche Erklärung

.